Glass Concrete Thin Sheets Reinforced with Prestressed Aramid Fabrics

Gregor Vilkner

Submitted in partial fulfillment

of the requirements

for the degree of Doctor of Philosophy

in the Graduate School of Arts and Sciences

COLUMBIA UNIVERSITY

2003

Abstract

Glass Concrete Thin Sheets Reinforced with Prestressed Aramid Fabrics

Gregor Vilkner

Thin sheet concrete products are receiving increased attention because of the large number of potential applications. By using crushed glass as aggregate, a multitude of different esthetic effects can be produced, which again open up numerous architectural and decorative uses. Such thin sheets are most effectively reinforced with fiber mesh, whether made of polypropylene, AR-glass, or other types of materials.

The experimental project presented in this work explored the possibilities of prestressing thin sheet glass concrete products with fabrics. Aramid fibers, known under their trade names Kevlar, Twaron, and Technora, have been found to be well suited for prestressing applications in the form of fiber-reinforced polymers (FRP). For prestressing thin sheets, however, the material was utilized to date in a more unprotected form, covered just with a thin coating agent.

The constitutive materials, aramid and glass concrete are introduced. Especially the deformation mechanisms of aramid fibers and their relaxation properties are explored in great detail. Glass concrete, which by now is produced commercially, was utilized as the matrix for the prestressed composite, because it offers several

advantages beside its esthetic potential, such as excellent workability, superior durability and high-early strength. Glass concrete beams with cross-sections of 1/4 in $\times$ 1 in have been produced with prestress levels varying from 0 to 2 ksi.

It has been observed that a large amount of the prestress force in the fiber rovings is lost during the first few hours of hydration, while they are still anchored against the formwork. Once the concrete has hardened, however, the prestress level stabilized. Understanding the interaction mechanisms between aramid fibers and hydrating concrete is critical to successfully produce thin sheets prestressed with high-performance polymeric fibers. The mechanical properties of prestressed thin beams correspond well with traditional prestressed concrete theory during three-point bending tests. The prestress delays the formation of distributed cracking and greatly enhances the stiffness of the section in the cracked state.

The next steps on the way to commercially produced prestressed thin sheets include optimizing the usage of the rather expensive reinforcing material by minimizing prestress losses. Most important is to identify promising applications and the corresponding design parameters, which may call for increased stiffness or large deformability. Suitable production techniques still need to be developed, especially for generating and maintaining the prestress force before concrete is cast. For outdoor applications, durability aspects gain additional significance, and the effect of moisture on the flexural response of prestressed thin sheets is to be further investigated.

Table of Contents

List of Tables

List of Figures

For Liesing Grohmann,

who was there for me all my life,

and whom I missed seeing one last time.

Acknowledgments

This has been four fantastic years in the Department of Civil Engineering and Engineering Mechanics. Besides the great academic challenge, the constant interaction with faculty and lab staff was most enjoyable. I am indebted to my fellow graduate students who became my closest friends. Thank you for all the help, talk, discussion, and fun we had together.

My stay in International House in the Heart of New York City has broadened my cultural understanding and had quite an impact on my personal development. There would have been no better place to live.

Many thanks to Dr. Shimanovich and Dr. Kozlova, who have always let me rely on their exceptionally broad body of knowledge in the fields of polymers, cement chemistry, and concrete technology. I also would have gotten nowhere without the superb assistance I received in the Carleton Laboratory from Lee Ping, Johnny, and Sam. Thank you, Roberto Felicetti and Bin Mu, for getting me on the right track with experimental techniques, and for letting me participate in your brainstorming sessions about closed-loop feedback control and the great mystery of the snap-back. The kind support by Hexcel-Schwebel and Strategic Materials is greatly appreciated, for there would have been no research without your aramid fabrics and waste glass.

I am much obliged to the members of the thesis committee, Prof. Testa, Prof. Smyth, Prof. Gryte, and Prof. Durning for their efforts reviewing this work and for their constructive criticism. I hope that I was able to communicate my keen interest

in aramid fibers and prestressed thin sheets through my thesis, and that the reading was enjoyable.

Finally I wish to express my gratitude to my advisor, Prof. Meyer. Thank you for inviting me to Columbia University, for giving me such a great opportunity. In the numerous talks and discussions throughout the last four years I always found you open-minded, patient and constructive in your criticism. Your mentorship has helped me find my own rhythm, improve my English, and fostered my passion for independent research. It was not planned at first, but I now consider continuing academic research - the credit for that belongs to you.

Gregor Vilkner

Columbia University

May, 2003

Chapter 1

Introduction

1.1 Thin Sheets

The recent development of high performance fibers has all but eliminated one major design limitation of reinforced concrete, namely the need for concrete cover. Because the alkaline nature of cement-based concrete matrixes protects reinforcing steel from corrosion, building codes around the world require that all reinforcing steel be covered by concrete, varying in thickness from 1/2 in (13mm) to 3 in (76mm) depending on size of reinforcement and application [1]. To non-corroding fibers no such restrictions apply, which eliminates a major limiting factor for the minimum thickness of concrete products. Standards usually require concrete members to be at least 3 times as thick as the diameter of the largest aggregate size used. When coarse aggregate is left out all together and fine-grained cement-based mortars are reinforced with high-performance fibers, highly orientated in the form of woven fabrics, there remains almost no lower limits for plate thickness. In fact, sheets as thin as 0.1 in (3mm) have been produced by researchers for the sake of demonstrating the possibilities. Sheets of such small thickness offer enormous flexibility, Fig. 1.1.

Structural slabs are traditionally reinforced with regular steel. For thinner and more slender plates, smaller bar diameters in the form of welded wire mesh are appropriate. As long as the reinforcing material is made of steel, however, the need for concrete cover remains. Fiber reinforcement in concrete applications was first

Figure 1.1: Prof. Shah with Thin Composite Sheet (as found on the cover of [9])

used in the form of short random fibers made of steel or polypropylene, mostly to control shrinkage cracking. Next, fibers with high strength and high stiffness were utilized to strengthen and toughen slabs, allowing larger deflections and controlled cracking. At that point, bond between fibers and matrix becomes an issue of major importance. If the fibers bond to the concrete matrix too strongly, they are likely to break after first cracking of the matrix, whereas if the bond is very weak, the fibers can pull out of the concrete matrix without much resistance. The art of high-performance fiber-reinforced cement composites (HPFRCC) is therefore to engineer materials, which allow elastic pull-out of reinforcing fibers, but under large energy dissipation, thereby causing strain hardening. This means, a structure subjected to tensile load or bending continues to increases its load response after initiation of cracking, as deflection or curvature increases [75, 59]. Only recently, it was suggested to differentiate between strain-hardening and deflection-hardening, depending

on whether a structure is subjected to uniaxial tensile loading or to bending [60].

The goal of reducing the thickness of slabs or sheets led to the use of continuous fibers and fiber bundles in the form of woven- or knitted fabrics [68, 37, 22]. One practical question that arose was how to ensure correct placement of such continuous fibers or fabrics. In traditional reinforced concrete, reinforcing steel is placed manually and held in place by spacers, or tied with metal wire to stirrups or other steel bars. Continuous fibers bend easily under their own weight and can not be arranged in the traditional way, unless they are stiffened by means of a coating such as epoxy (The result is reinforcing concrete with fiber-reinforced polymers (FRP) [61, 25], which is not the subject of this study). Regardless of the application, thin sheets can be produced practically only by precasting. Cement-based thin sheets are already used as drywall and tile backer boards (for instance, USG's DUROCK Brand Cement Board Panels [36]). Other potential applications include architectural products, especially combined with glass concrete for facade elements, table top counters, elevator panels, etc.

1.2 Glass Concrete and the Challenge of Controlling ASR

Over thousands of years concrete has been produced with hydraulic cement, sand and stone. Just as certain environments are aggressive to concrete structures, particular kinds of sand and stone are known to be harmful or incompatible aggregates for concrete. Typical problems that can occur if the wrong kind of aggregate is chosen are the delayed formation of ettringite, alkali-silica reaction (ASR), sulfate attack or carbonisation.

Glass as an aggregate is considered harmful for concrete because it generally

will cause ASR. The exact mechanisms of ASR are still not fully understood. However, it is clear that the silicious glass reacts in a moist alkaline environment of a Portland cement based matrix to form a gel, which is of larger volume than its constituents. The gel presses into the pores of the concrete matrix and sets it under tension until it eventually causes cracking and deterioration. This mechanism may occur rapidly and early in the life of a structure, or its effects are noticeable only after decades, which makes ASR a difficult problem to research. For example, it is a great challenge to establish accelerated testing techniques that allow to investigate any new concrete mix in a reasonable time to determine whether or not ASR will occur in the lifespan of a concrete structure. Two of such testing methods that have been standardized, ASTM C-227 and ASTM C-1260, were originally developed to test certain aggregates in a standardized cement-based matrix. Nowadays the Portland cement-based matrix itself is sometimes modified to adjust for potentially harmful aggregate like glass. For such non-conventional aggregates, none of the testing methods standardized by ASTM seem to be suitable. The academic discussion on which technique to use is still ongoing [32]. The relatively rapid method of ASTM C-1260 is said to be overly aggressive because of the high temperature and alkalinity, which far exceed the expected service life conditions of actual structures. The test method of ASTM C-227, on the other hand, has the disadvantage that it takes at least nine months to yield useful results. There are also concerns that alkali could be removed from the concrete system by means of leaching due to poorly specified test apparatus [77].

Other suggested tests, which use hot water environments to accelerate aging [50] are also controversial especially in connection with glass fibers or glass aggregate, since such tests change the intrinsic nature of the matrix composition rather than

simply accelerate hydration [72]. Finally, a wide range of ultra-accelerated tests using autoclave technology to artificially modify the aging environment have been proposed in the recent years. Such testing methods, although controversial [33], provide results already after a few days.

1.3 Why Aramid Fibers?

Fibers can be classified as either inorganic or organic. The inorganic category includes materials such as metals, graphite, ceramics, carbon and glass. The list of organic fiber materials, on the other hand, seems to be limited only by the creativity of nature and the chemical industry. Interestingly enough, nature still holds the record for the strongest fibers, which are spun by spiders[1]. Cellulose, silk, and cotton are also examples of natural fibers. Man-made organic fibers include nylon, polypropylene, polyvinyl alcohol (PVA), polyethylene, and aramid, among many others. Throughout the last decades aramids have been used in a variety of applications. Probably best known among these are soft body armor because of their capacity to absorb large amounts of energy. This capacity is realized primarily by the ability of the high-strength fibers to undergo large deformations.

High-strength steels, which traditionally have been the only materials used for prestressed concrete applications, need to be protected against corrosion. Stainless steels are available, including piano wires, but are very expensive. Also, they are not being offered in the form of woven or knitted meshes, in parallel alignments. Most of the commonly used polymeric materials, such as polypropylene, nylon, and polyvinyl

[1] "Recently, there has been much interest in spider dragline silk because of its stretchable and strong properties. Nephila spider dragline has a strength of 190 ksi (1.3 GPa), a breaking elongation of 40%, and toughness (breaking energy) of 16×10^4 Jkg^{-1}." [58]

alcohol, have relatively low melting points and exhibit excessive creep and relaxation behavior, which makes these materials unsuitable for prestress applications.

Alkali-resistant (AR) glass, aramid, and carbon are more appropriate in that regard. Because of their very high unit strengths, relatively low creep deformations, and high melting points, these materials are now being used, mostly in form of fiber reinforced plastics (FRP), in large-scale prototype projects around the world, such as for post-tensioned elevated roads and cables for suspension bridges.

All three materials have in common, in contrast to metals, that they exhibit highly linear elastic-brittle behavior. They are available in the form of woven or knitted fiber mesh. Alkali-resistant glass, although popular as short fiber reinforcement for concrete, mainly to control shrinkage cracking, has a rather low static fatigue limit and therefore is not likely to be suitable for prestressed applications. Aramid and carbon fibers, on the other hand, have reasonably high static fatigue limits, relative to their ultimate strengths. A disadvantage of carbon and glass fibers is their brittleness. However, in the case of extremely small diameters, brittleness is rendered a moot issue, to the extent that one can make a knot into a fiber and still be able to stretch it without causing failure. However, each single fiber is a solid structure. Small defects or cracks on its surface cause stress concentrations and can lead to accelerated degradation. Polymeric fibers, on the other hand, are flexible and fibrous down to basic polymer chains and surface defects are relatively harmless.

Carbon is chemically very well suited for concrete applications. Aramid fibers can be degraded by hydrolysis in environments with extreme pH values and are known to decompose under the influence of ultraviolet radiation, i.e. unprotected exposure to sunlight. Glass can be used in concrete only in its alkali-resistant form (AR-Glass).

The costs of aramid fiber mesh is still relatively high, however, manufacturers are steadily improving their production technologies. The resulting price reductions will make new applications feasible, and the increased demand for these materials is expected to prompt further cost reductions due to the economy of scale. Whereas it was difficult to obtain suitable carbon samples for this study, Hexcel-Schwebel kindly provided non-woven aramid fabrics of sufficient quantity, which shifted the focus of this work to aramid fibers exclusively.

1.4 Prestressing Thin Glass Concrete Sheets - Research Objective

Thin glass concrete sheets reinforced with prestressed continuous aramid fibers fall into a category referred to as *"textile-reinforced concrete"*. There is a major nationally funded project in Germany on this topic, shared between the Universities of Aachen and Dresden [37]. Also underway is a cooperative project on textile reinforced concrete composites between the Arizona State University, the Techion in Haifa, Israel, and the Ben-Gurion University in Beer Sheva, Israel [67, 57]. The only attempt to engineer thin sheet Portland cement-based composites prestressed with high-performance textile fabrics, has been reported from the University of Stuttgart, Germany[74]. The suitability of aramid fibers for prestressed concrete applications were also studied at the University of Cambridge, UK[17, 3, 48].

The key issue in the field of textile-reinforced concrete is the compatibility between fabrics and matrix, ranging from chemical aspects and bond to durability. Only carbon fibers come close to steel for stiffness. The other high-modulus fibers, aramid and glass fibers, are so soft that large cracks will develop before the fibers' load carrying capacity is developed [16]. The question arises, whether under such circumstances it is feasible to prestress thin sheets to control cracking, increase flex-

ural performance and improve durability by generating a compressed matrix, which destructive ions can permeate only with difficulty. While this is without doubt technically feasible, the question remains whether it is also practical and economical.

To avoid movement of the fiber mesh or fabric during concreting, it must be anchored against all sides of the formwork and held in the proper position until the matrix material is placed. It has been observed that slight stretching of the fibers to ensure improves the flexural performance of the composite. If the fibers can be anchored externally prior to placement of the mortar, it is straight forward to also apply larger tension into the reinforcement and arrive at a prestressing system similar to those used in regular pretensioned concrete, such as the stretchbed[2], which relies on load transfer via mechanical bond between the prestressing steel and the concrete matrix. If not enough bond can be developed, steel tendons require separate anchoring devices.

In connection with HPFRCC much work has been done on pull-out characteristics of single short fibers. Working with continuous fiber bundles, however, complicates the matter:

1. There is a difference between the friction between fibers on the inside of a fiber bundle and the friction between fibers located on the outside of a fiber bundle and the matrix material. Different numbers of fibers per bundle will surely display different bond characteristics.

[2]Typical stretchbeds are hundreds of feet long. After the concrete has hardened, load transfer is achieved by releasing the ends and then dividing the single long slab into pieces of desired size. During stretching the cross section of steel wires decreases due to Poisson's ratio. When the wires are cut to transfer the load to the concrete, their cross sections tend to increase again near the ends, thereby increasing the mechanical friction and in this way anchoring the wires. This is known as the "Hoyer" effect.

2. It is uncertain, how well the matrix material penetrates into the fiber bundle. Cement pastes are generally considered too viscous to penetrate into spaces as small as 10 μm (the diameter of a single aramid fiber), but during the concrete hardening process hydration products can eventually grow into fiber bundles.

3. Whether or not and how fibers or fiber bundles are coated by the manufacturer greatly influences their bond properties. The problem here is, that details of such coatings, which have a large influence on composite performance, are withheld by the industry as proprietary information.

All details on fibers, rovings, matrix, and the loading conditions affect the performance of the composite. A complete study of all the mechanisms involved would be therefore extremely complex and beyond the scope of a single project. The work presented here takes a practical approach and investigates prestressed thin beams in an empirical and experimental, rather than a theoretical and mechanics-based manner.

It was the aim of this study to develop an experimental setup to prestress thin beams. In a best-case scenario the technology used to produce these thin beams should be applicable to large thin sheets as well. Aramid fibers were studied in uniaxial tension experiments and the mechanical properties of prestressed thin beams were investigated by experimentally testing their flexural performance. All experiments described in the following chapters serve primarily qualitative, rather than quantitative purposes. They are meant to show trends and visualize theoretical principles. The results summarized in the various graphs and tables are usually mean values, and it should be realized that they display the kind of statistical scatter commonly experienced in concrete experiments.

Chapter 2 presents a detailed discussion of aramid fibers to understand their deformation mechanisms, chemical compatibility aspects, and relaxation properties. It was decided to select glass concrete as the cement-based matrix for various reasons, such as architectural potential and the experience gained with this particular building material within the research group throughout the last years. Chapter 3 reviews the main issues and the glass concrete mix design that had to be developed to combine excellent workability with development of high-early strength.

Chapter 4 describes the experimental setup needed to stress the fiber mesh, to anchor it until load transfer, and to monitor concrete shortening during load transfer and due to combined shrinkage and early creep. The experimental test program is described in Chapter 5. Test specimens were produced with different prestress levels, and their flexural performance in three-point bending tests are described in detail. Chapter 6 presents the major conclusions of this work and summarizes the numerous open questions that require further study.

Chapter 2

Aramid Fibers

2.1 Chemical Composition of Aramid Fibers - Review

Aramids are a family of high-strength nylons that includes fibers known under trade names like Kevlar, Twaron and Nomex. Aramid is a generic term applied to aromatic polyamides. A summary of aromatic high-strength fibers is compiled in [94]. Figure 2.1 shows the poly-para-phenylene terephtalamide (PpPTA) repeat unit, which in series builds polymer chains and forms highly ordered crystallite structures. Such crystallites are the building blocks of fibrils that, finally, form aramid fibers. The typical features of such aramid monomers are the aromatic phenyl rings, as well as the amide (-NH-) and carbonyl (-CO-) groups.

The small but important difference between different aramids such as Kevlar and Nomex can be pointed out by comparing Figs. 2.1 and 2.2. In the first case, the carbonyl-amid connections are attached to para-phenylene groups at carbon atoms

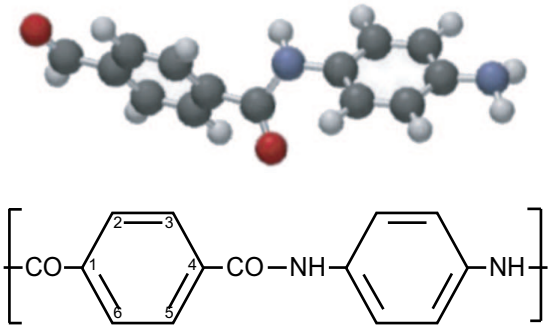

Figure 2.1: Para-Aramid Repeat Unit (e.g. Kevlar, Twaron, Technora) [40]

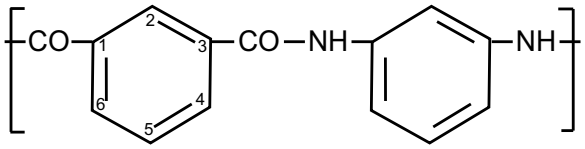

Figure 2.2: Meta-aramid Repeat Unit (e.g. Nomex)

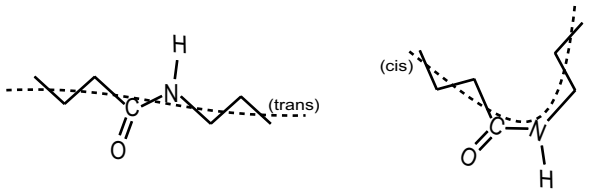

Figure 2.3: Trans- vs. Cis- Configuration of Amid-Carbonyl Connection

directly across from each other, i.e. at positions 1 and 4. In the second case, carbonyl-amid connections attach to meta-phenylene groups at the 1 and 3 positions. Both aramid forms are very resistant to high temperatures and chemical attack. Para-aramids form almost perfect lines, whereas meta-aramids do not. Therefore, para-aramids can pack polymer chains more closely. The result is a stiffer fiber [47].

The aromatic rings distinguish aramids from non-aromatic polyamides that form fibers like Nylon 6,6. In the case of Nylon 6,6, the connection between the amid and the carbonyl groups is found in both, the trans- and cis-configurations as illustrated in Fig. 2.3. The trans-configuration enables polymer chains to line up in an almost linear fashion, whereas the cis-configuration causes the fiber path to change direction. A valid and often used analogy is comparing cooked with uncooked spaghetti [47]. The relatively large phenylene rings in aramid polymers cause the bonds between the amide and the carbonyl units to be highly resistant to rotation. As a result, the amide-carbonyl connection is formed almost exclusively in the trans-configuration, which allows for perfectly straight polymer chains [23].

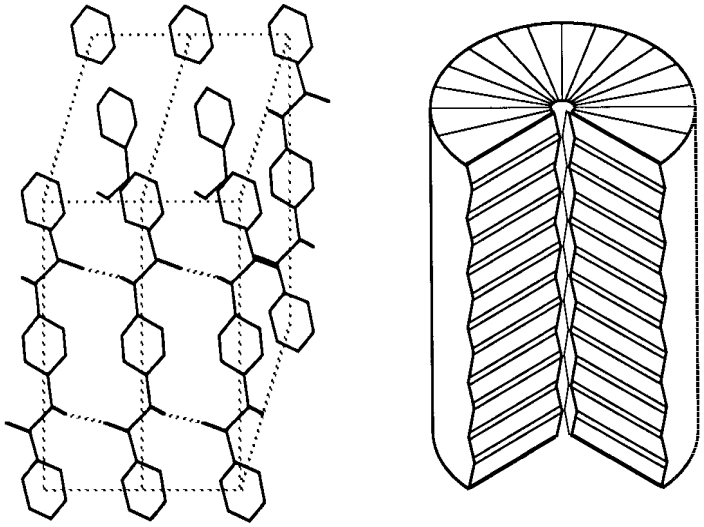

Figure 2.4: Aramid Unit Cell and Crystallite [24]

The chains align parallel to each other and connect via hydrogen bonds to form planar sheets. The sheets can stack, held together by Van der Waals forces and build crystallites of considerable size. Figure 2.4 illustrates such a crystallite and a typical unit cell of which it is composed [24]. According to Northolt [63] the size of such crystallites is of the order of 5×25 nm. The production of aramid fibers begins with such crystallites dissolved in highly concentrated sulfuric acid solution, referred to as a liquid crystalline state. When applying X-ray diffraction techniques, such solutions behave exactly like single crystal powder samples. They contain single crystals, crystallites in this case, but with perfectly random orientation.

These crystallites orientate along the direction of shear during flow. In an industrial spinning process, the polymer solution, also referred to as dope, is extruded through fine holes. During that operation the crystallites undergo significant reorientation [30, 86]. Under controlled temperature and pressure the surfaces of the crystallites are activated. They connect and form long fibrils that finally build

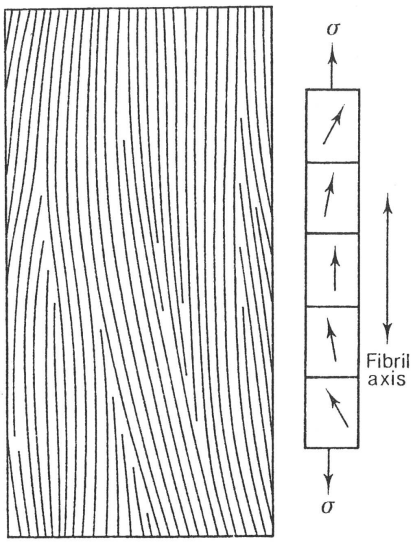

Figure 2.5: The Single Phase Structural Model for a Polymer Fiber. [13]

actual continuous fibers with diameters of the order of 10 μm, Fig. 2.5.

The fibrils and the crystallite domains they are made of do not orientate perfectly parallel along the fiber axis. Instead, an orientation distribution is observed, usually described statistically using the Weibull distribution, with angles between domain and fiber axis less than 20° for low-modulus aramid fibers and not exceeding 10° for high-modulus aramid fibers [66].

Compared to the covalent bonds along the molecule chains, the bonding between the fibrils is not very strong. Also voids and other imperfections can not be avoided. This is the reason for the fibrillar nature of aramid fibers. They can wear off on the outside or split. At the same time this also explains their toughness and the fact that they do not fail in as brittle a manner as glass or carbon fibers do [70].

DuPont developed the most popular of these fibers in 1966 under the trade names Kevlar 29 and Kevlar 49. Briefly afterwards, the AKZO Group developed

para-aramid fibers in Europe under the trade name Twaron. In early 2001, however, the multi-national Teijin Corporation, which before had been the producer of the third traditional para-aramid fiber, called Technora, acquired Twaron Products and since then is the producer of both, Twaron and Technora fibers.

In this study, Twaron fibers are used exclusively.

2.2 Deformation Mechanisms of Aramid Fibers - Review

The viscoelastic properties of polymer fibers are not at all comparable with the behavior of classic reinforcing materials, like for instance steel. The behavior of aramid fibers over short or long time spans, subjected to various environments, is largely influenced by their chemical composition well below the 10 μm level, which would be the diameter of a single fiber. Most of the work on aramid fiber behavior was done long before the material attracted the attention of civil engineers. This time lag, combined with the fact, that such work was mostly carried out by chemists and crystallographers, specialized in polymer science, trying to understand single fibers, makes it difficult to communicate their findings and models to the engineering community, which is interested in resisting forces that are usually about 6 orders of magnitude larger than those that will break a single fiber.

In the following sections an overview is given of the time-dependent mechanical properties of aramid fibers. For completeness, four such viscoelastic properties should be considered: tension and compression, both parallel and perpendicular to the fiber axis. Because of only limited interest not much is known about the properties perpendicular to the fiber axis, which becomes an issue in applications that utilize woven fabrics. The fibrillar nature of aramid fibers suggests rather poor performance

in both, tension and compression, perpendicular to the fiber axis. Of course, fibers are meant to be loaded exclusively uniaxially, i.e. in the fiber direction. When fibers are used in composites, their tensile and compressive properties need to be known. In this study, however, aramid fibers are used to prestress Portland cement-based thin glass concrete sheets. It is therefore logical to pay attention primarily to their tensile properties and to give only a brief summary of the work that has been carried out on their compressive properties.

a) Tensile Deformation Mechanisms

The initial crystallite orientation distribution is responsible for the fiber's initial uniaxial stiffness. As the fiber is stretched, e.g. in a strain-controlled experiment, two mechanisms simultaneously determine the fiber's stress level and tangential stiffness.

For one, obviously, the crystallites stretch on the molecular chain level. The stiffness of the polymeric chain structure corresponds to the stiffness of the carbonyl and the amid bonds, as well as to the stiffness of the phenylene rings. In one molecular chain these three components act in series. On a small scale, little stiffness is provided by secondary bonds, such as hydrogen bonds between single polymer chains and Van der Waals forces between their planar arrangements. Over long distances, however, stresses are transferred between fibrils ultimately by secondary bonds. As long as there is no shear slip, all of the above processes are reversible and can be experimentally observed using Laser Raman Spectography. The technique is based on the scattering of light beams as they pass through a material, in this case aramid fibers. It utilizes an intense response at a wavelength of 1615 cm^{-1}, which corresponds primarily to in-plane benzene ring stretching vibrations. Being so char-

acteristic makes it ideal for monitoring deformation effects in the polymer backbone [88, 89, 95].

The second, much more important mechanism is the rearrangement of the crystallites towards the fiber axis, well described in [65] and known as yielding of polymers. The highly ordered crystallites, which are not parallel to the fiber axis, according to some initial orientation distribution, start to rotate under load towards the fiber axis. This rearrangement process is rotational shear slip between crystallites and not reversible. This process is thus somewhat comparable to yielding due to crystal slip in metals. It can be experimentally detected by X-ray diffraction, since it produces a more ordered crystallite network, which ultimately produces a sharper peak in the orientation distribution. It requires a certain level of strain to start such a reorientation process. Especially lower-modulus fibers, for which this mechanism is more pronounced, exhibit a yield point in the stress-strain diagram at strain levels between 0.5% and 1%.

Once those two basic processes are understood, the basic stress-strain behavior of aramid fibers in a uniaxial tension test can be modeled, as well as phenomena observed in cyclic loading experiments and long-term deformations due to creep or relaxation [13, 11, 12].

b) Aramid Fibers under Compression

Laser Raman Spectography has been used by different researchers to study the mechanical performance of aramid fibers in compression [6, 88, 89]. The assumption that the moduli in compression and tension are equal was found to be inappropriate. Values for low-, high- and very high-modulus Kevlar fibers are summarized in Table 2.1. In all cases the compressive modulus is lower than the tensile modulus. The

difference is not significant for the low-, but considerable for the high-modulus fibers. The more narrow the orientation distribution, i.e. the higher the fiber modulus, the more similar the behavior of a network of fibrils is to a set of independent slender columns. Low-modulus fibers are interconnected, which increases shear resistance and can be understood as a form of lateral bracing. This explains why the ultimate compressive strength decreases with increasing modulus.

Table 2.1: Uniaxial Stiffness of Different Kevlar Types [88]

Kevlar Type	$\mathbf{E}_t$**(GPa)**	$\mathbf{E}_c$**(GPa)**	$\mathbf{E}_c/\mathbf{E}_t$
Kevlar 29	80	76	0.95
Kevlar 49	130	85	0.65
Kevlar 149	160	115	0.72

The experimental determination of compressive properties of fibers of 10-12μ diameter is not trivial. In the composites industry, however, knowledge of the mechanical behavior of reinforcing fibers under compression is crucial. In the past, a number of test setups were developed, and a controversial discussion took place on how to interpret certain experimental results and, ultimately, which test method was most reliable. A detailed account of the various available test methods is given in [45]. The most popular method appears to be the so-called bending beam setup, where a single fiber is attached to the compressed face of a thin metallic beam, which is then subjected to bending.

When an aramid fiber is subjected to uniaxial compression it deforms in a linear elastic manner up to a strain of ≈0.5%, at which yielding can be observed. Fiber micro-buckling as visualized in Fig. 2.6 leads to the development of pronounced macroscopic kink bands, Fig. 2.7. The fiber fails at an ultimate compressive strain of ≈1.5%. A detailed theoretical approach and general discussion of kink bands are

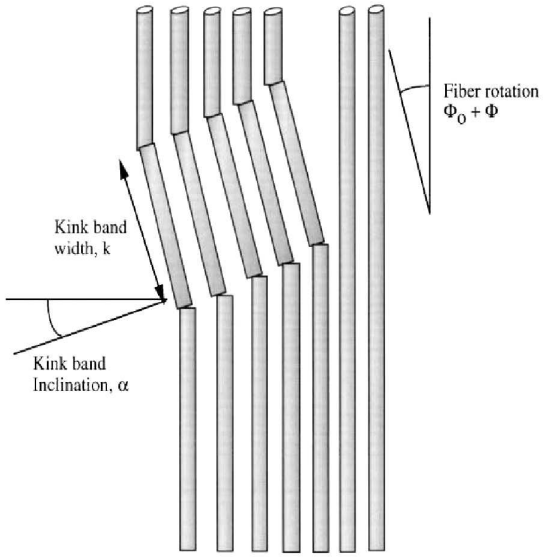

Figure 2.6: Scheme of Kink Band Development [31]

given in [31].

2.3 Mechanics of Aramid Rovings

Most of the researchers who studied deformation mechanisms of aramid fibers, used single fibers. In the context of the present work, however, rovings consisting of many thousand fibers were used. Just as the strength of a fiber is controlled by the weakest link among its fibrils [4], so is the strength of a roving determined by the weakest of its fibers. In both cases, statistical parameters can be used to model the respective relationships. Not all fibers will start to take load at the very beginning of a tension experiment and, ultimately, one fiber will fail first. The result is that in a 2,200 denier (244 tex)[1] roving, for example, many of the approximately 2,000 fibers will

[1]In the fiber industry, it is common to specify fibers in units of tex or denier, which indicate the weight of a 1000 m or 9000 m long single fiber, respectively, i.e. denier = 9 × tex.

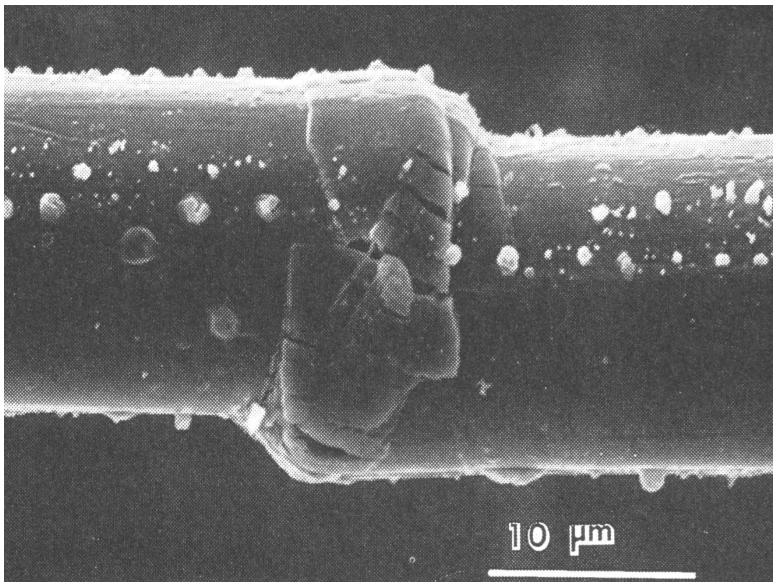

Figure 2.7: SEM Image of Kink Band [45]

reach only 70% of the theoretical strength of an absolutely perfect fiber bundle, with all fibers having the same diameter, length and imperfections [5].

A nontrivial problem in fiber testing is how to pull a fiber without premature failure at the anchorages, due to strain discontinuities that may cause stress concentrations. Single fibers are usually fixed on paper, which is cut directly before the test and strengthened on the ends by epoxy glue. Gauge lengths range from 2 in (5cm) to 20 in (50cm). It is well known, that the longer the fiber, the more likely is a failure away from the ends. The strengthened fiber ends are usually held by mechanical clamps. Load cells must be extremely sensitive, since failure loads are usually below 0.1 lbs (50g). Strain is preferably measured optically. Similar approaches can be used to test rovings, i.e. with ≈2,000 single fibers. In connection with an investigation of coated fabrics[84], special aluminum clamps were developed in the Carleton Laboratory in the 1980's that have proven to be suitable for clamping rovings without the

necessity of strengthening their ends with epoxy glue.

a) Tensile Loading to Failure

Single 1,100 (Low Modulus) and 2,200 (High Modulus) denier rovings (122tex and 244tex, respectively), tested in the present investigations, failed at tensile loads of about 40 lbs (180N) and 100 lbs (450N), respectively, stretched to ultimate strains between 2% and 2.5%, Fig. 2.8. Assuming such single rovings contain 1,000 and 2,000 circular fibers of 10 μm diameter each, the failure loads of 40 lbs (180N) and 100 lbs (450N) correspond to ultimate stresses of 334 ksi (2.30GPa) and 421 ksi (2.90GPa), respectively. The moduli of the fibers are therefore 17×10^6 psi (115GPa) and 21×10^6 psi (145GPa). These values are slightly higher than those measured on single low-modulus and high-modulus Twaron fibers, 13×10^6 psi (90GPa) and 17×10^6 psi (120GPa), respectively [65].

The stress-strain curve of the low-modulus roving shows clearly the yield point early in the loading process and non-linearity due to reordering of crystallites up to failure. As described in the literature, the high-modulus fiber shows almost no non-linearities and a yield point is not easily noticeable [10]. No dependency of stress-strain data on the loading rate was found for the high-modulus fiber.

b) Cyclic Loading

Response of single aramid fibers to cyclic loading is described in the literature [2, 64]. Two experiments carried out in the Carleton Laboratory using 2,200 denier (244tex) single high-modulus aramid rovings show the typical behavior particularly well.

Fig. 2.9 presents the results of an experiment where a 2,200 denier (244tex) Twaron roving was loaded twice to 50lbs (222N) and unloaded, each time keeping

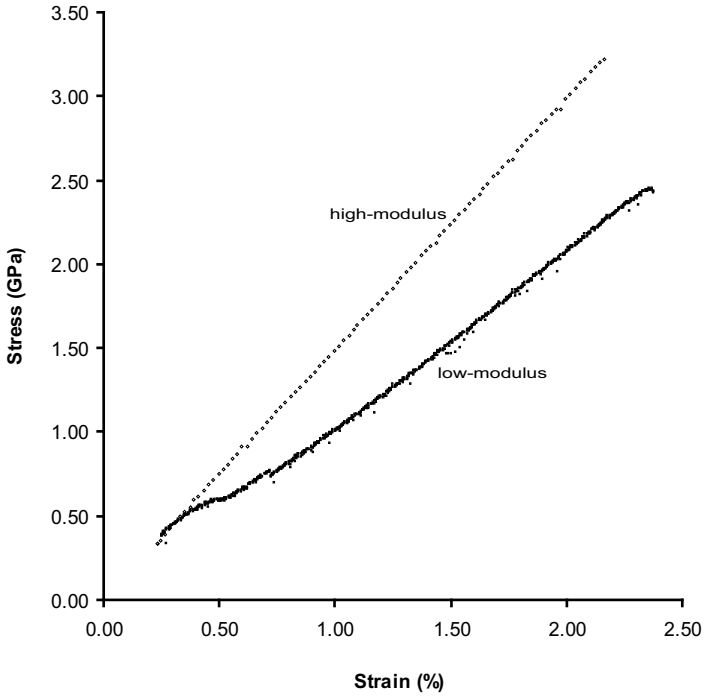

Figure 2.8: 1,100 Denier (122tex) Low-Modulus and 2,200 (244tex) Denier High-Modulus Single Roving Stress-Strain Diagram

the strain constant for 1 min after reaching the target load before unloading. Then the roving was loaded twice up to 60 lbs (267N), held again at constant strain for 1 min before unloading both times and so forth, until failure. It can be seen how the permanent set increases at each load increase, due to change of the orientation distribution within single fibers. In other words, the loading curve consistently shifts towards the right on the load vs. strain diagram. As predicted by the deformation mechanisms, the first loading shows the lowest stiffness, whereas with each consecutive loading to a higher strain level the slope of the stress-strain curve increases. The same holds for the permanent set. The first loading causes a large permanent set, whereas each subsequent load increases the set in an almost linear fashion. Both, stiffness and permanent set, are summarized in Fig. 2.10. It may be pointed out, that an extrapolation of the first loading curve connects the peaks of the subsequent load cycles, i.e. all of them form approximately a straight line.

The results of a similar experiment, following an exactly reversed loading sequence, i.e. decreasing the load levels after loading the roving twice, are shown in Fig. 2.11. Almost all permanent deformation is achieved in the first loading cycle up to the highest load, Fig. 2.12. During subsequent load cycles to lower load levels almost no new permanent set is introduced. At the same time the stiffness observed during the initial loading is, again, lower than that observed throughout all subsequent loading cycles, during which it appears to remain almost constant. This observation is very important in regards to preconditioning fibers for long-term loading, i.e. in prestressed thin sheets.

c) Viscoelastic Properties

Creep and relaxation have been studied on single fibers [27, 90, 93] and on

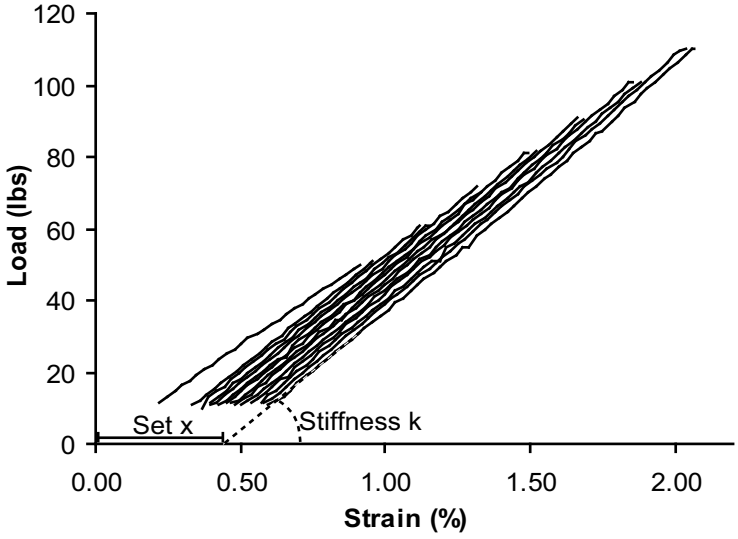

Figure 2.9: Repeated Loading of a Single Roving (Load Increasing). Unloading Branches are not Shown.

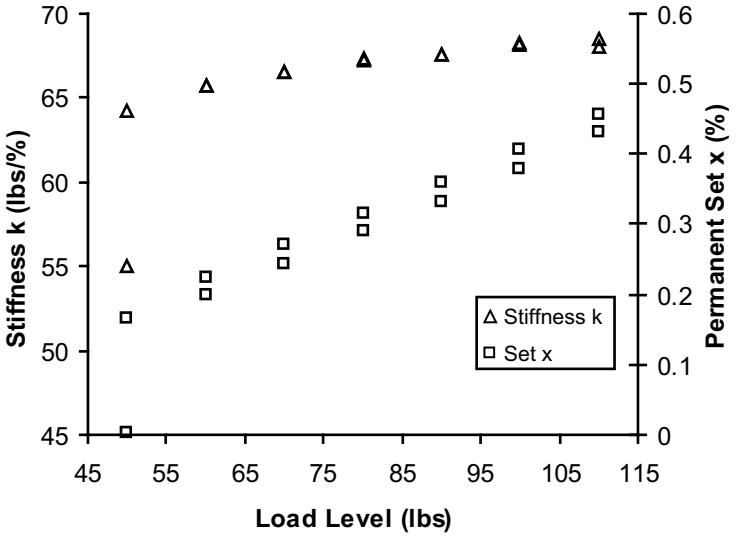

Figure 2.10: Stiffness and Permanent Set as Functions of Increasing Load Levels (Single Roving).

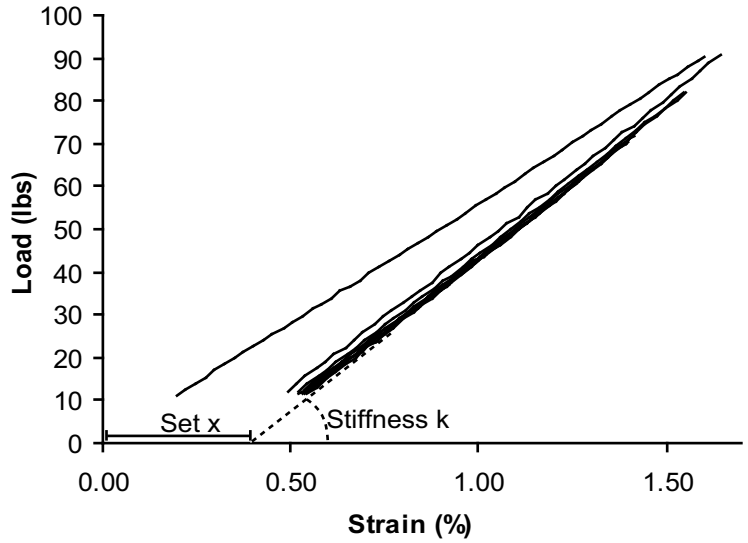

Figure 2.11: Repeated Loading of a Single Roving (Load Decreasing)

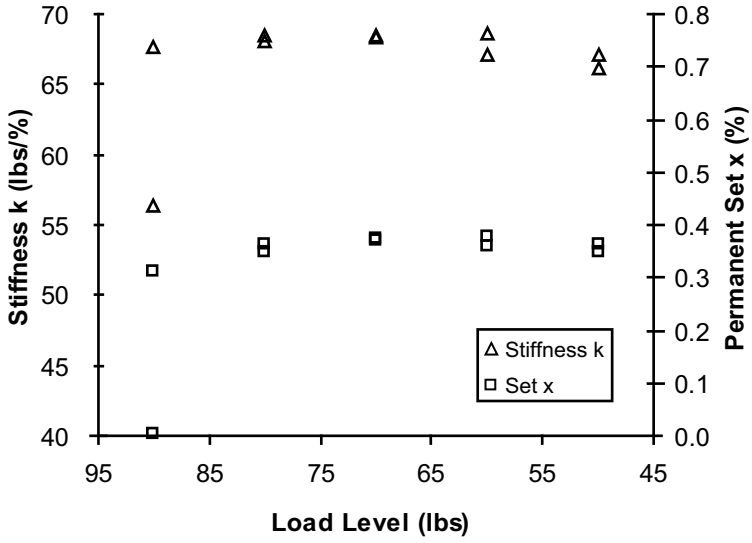

Figure 2.12: Stiffness and Permanent Set as Functions of Decreasing Load Levels (Single Roving).

fiber bundles [18, 35]. The higher the fiber modulus, the lower the creep rate. Three different stages can be observed in a creep experiment: primary, secondary and tertiary creep. Whereas secondary creep is reversible by means of recovering of creep losses, the often large primary creep strains can not be recovered. The secondary creep is low and easily fit by exponential or logarithmic functions. During the third creep stage the rate of creep increases until failure occurs.

The mechanisms that control the large primary creep are the same ones that are explained in the previous chapter: the crystallites rotate towards the fiber axis and the orientation distribution changes towards a more perfectly orientated fiber. Such reorientation can be carried out deliberately up front by prestretching the fibers. The possibility of preconditioning fibers to almost eliminate primary creep was only pointed out in the literature dealing with single fibers. Most importantly, the fibers should be stretched well beyond the maximum life strain before they are placed in a creep or relaxation environment.

Among many relaxation experiments carried out during this investigation, one illustrates the effect of different preconditioning levels very well. 2,200 denier (244tex) Twaron rovings were subjected to constant strain of about 60% of their failure strain for 4 hours. However, immediately before the 4-hour relaxation experiment they were stretched to different higher strain levels for a 1 min period.

Fig. 2.13 illustrates one such experiment, carried out on an Instron Universal Testing Machine, which is controlled by mechanically moving the crosshead up or down. The loading path was as follows: The roving was loaded to 70 lbs (311N) and the corresponding strain was held constant for 1 min. In this one minute the load decreased from 70 lbs (311N) to 67 lbs (298N). The load was then lowered to 60 lbs

(267N) and the strain again held constant, this time for 4 hours, during which the load decreased from 60 lbs (267N) to 56 lbs (249N). The roving was then unloaded to 10 lbs (44N) and immediately reloaded to failure, which occurred at 120 lbs (534N). Again, the load-strain diagram verifies the deformation mechanisms. The stiffness of the roving during the second loading is clearly greater than during the initial loading. Yet, after reaching the preconditioning load level of 70 lbs (311N), the slope decreases towards a value similar to the one observed during initial loading. Fig. 2.14 shows a typical load vs. time response for the 4-hour relaxation part of the experiment. The time history curve can be conveniently fitted using an exponential function, which in this particular case yields a relaxation coefficient of -0.014. Fig. 2.15 summarizes the results of similar experiments, but for preconditioning of the rovings at levels of 0, 10, ..., 40 lbs (0, 44, ..., 178N) above the target load of 60 lbs (267N). As expected, the higher the level of prestretching, the lower the relaxation rate. Not only that, but the relaxation coefficient appears to be linearly dependent on the level of preconditioning. Charts for low-modulus aramid fibers and for different target loads could be constructed following the scheme described above. However, for the purpose of this study, the representative results presented here shall suffice to illustrate the time- and strain-dependent behavior of aramid fibers.

2.4 Aramid Fibers in Alkaline Environments

Like all aramid fibers, Twaron fibers have basically good chemical resistance, except in environments with extreme pH values. Because of this, fibers are often provided with protective coatings such as PVC, polyester or epoxy. Still, concerns do exist that the alkalinity of the pore solution in Portland cement paste can cause deterioration.

When unstressed fibers were stored in concentrated NaOH solution for 24

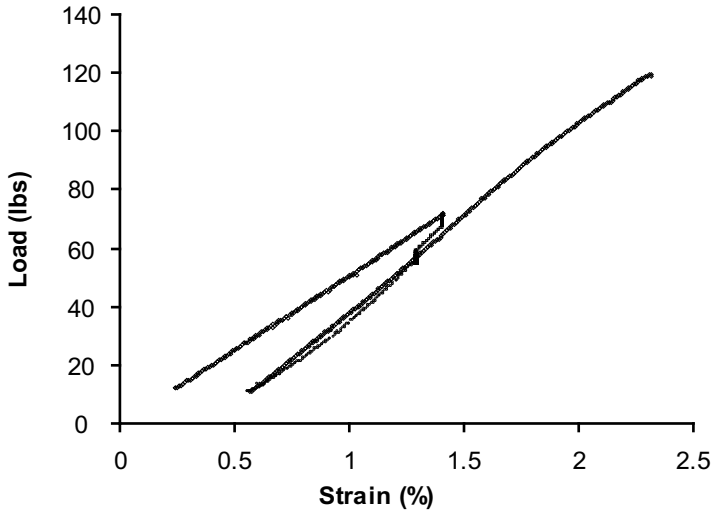

Figure 2.13: Typical Loading Path (10 lbs (44N) Overstretch)

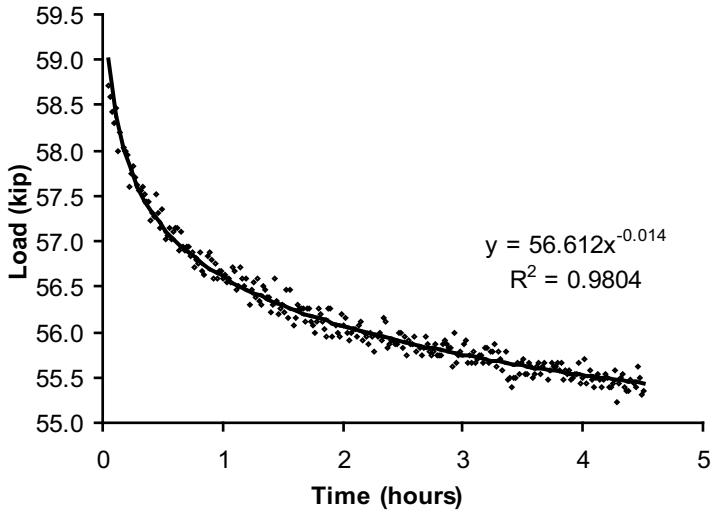

Figure 2.14: Typical Relaxation Time History (10 lbs (44N) Overstretch)

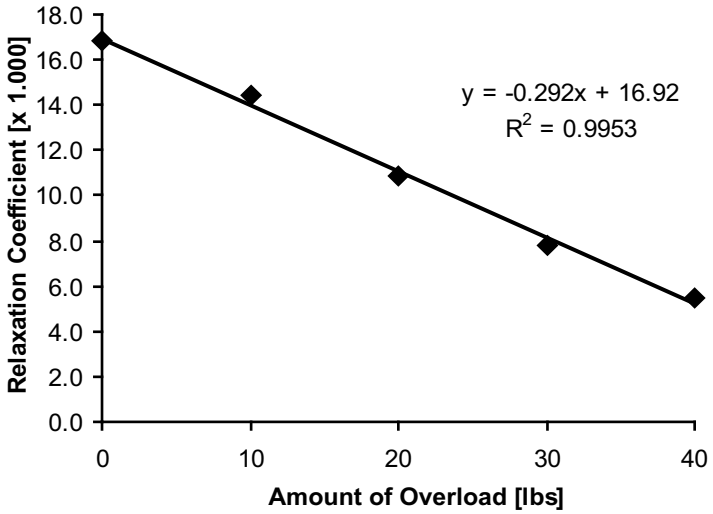

Figure 2.15: Relaxation Coefficients vs. Amount of Preconditioning

hours, no loss of stiffness nor ultimate strength was found afterwards. Originally, this outcome was attributed to the protective coating of the fibers. If the fiber is stretched, however, coating and fiber deformations are not necessarily compatible. As the fiber stretches, the coating may crack, which introduces areas, where an alkaline solution can attack the aramid fiber surface. A simple relaxation experiment was carried out to explore the impact of concentrated NaOH solution on the stress level of an aramid roving. A 6-hour load-time history is plotted in Fig. 2.16. Note the high primary relaxation rate, caused by the fact, that the fiber was not preconditioned. After 1.5 hours, a straw, that was aligned around the fiber and sealed at the bottom, was filled with concentrated NaOH solution. The fiber stress level decreased immediately by a small amount, but the effect decayed in time. Loading the fiber after the relaxation experiment, however, did not show a strength drop, Fig. 2.17. Also, the typical increase of fiber stiffness, due to preconditioning, which occurred during the initial loading to the relaxation target load, was observed.

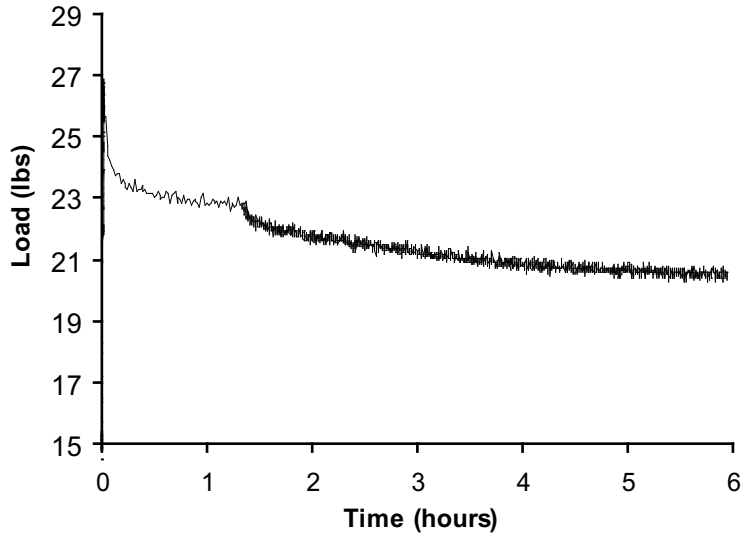

Figure 2.16: Relaxation Experiment with the Introduction of NaOH after 1.5 Hours

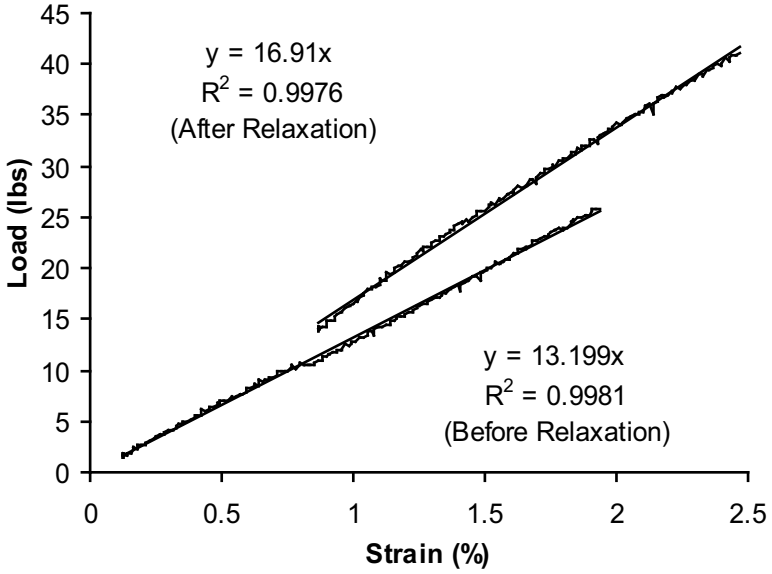

Figure 2.17: Initial Loading of the Roving Before Relaxation Experiment with NaOH Impact and Final Loading to Failure.

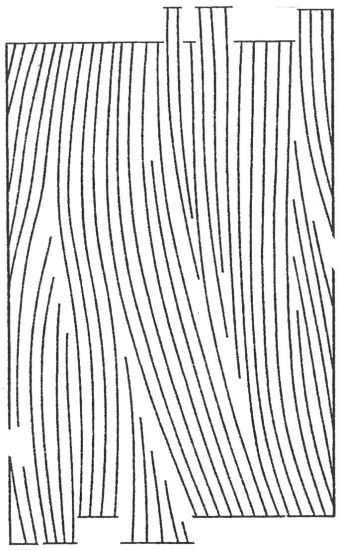

Figure 2.18: Suggested Yielding Mechanism During Impact of Alkaline Solution. Based on the Single-Phase Structural Model for Polymer Fibers. [13]

The observations suggest that no cross-sectional area is lost due to deterioration caused by the alkaline solution. Instead, the alkaline solution can be interpreted as a catalyst for fiber reorientation. The secondary bonds between fibrils within single aramid fibers are weakened and therefore rotation of crystallites towards the fiber axis is made easier. The failure of the roving itself is much more fibrillar, which supports this argument. At the same time it is unknown to what extent the whole fibril network is irreversibly torn apart, as suggested in Fig. 2.18. Clearly, the NaOH solution was not strong enough to break polymer chains.

The main concern, however, about the above experiment is, that the impact of a more realistic pore solution is expected to be quite different. Almost liquid fresh mortar turns into gel and hardens within a few hours. The effect that causes a loss of prestress may decay faster than it does with liquid NaOH solution. The interaction between prestressed aramid fibers and a Portland cement-based matrix will therefore

be revisited in a later chapter, after the glass concrete matrix has been described in sufficient detail.

Chapter 3

Glass Concrete

3.1 Hydration of Regular Portland Cement - Review

The hydration process of regular Portland cement is well understood and described in great detail in textbooks on concrete materials [62, 51, 83]. The main components of regular Portland cement are tricalcium silicate (C_3S, also *"alite"*), dicalcium silicate (C_2S, also *"belite"*), tricalcium aluminate (C_3A) and calcium ferroaluminate (C_4AF) [1]. Different types of Portland cement are standardized in ASTM C-150 as listed in Table 3.1, while Table 3.2 summarizes the main hydration reactions of the cement components.

Table 3.1: Compositions of Portland Cement Types in the US [56]

	Mineral Component [%]				
Cement Type	**C_3S**	**C_2S**	**C_3A**	**C_4AF**	**$C\overline{S}H_2$**
I	55	18	10	8	6
II	55	19	6	11	5
III	55	17	10	8	6
IV	42	32	4	15	4
V	55	22	4	12	4

The hydration of regular cement can be summarized as follows. Upon the addition of water the aluminates, especially C_3A, quickly engage in reaction and

[1] Shorthand in concrete chemistry: C=CaO, S=SiO_2, A=Al_2O_3, F=Fe_2O_3, $\overline{S}$=SO_3, $\overline{C}$=CO_2, H=H_2O. For example, C_3A = $3CaO{\cdot}Al_2O_3$

harden, while generating large amounts of heat of hydration. Portland cements contain small amounts of gypsum ($3C\overline{S}H_2$) to retard this process. The addition of gypsum largely increases the time available for the placement of fresh concrete before setting and helps to synchronize the rapid reaction of the aluminates with the much slower hydration of the silicates. The aluminates form mainly calciumaluminate-(C_4AH_{13})and calciumferrit-hydrates (C_4FH_{13}) and, in connection with gypsum, ettringite ($C_6AS_3H_{32}$) and monosulfate ($C_4A\overline{S}H_{18}$). Ettringite can also be transformed into monosulfate, at a later point in the hydration process. The silicates form the main constituents of a hardened cement matrix, which are Portlandite (CH) and calcium silicate hydrates (C-S-H). Unlike the other hydration products, Portlandite forms large chemically active crystals and is considered responsible for poor durability, creep and strength characteristics of concrete. At the same time Portlandite guarantees for high alkalinity of the pore solution, which protects reinforcing steel from corrosion.

Table 3.2: Portland Cement Hydration Reactions [83]

	Aluminate Reactions
1.	$C_3A + 3C\overline{S}H_2 + 26H \rightarrow C_6A\overline{S}_3H_{32}(ettringite)$
2.	$C_3A + C\overline{S}H_2 + 16H \rightarrow C_4A\overline{S}H_{18}(monosulfate)$
3.	$C_6A\overline{S}_3H_{32}(ettringite) + 2C_3A \rightarrow C_4A\overline{S}H_{18}(monosulfate)$
4.	$C_4AF + 4CH + 22H \rightarrow C_4AH_{13} + C_4FH_{13}$
	Silicate Reactions
5.	$2C_3S + 6H \rightarrow C_3S_2H_3$(C-S-H) $+ 3CH(Portlandite)$
6.	$2C_2S + 4H \rightarrow C_3S_2H_3$(C-S-H) $+ CH(Portlandite)$

3.2 Optimizing Concrete Mixes - Review

Engineering high-quality concrete matrices is a complex task. Basic mixture proportions can be modified and admixtures added to modify specific hydration parameters

and properties of the hardened concrete matrix. A frequent goal is to produce a dense matrix and eliminate as much pore volume as possible.

The particle size distributions of cement, sand and coarse aggregate can be optimized by means of simple geometry to achieve maximum compactness even before water is introduced to start the hydration process. In addition, a large variety of mineral fillers is available to occupy the remaining voids between particles. Inert fillers, such as ground limestone or quartz, are differentiated from active fillers, which have pozzolanic properties and actively take part in the cement hydration [55].

Theoretically, a water/cement (w/c) ratio of only about 0.21 is needed to achieve complete hydration of cement. To assure adequate workability, which can be determined by slump or flow tests, higher w/c ratios are needed. In this case, not all water is used up by hydration reactions. The excess water in the hardened cement matrix may eventually evaporate, which causes shrinkage and creates pores in the concrete. High-range water reducers, also called superplasticizers, can be used to ensure good workability at lower w/c ratios, producing a denser concrete matrix. The mechanisms of how typical superplasticizers work are summarized in detail in [76].

Even if the size distributions of the constituent particles are optimized and the water content minimized, the very structure of the hydrated cement paste is still inherently heterogeneous due to the different phases, primarily C-S-H and CH [8]. Upon complete hydration, up to 28% by weight of cement can theoretically be transformed into Portlandite. Pozzolans can be utilized to partially replace cement and, by actively participating in the cement hydration, decrease or even fully transform harmful Portlandite into more durable C-S-H phases. Examples of widely

used materials with pozzolanic properties are fly ash and silica fume, both industrial by-products, and metakaolin, which is thermally activated kaoline (clay). The main advantage of fly ash is that it increases workability, slows the cement hydration and greatly reduces heat of hydration, which makes it most valuable in the production of mass concrete, such as dams and massive foundations [51]. Silica fume acts as a filler, since particles are as fine as 0.1 μm. Due to its large surface area it is highly reactive, but also greatly decreases workability. It is widely used in combination with superplasticizers to achieve high early strength. When used in conjunction with fiber reinforcement, the durability of concrete produced with silica fume has been questioned [81]. It was observed that the small-sized hydration products can grow into fiber bundles which can cause mechanical degradation of the fibers. Metakaolin is not as fine as silica fume but chemically also very reactive. It also compromises the workability of fresh concrete and therefore is normally used together with superplasticizers. It has the potential to greatly improve durability and mechanical properties of concrete systems as described in more detail in the following paragraphs.

3.3 Cement Matrices Modified with Metakaolin - Review

Metakaolin is a calcined china clay produced by the controlled thermal activation of kaolin in air at $750-800°$C. It contains $SiO_2(52\%)$, $Al_2O_3(44.6\%)$ and $Fe_2O_3(0.5\%)$. Its degree of reactivity depends on the purity of the kaolin used and on the production process. Depending on the purity of the kaolin, the end products are referred to as either metakaolin or high-reactivity metakaolin. Metakaolin is almost perfectly white, with a Hunter L whiteness value greater than 90, on a scale from 0 (black) to 100 (white) [34]. Its hydration products do not darken with time, which makes it valuable especially for architectural concrete applications. Its large surface area requires more

water for adequate workability, unless superplasticizers are used. The effects of replacing of cement with metakaolin on the development of concrete strength are threefold [92]:

1. There is a filler effect. Although not as fine as silica fume, the metakaolin particles are still of much greater fineness than cement particles. Typical specific surface values are $0.35m^2/g$, $12m^2/g$ and $20 - 25m^2/g$ for ordinary Portland cement, metakaolin, and silica fume, respectively.

2. Because of its high specific surface and chemical activity, metakaolin outperforms other pozzolanic materials like fly ash and silica fume in its ability to consume CH, Table 3.3. By the rapid removal of CH from the cement system, the hydration reaction is set off balance, causing the Portland cement to hydrate faster and to keep up with the production of Portlandite. This hydration acceleration effect can be demonstrated by measuring the increased 24 hour strength as well as the increased generation of heat of hydration.

3. Most of the pozzolanic reaction takes place between the 7th and 14th day. Lime is removed from the system and transformed into C-S-H and C-A-H phases with crystals that are smaller than in Portlandite. They form a denser and much more homogeneous matrix, which is chemically more stable than Portlandite. The pozzolanic reaction continues beyond the 14th day, but at a greatly reduced rate [91].

The full potential of metakaolin was discovered only recently, unlike that of fly ash and silica fume. Especially the pozzolanic reaction has received great attention lately[78]. Fundamental questions, like what replacement levels of cement by

Table 3.3: Pozzolanic Activity of Different Mineral Admixtures [78]

	Reactivity [1/1000 g CH per g pozzolan]
Silica Fume	427
Fly Ash	875
Metakaolin	1050

metakaolin cause what levels of CH removal from the concrete matrix, have only been answered a few years ago. The influence of metakaolin on the hydration of ordinary Portland cement is of great complexity, e.g. how the replacement of cement by metakaolin affects strength and alkalinity, both as functions of time. Lime content can be greatly reduced, as shown in Figure 3.1. As a result, the concentration of hydroxide ions can be decreased below 0.2M, Figure 3.2, which is considered a critical level to initiate and sustain alkali-silica reaction (ASR) [34]. Because of the improved matrix properties, metakaolin was also found to reduce creep deformations by more than 50%, compared to regular concrete, Figure 3.3. The illustration refers to concrete specimens loaded to 20% of their compressive strength after 28 days.

3.4 Glass as Aggregate in Concrete - Review

Glass has attracted researchers in the field of concrete materials for a number of decades. The use of glass chips was tried to produce architectural exposed aggregate concrete as early as 1963 [79]. In the following years other efforts were made to utilize glass as aggregate in concrete [69, 43, 49, 28, 82]. All of these early attempts confirmed that the use of waste glass as an aggregate in Portland cement-based concrete leads to unacceptable durability problems caused by ASR. Some researchers attempted to solve the problem by using fly ash and low-alkali cements, but with

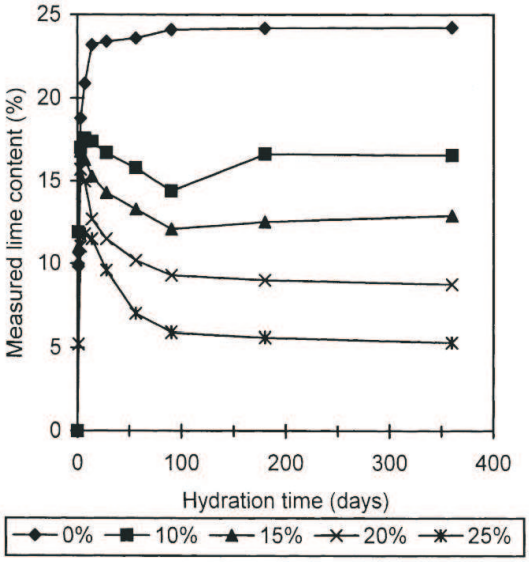

Figure 3.1: Partial Replacement of Cement with Metakaolin (0 - 25%): Lime Content vs. Hydration Time [29]

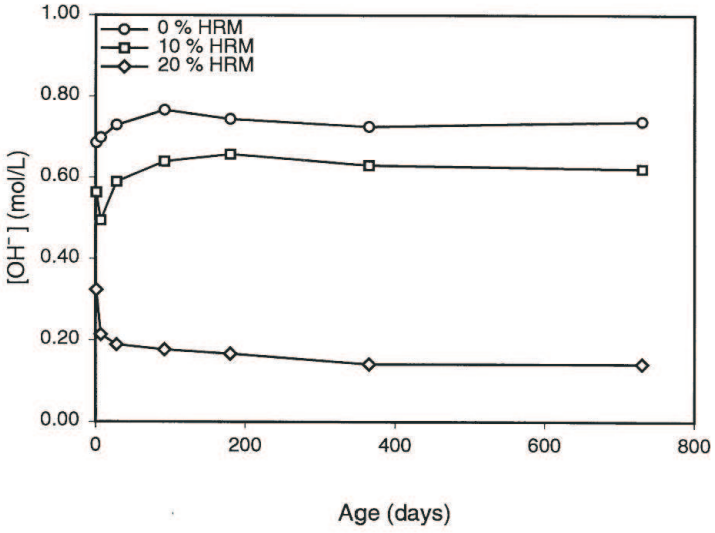

Figure 3.2: Partial Replacement of Cement with Metakaolin (0 - 20%): Hydroxyl Ion Concentration vs. Hydration Time [73]

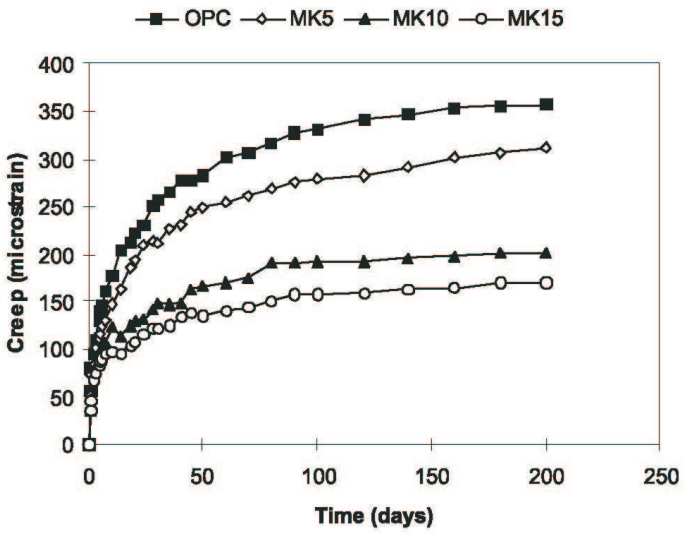

Figure 3.3: Partial Replacement of Cement with Metakaolin (0 - 15%): Creep vs. Hydration Time [15]

limited success. The characteristics of ASR involving glass aggregate appear to be different from those caused by other reactive, but porous materials. For example, an interesting pessimum effect was observed, which links the expansion due to ASR to the size of glass particles [71, 41].

Starting in the early 1990's, interest in glass as an aggregate in concrete revived, partially prompted by the growing solid waste disposal problem in most developed countries [52, 53]. In some countries, for instance Japan and China, there are large regions with limited sources of suitable natural sand and stone. This raises the cost of natural aggregate and thereby makes alternate materials economically attractive, even reactive materials like glass [82, 44].

Glass is an amorphous material which consists mainly of SiO_2. It further contains small amounts of alkalis, such as K_2O and Na_2O. Compositions for typical clear, green and amber glass are summarized in Table 3.4. Compared with quartz, which

is of similar chemical composition, but with a highly ordered crystalline structure, glass is chemically not very stable. It can be easily degraded in alkaline solutions. According to its chemical composition, it should have pozzolanic properties and react with Portlandite to form C-S-H in the course of cement hydration. This fact has been observed experimentally, but only for very small particle sizes. Glass also causes harmful ASR at a later stage in the hydration history. The pozzolanic and ASR reactions are chemically similar, except they occur at different times during the hydration process [26]. One further noteworthy point is that even if the alkali content in the hardened cement paste is lowered by the use of pozzolanic additives or other admixtures, glass can still leach out silica and alkali and therefore cause ASR.

Table 3.4: Compositions of Soda-Lime Container Glass [87]

	Clear Glass	**Amber Glass**	**Green Glass**
SiO_2	73.2 - 73.5	71.9 - 72.4	71.27
Al_2O_3	1.7 - 1.9	1.7 - 1.8	2.22
$Na_2O + K_2O$	13.6 - 14.1	13.8 - 14.4	13.06
$CaO + MgO$	10.7 - 10.8	11.6	12.17
SO_3	0.2 - 0.24	0.12 - 0.14	0.052
Fe_2O_3	0.04 - 0.05	0.30	0.599
Cr_2O_3		0.01	0.43

In a major study at Columbia University the accelerated mortar bar test method of ASTM C-1260 was used to investigate the suitability of glass as aggregate in concrete. Initially the following parameters where studied: size of glass aggregate, amount of aggregate replaced with glass, and glass color. The results can be summarized as follows [41, 42, 54]:

1. When glass is added as partial fine aggregate replacement in regular concrete, ASR starts almost immediately after the begin of cement hydration. The more

regular aggregate is replaced with glass particles, the larger the observed expansions. A pronounced pessimum size with the largest expansions was identified.

2. If glass is ground finely enough, i.e. finer than the openings of a standard sieve size #400 ($\approx 38\mu m$), it has pozzolanic properties and actively participates in the concrete hydration. This important observation was also made by other researchers [80, 26, 38].

3. Unlike clear or brown glass, green glass showed no sign of causing ASR, which has been explained by the chromium oxide added during the production of green glass. The fact that clear glass is more reactive than colored glass was confirmed in [26].

4. Besides chromium oxide, present in green glass, lithium was found to be an effective inhibitor of ASR [14], suggesting the development of either ASR-resistant cement or glass.

The preceding observations suggest several possibilities for using glass in concrete. Grinding the glass very fine is certainly possible, but such glass powder has to be considered as an active filler, rather than aggregate. The amounts of glass that could be utilized in this way would be considerably smaller than if the glass were used as regular size aggregate. Architectural concrete does not benefit from finely ground glass at all, since it would not be visible.

To prevent damaging ASR in concrete containing glass aggregate, a number of mineral and chemical admixtures are available, some of which are proprietary. They have been proven to be sufficiently effective so that glass concrete has been applied in engineering practice. For instance, the tower which held the Olympic flame of the

Figure 3.4: Architectural Glass Concrete: Olympic Flame in Lillehammer '94 [7], Park Bench Assembly [39], Bird Bath [21]

Winter Olympic Games of Lillehammer in 1994 was made of Portland cement-based glass concrete and appears to be in good shape today [7], Fig. 3.4).

At Columbia University, a combination of metakaolin and a proprietary admixture has been used successfully. This forms the basis for terrazzo glass concrete tiles and paving stones that are now being produced commercially. Although full-scale commercial production in the greater New York area requires the solution of political and commercial problems, which are beyond the scope of this work, the potential exists that all waste glass recycled in New York City can be utilized by a single paving stone manufacturer.

The challenge faced today is no longer how to use glass as an aggregate in high-performance concrete, but how to provide reliable sources of glass of high quality and sufficient quantity at a reasonably constant price. The latter aspects are solely of commercial nature. For high-quality applications the glass must be washed and graded for size, and architectural applications may call for color-sorted glass.

3.5 Glass Concrete Matrix for Prestressed Thin Sheets

A number of criteria need to be considered when designing a glass concrete formula suitable for prestressed thin sheets: optimum grading of glass aggregate, high early strength, upper limit for aggregate size, workability, excellent spread, and low creep.

The smallest clear spacing between rovings of fibermesh determines the largest aggregate size that may be used. Several mesh layers separated by as little as 0.06 in (1.5mm) are needed to achieve the desired level of prestress. This limits the largest aggregate size for the presented study to particles passing a standard sieve #16 ($\approx$ 1.2 mm). According to standard terminology, a cement composite with such small aggregate should be referred to as "mortar". However, concrete with glass aggregate has become known as "Glass Concrete", and it shall be referred to as such in this work.

As a first step of the iterative process to develop a suitable glass concrete mix design, a simple experiment was carried out to determine an optimum grading of glass aggregate sizes. A glass container was filled with 50 grams of the largest aggregate fraction, i.e. #16, and the required volume recorded. Then glass of size #30 was added in increments of 5 grams. For each increment, the volume was measured and the density computed. Upon reaching a maximum density, the ratio of #16 to #30 aggregate was fixed. Next, glass of size #50 was added to 50 grams of the optimized mix containing glass of sizes #16 and #30 in a similar manner, until the the optimum mix ratio of glass fractions #16 : 30 : 50 was found. The end results are summarized in Table 3.5. 5% of the size #100 fraction was added, because glass powder of such size is partly reactive and also a good filler.

Because of the small spacings of the fiber mesh that need to be filled with

Table 3.5: Optimized Glass Aggregate Grading (% by weight)

Sieve Size	**#16**	**#30**	**#50**	**#100**
Fraction	49	24	22	5

material, an exceptionally high flow of more than 5 in (130mm) had to be achieved to guarantee good workability, even if the matrix is compacted by vibration. This requirement is coupled with the need for high early strength, so that the prestress may be applied after only 20 hours. To address this coupled problem, three weight ratios were varied: superplasticizer-, aggregate-, and water-to-binder[2], s/b, a/b, and w/b, respectively. In the particular case of glass concrete, s/b = 0.0125 was found to be optimal. In industrial production of fiber-reinforced cement thin sheets, a/b ratios as low as 1/1 are used. In an iterative process, an a/b ratio of 1.72 was found to produce good workability at a w/b ratio of 0.38 and at the same time achieve a targeted compressive strength of 5 ksi (35 MPa) after 24 hours. The mix design is summarized in Table 3.6.

Table 3.6: Glass Concrete Mix Design

Component	**Weight Ratio**
Glass Aggregate	1.72
Type III Cement	0.80
Metakaolin	0.20
Water	0.38
Superplasticizer	0.0125

The key performance characteristics are summarized in Table 3.7 and illus-

[2]Since it has become common to replace parts of the cement with other pozzolanic materials, the sum of all cementitious materials is referred to as binders. The ratios w/c, a/c, s/c, etc. are therefore replaced by w/b, a/b, s/b, etc.

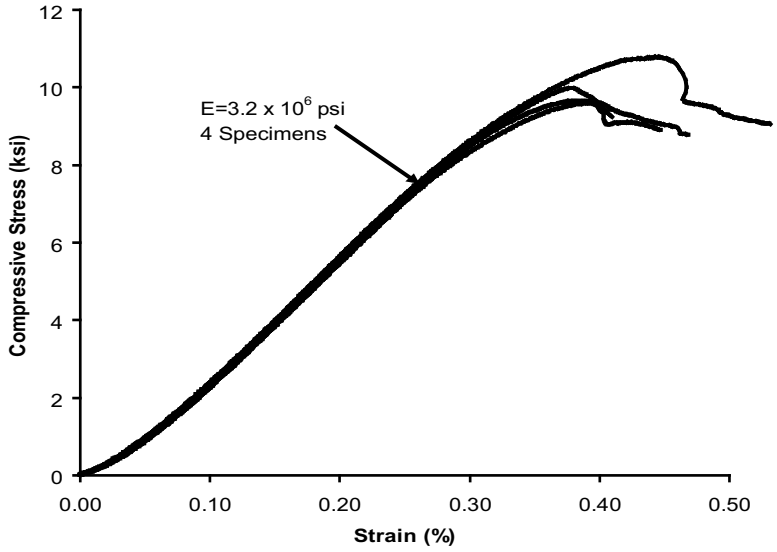

Figure 3.5: Stress-Strain Behavior of Glass Concrete at age 7 days (2×2 in Cylinders)

trated in Fig. 3.5 (stress-strain behavior after 7 days), Fig. 3.6 (3-Point bending[3] test after 7 days), Fig. 3.7 (shrinkage of glass concrete mortar bars) and Fig. 3.8 (ASTM-C277 Test for ASR). No creep properties were obtained experimentally. As illustrated in Fig. 3.3, metakaolin-modified concrete matrixes clearly outperform regular concrete mix designs in their creep behavior. Still, since creep data is of great importance for the modelling of prestressed concrete, tests need to be performed in the future to study the creep behavior of prestressed glass concrete beams using a test setup described in the next chapter.

[3] *"Strain"* in bending tests refers to the displacement measured with a clip gage on the tension side of the specimen, as discussed in Chapter 4.6.

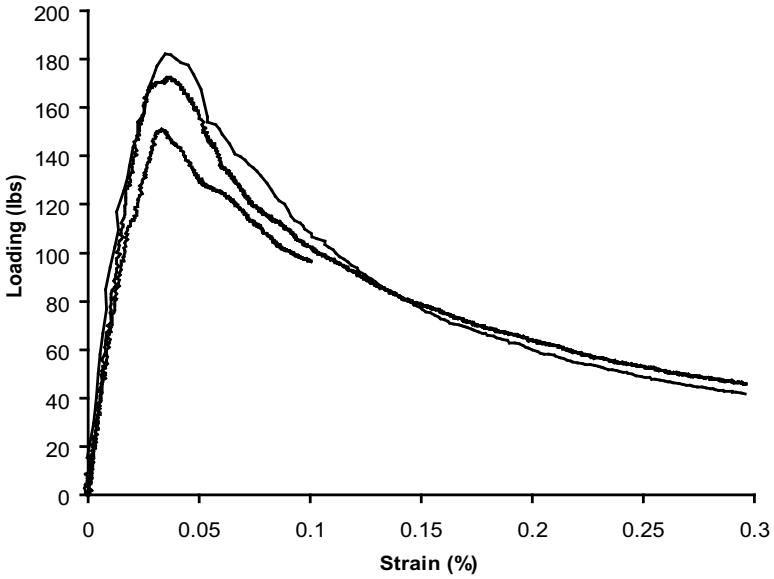

Figure 3.6: 3-Point Bending of Glass Concrete at age 7 Days ($1\times1\times6$ in^3 Beam Specimens on a 4.5in Span)

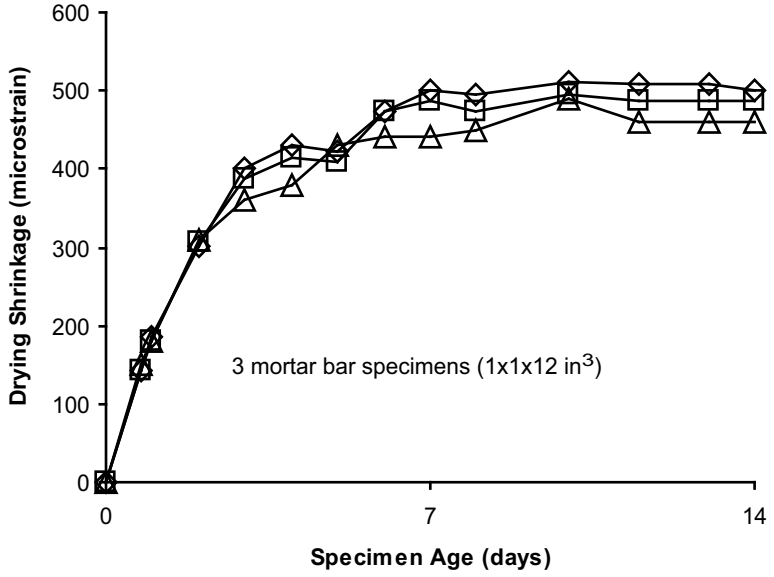

Figure 3.7: Drying Shrinkage of Glass Concrete

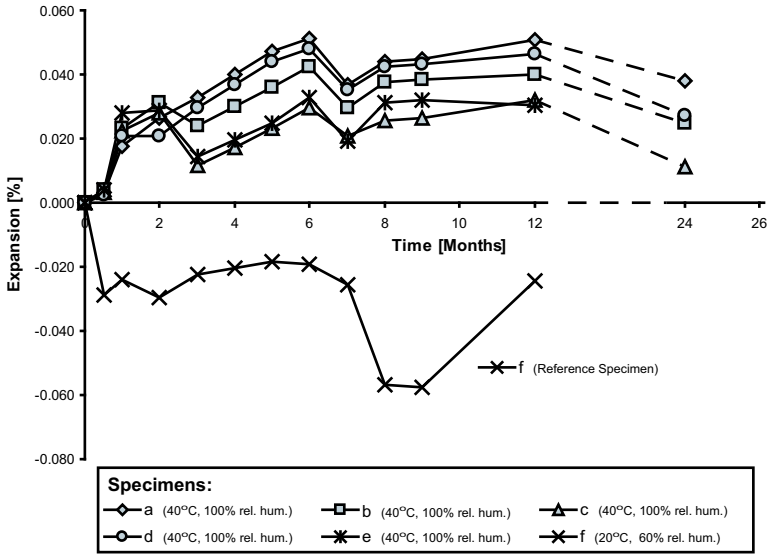

Figure 3.8: ASTM C-227 Test for ASR Performance of Glass Concrete (Final results after 24 months were obtained after drying of specimens.)

Table 3.7: Glass Concrete Properties

	20 Hours	**7 Days**
Compressive Strength [ksi]	5	10
Young's Modulus [$\times 10^6$ psi]	1.5	3.2
Modulus of Rupture (3-Point Bending)[psi]		1080

Chapter 4

Prestressed Thin Sheets - Experimental Setup

4.1 Preparation of Roving Systems

A trial-and-error investigation led to a system that binds the rovings in epoxy end-blocks, which can be mechanically held by clamps. Figure 4.1 shows such an end-block with 15 encased aramid rovings - 3 layers of fabrics with 5 rovings each. The spacing between layers is 0.08 in (2mm) and the total thickness of the epoxy end-block is 1/4 in (7mm), which is the target thickness of the thin glass concrete beams.

In the prototype phase of the project two different roving systems were considered. First, a system of 7 layers of fabric with 5 rovings each was produced, using 1,100 denier (122tex) low-modulus Twaron rovings. The system was successfully anchored, tensioned and then used to produce a small number of prestressed glass concrete beams. Though the system gave promising results, it was concluded that 7 layers of fabric were too difficult to handle. In an attempt to decrease the number of rovings needed to prestress a 1/4 in $\times$ 1 in (7 mm $\times$ 25 mm) cross-section with a load of 500 lbs (2.2kN), a fabric with larger 2,200 denier (244tex) high-modulus rovings was considered, with a failure load of 120 lbs (534N) per roving, compared with 40 lbs (178N) for the 1,100 denier (122tex) low-modulus rovings. After producing 1 inch (25mm) long epoxy end-blocks with 3 layers of aramid fabric with 5 rovings each, it was discovered that it was not possible to hold the targeted load of 500 lbs (2.2kN) without slip between the aramid fibers and the epoxy matrix and pullout of complete

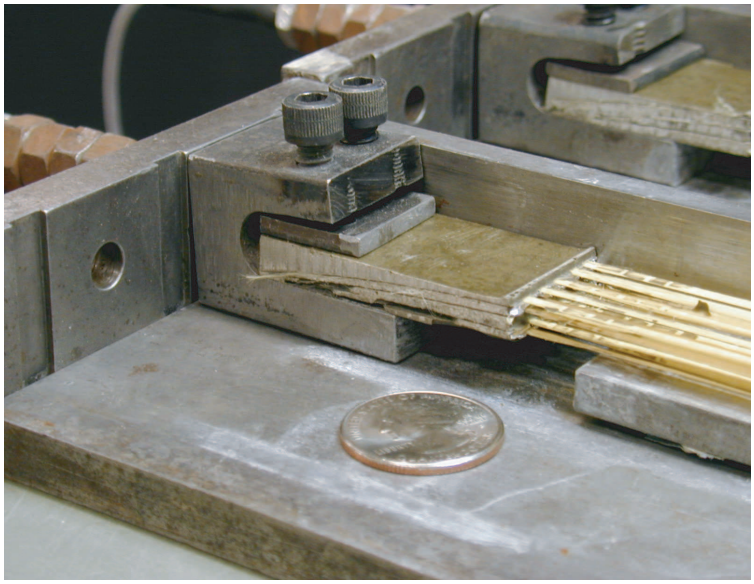

Figure 4.1: Epoxy End-Block Holding 15 2,200 Denier (244tex) Aramid Rovings

rovings. In a displacement-controlled experiment the load level decreased from over 500 lbs (2.2kN) to 300 lbs (1.3kN) before it eventually stabilized. The performance of a typical system with 35 low-modulus 1,100 denier (122tex) rovings and a system with 15 high-modulus 2,200 (244tex) denier rovings is shown in Fig. 4.2.

The following list summarizes the effects that were considered to explain the observations and presents the measures that were tried to overcome the problem.

1. The number of rovings that were used to transfer the target load of 500 lbs (2.2kN) decreased from 35 to 15, but the circumference of the cross section of a single roving increased from 2 x(0.15 mm + 1.2 mm) = 2.7 mm to 2 × (0.3 mm + 1.8 mm) = 4.2 mm. Thus, the total surface area available for bond within the 1 inch (25 mm) end-block decreased from 35 × 2.7 mm × 25.4 mm = 2400 mm^2 to 15 × 4.2 mm × 25.4 mm = 1600 mm^2. To increase the available

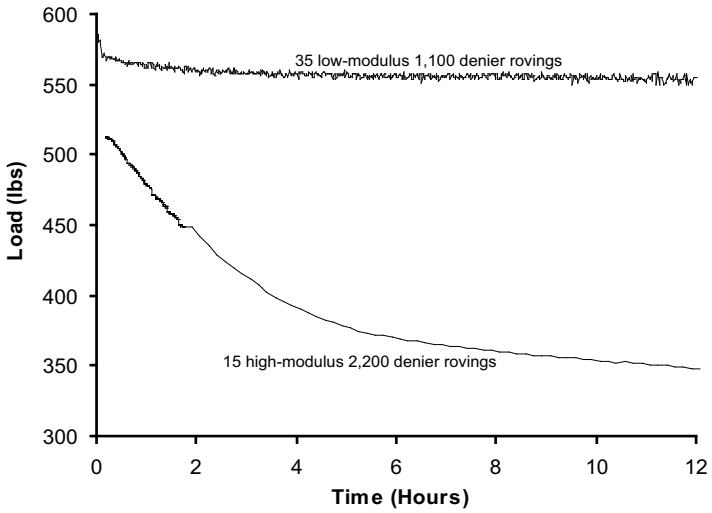

Figure 4.2: Well-Bonded vs. Poorly-Bonded Roving Systems

surface area, the length of the end-block was increased from 1 inch (25 mm) to 2 inches (51 mm). However, even with such an elongated end-block it was not possible to maintain a load level of 500 lbs (2.2kN).

2. The role of the coating of the rovings remains to be investigated. 1-in (25 mm) and 2-in (51 mm) epoxy end-blocks were produced with rovings of which the coating was washed off with regular detergent with the intent to increase the bond strength. The results were discouraging, and this approach was abandoned.

3. When larger rovings were used, a higher porosity of the epoxy matrix was observed below the rovings. Such porosity lowers the effective bond strength. The reason for the increased porosity was found to be the greater difficulty for the epoxy to completely encase the larger rovings, especially in the lower layers, without entrapping air pockets. To improve the bonding, the roving ends were dipped into epoxy immediately before production of the epoxy end-blocks, but

again without success.

4. The final approach was to use an epoxy with a proprietary filler consisting of very fine particles, and to use 4 layers of 5 rovings each, stressed to 3/4 of the previous level to obtain the target prestress load of 500 lbs (2.2kN). This approach proved to be successful in that all rovings could be properly anchored.

The end result of this trial-and-error phase was the choice of 4 layers with a total of 20 high-modulus 2,200 denier (244tex) aramid rovings to prestress thin glass concrete sections of 1/4 in × 1 in (7 mm × 25.4 mm) dimensions such as to generate uniform stresses of either 0, 0.5, 1.0, 1.5, or 2.0 ksi (0 - 14 MPa). Roving systems with 3 layers of mesh were used to produce 1/8 in × 1 in (3 mm × 25.4 mm) thin beams prestressed to uniform stress levels of 0, 1.0, and 2.0 ksi (0 - 14 MPa). The epoxy end-blocks were produced as illustrated in Fig. 4.3.

4.2 Preparation of Formwork

The formwork setup utilizes regular steel formwork for the production of 1 × 1 × 12 in^3 (2.5 × 2.5 × 30 cm^3) mortar beams, usually used for ASR tests. The thickness of the epoxy end blocks is the same as the target thickness of the glass concrete beams. As shown in Fig. 4.1, the thickness of the clamps requires that the bottom of the formwork be raised. This feature allows at the same time to vary the concrete cover, for example, to study surfaces with exposed aggregate or to introduce eccentricity of the prestress force. Fig. 4.4 shows the equipment used to monitor prestress and strain. A strain-gaged bolt monitors the load, and a magnetic clip-on device allows the installation of an LVDT to measure the distance between the clamps and therefore the relative strain in the roving system. The system was found to work

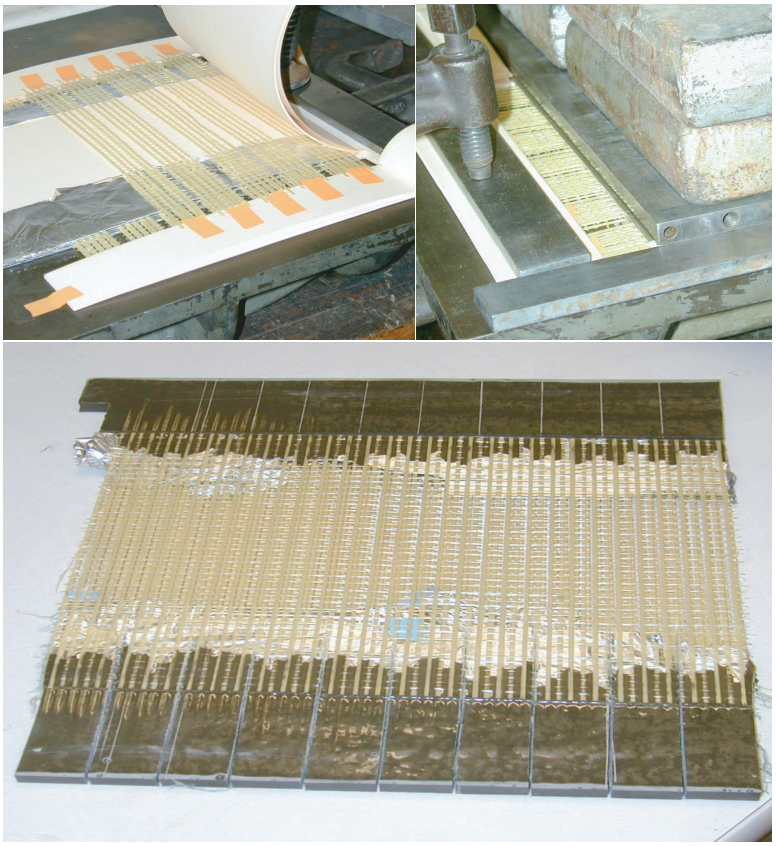

Figure 4.3: End-Block Production

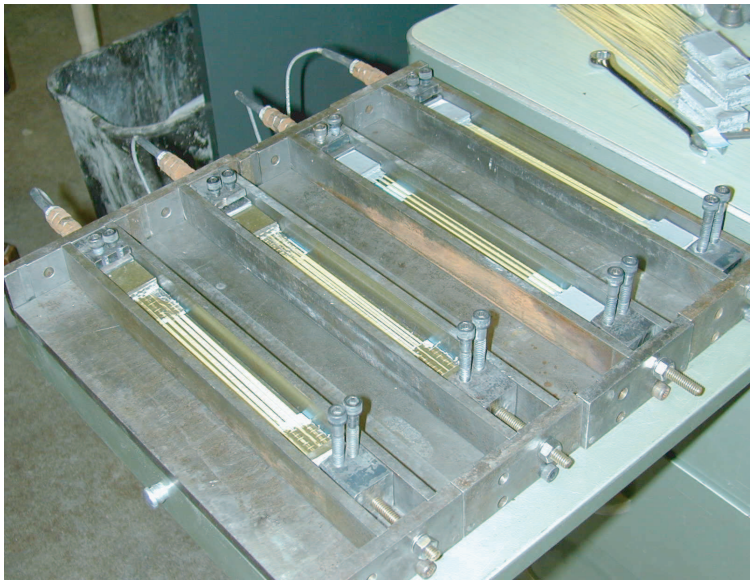

Figure 4.4: Mold Setup

well and reliably. The stressing operation was done by manually tightening a nut located on the side opposite to the strain-gaged bolt.

4.3 Prestretching of Roving Systems

The roving systems were first loaded up to 150% of the target load, for 1 hour, then unloaded completely. This preconditioning technique, carried out to lower the relaxation coefficient of the aramid fibers, was discussed in Chapter 2. After final preparation of the mold, which included installing the piece of steel to raise the bottom of the mold between the clamps, and applying a release agent, the roving system was stretched to 110% of the target load level. Immediately afterwards, glass concrete was mixed and placed. Finally, after concrete placement the load was adjusted to the target prestress level. Monitoring of the tensile load of the roving system with the strain-gaged bolt was continued until load transfer. Fig. 4.5 shows

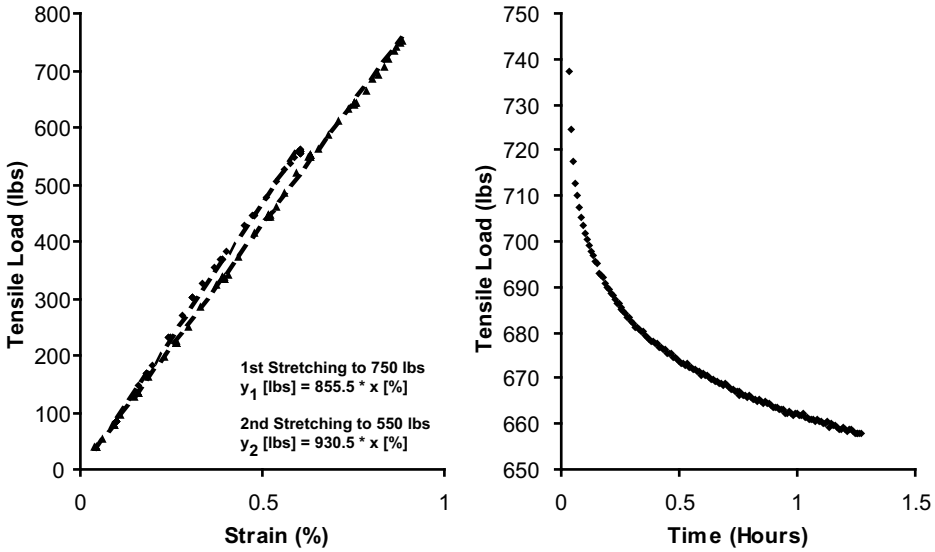

Figure 4.5: Preconditioning of Roving System Prior to Glass Concrete Placement

a representative load history obtained throughout the preconditioning period of 1 hour (Note the large loss of prestress force due to primary relaxation). It also shows load-strain responses for the first and second loadings, which illustrate the stiffness increase due to prestretching observed during the second stretching.

4.4 Placing of Concrete and Early Hydration Period

The glass concrete was mixed for 3 min. Because of the metakaolin the fresh glass concrete mix was very sticky, but with external vibration, it flowed easily and completely filled the spaces between the layers of aramid fabric. About 2/3 of the needed amount of glass concrete were placed and vibrated for about 10 seconds. Then the remaining material was placed and vibrated for another 10 seconds. Excess material was removed and the beam thickness verified to ensure the correct value of 1/4 inch (7 mm) or 1/8 inch (3 mm).

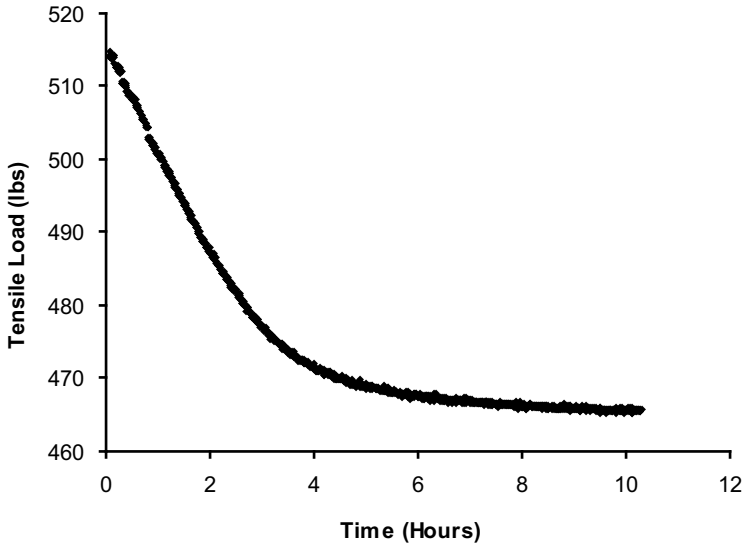

Figure 4.6: Monitoring of Prestress Level Throughout Hydration

A typical batch yielded 4 specimens, which were covered with plastic foil to minimize drying shrinkage. Because of the computer-aided monitoring of the prestress levels, the molds were not placed in a moisture room.

Fig. 4.6 illustrates a typical load-history during the first 10 hours after concrete placement, as monitored by the strain-gaged bolt. The loss of prestress during the first hours of hydration is a measure of the chemical impact of fresh glass concrete on the prestressed roving system. Different concrete mixes may cause different prestress losses. Also the prestress level influences the total amount and the rate of the prestress loss.

4.5 Load Transfer and Removal of Formwork

Twenty hours after concrete placement, the magnet clip-on LVDT was reinstalled to allow monitoring of the elastic shortening of the glass concrete beam caused by

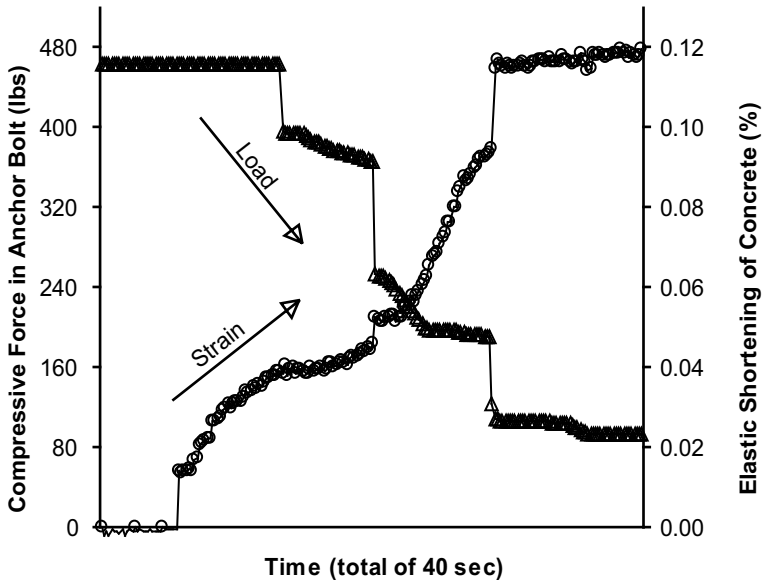

Figure 4.7: Load Transfer

the transfer of the prestress force from the formwork into the young concrete. The prestress force was transferred by manually loosening the nut on the side opposite to where the strain-gaged bolt was installed. Friction between the concrete beam and the formwork interfered with a smooth load transfer. It was all but impossible to obtain a linear relationship between transferred prestress force and elastic shortening. Fig. 4.7 shows that the strain-gaged bolt was unloaded in stages, rather than continuously. By noting the difference between LVDT readings before and after load transfer, and the complete amount of prestress, which was transferred, it is possible to determine Young's modulus of the young concrete and the prestress loss due to elastic shortening.

It would be instructive to record the strain vs. time relationship after load transfer by leaving the clamps connected to the thin beam and continuing to monitor the LVDT, i.e. measuring combined shrinkage and early creep deformations of the

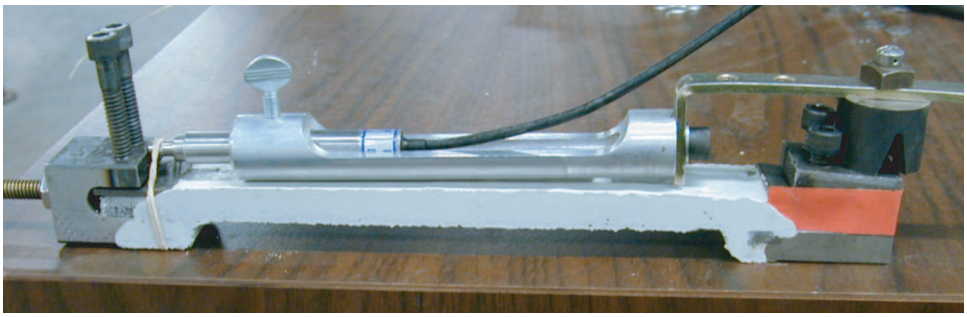

Figure 4.8: Test Setup for Monitoring of Early Shrinkage and Creep

specimen, Fig. 4.8. In one trial case, an additional 0.085% strain was recorded during the first 7 days, Fig. 4.9. However, the results are greatly influenced by curing conditions, temperature and relative humidity. As stated in the previous chapter, creep data on metakaolin-modified concrete systems is rare, and creep and shrinkage data for glass concrete, which is prestressed at 2 ksi (14MPa) after only 20 hours does not exist.

4.6 Post-Load Transfer Experiments

Beams were subjected to three-point bending on a 4.5 in (114mm) span 7 days after concrete placement. Prior to loading the epoxy end-blocks of 2 out of 4 specimens per batch were cut off. It was expected that bond between rovings and matrix would not be sufficient to maintain the prestress in specimens without the end-blocks. The result would have been less stiffness of the cracked specimens and noticeable permanent deflections after three-point bending, caused by fiber slip. Load, vertical displacement, and strain on the tension side of the specimens were measured. The strain data was obtained using a 1 in (25mm) clip-gage, Fig. 4.10. For an uncracked section, this measurement corresponds to the tensile strain of the concrete bottom face averaged over the 1-inch (25mm) gage length. Once cracking starts, the clip-

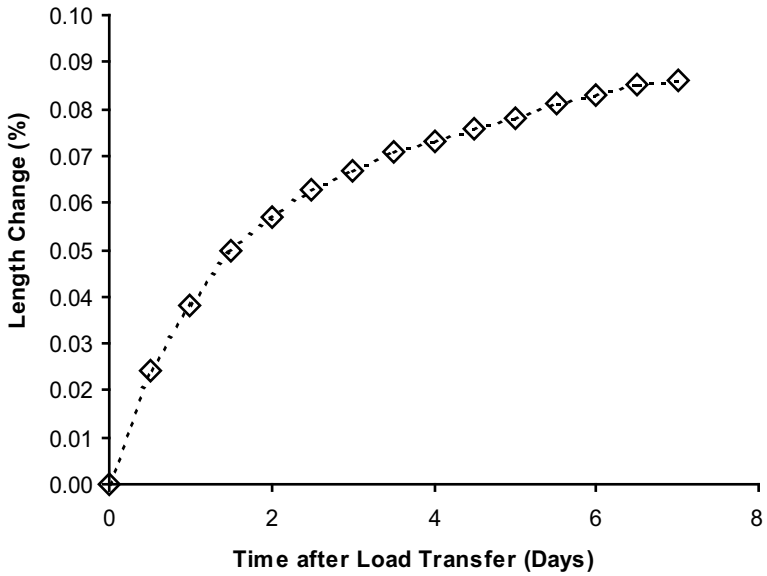

Figure 4.9: Early Shrinkage and Creep of Prestressed Glass Concrete Thin Beam

gage bridges over a number of cracks. The measurement thus does not correspond to strain, nor to CMOD (crack mouth opening displacement), but to an average strain with the crack openings smeared over the 1-in (25mm) distance. Since the clip-gage feedback (and not the displacement of the hydraulic jack) was used to control the bending tests, the resulting loading curves were plotted against this quantity, which will be referred to as *"strain"* in the remainder of this report. Three-point bending tests were carried out in a cyclic fashion with increasing strain levels, Fig. 4.10. A specimen was loaded to a strain of 0.5%, then unloaded, followed by reloading, but up to a strain of 1% and finally 1.5%. To observe the development of the prestress level over time, the same specimens were bent again straight up to 1.5% and back, after 14, 21, and 28 days. Further preliminary tests were carried out to investigate durability properties and the effect of moisture uptake in a wet environment on the bending performance of prestressed thin beams.

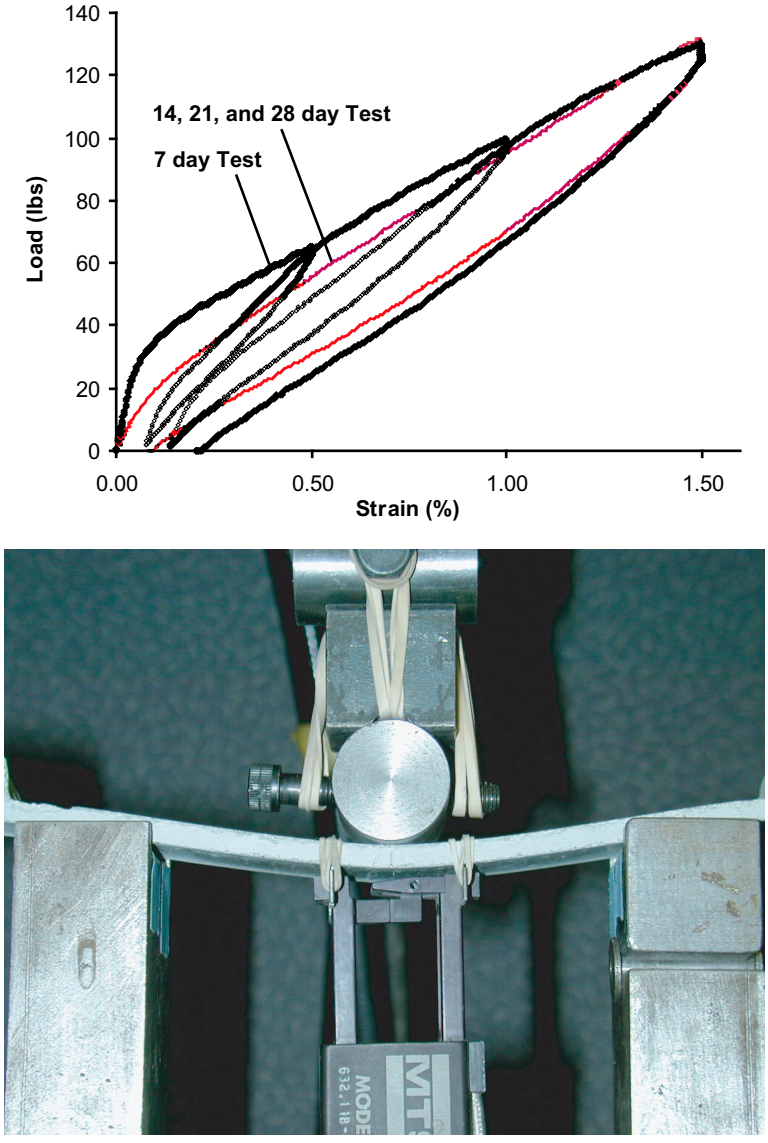

Figure 4.10: Three Point Bending Test Setup and Typical Load Deformation Curve

Chapter 5

Prestressed Thin Sheets - Experimental Results, Analysis, and Discussion

5.1 Test Program

Eight series, *a1* - *a8*, of uniaxially prestressed glass concrete beams were prepared. Each consisted of 4 specimens, 7 inch (175mm) long. Series *a1* - *a5* consisted of beams with cross-sections of 1/4 in × 1 in (7 mm × 25 mm), which contained 4 layers of aramid fabric with 5 rovings each. The average stiffness of the roving systems, containing 20 rovings each, was found to be 765 lbs/% (3.4kN/%)[1] and 820 lbs/% (3.6kN/%), before and after preconditioning, respectively. Beams of series *a1* - *a5* were prestressed at 0[2], 0.5, 1, 1.5, and 2 ksi (0 - 14 MPa), respectively. This implies, that the roving systems were stressed to 1, 5, 10, 16, and 21% of their theoretical load carrying capacity[3]. The main focus of this study was on these five

[1]The mechanical properties of solids are always specified in terms of stress and strain, i.e. stiffness in psi or GPa. In this work, the properties of roving systems were measured in denier per roving, number of rovings per roving system, load, and strain. Converting denier into cross-sectional areas and stiffness into psi would not be very meaningful. A stiffness of a roving system with 20 2,200 denier rovings of 765 lbs/% means that it requires 765 lbs to stretch the system by 1%. This corresponds to 765lbs/(20 rovings × 2000 fibers/roving × Pi/4x$(10\mu m)^2$/fiber)/% = 15.7×10^6 psi = 108 GPa, which is about 2/3 of the stiffness of a single roving, Fig. 2.8. The stiffness of a single roving is only a fraction of 2,000 × the stiffness of a single fiber, which again has only a fraction of its theoretical stiffness and is different for different aramid products.

[2]Placing and consolidating the concrete proved to be very difficult in specimens with no tensile force applied to the rovings at all. For this reason, a small prestress load of 50 lbs was applied, which resulted in a uniform compression of 100 psi. For convenience, all test results obtained on specimens prestressed at 0.1 ksi shall be presented as the "non-prestressed" reference cases.

[3]For instance, to generate a prestress of 2 ksi the roving system had to be stressed to a tensile force of 500 lbs. This force is devided among 20 rovings at 25 lbs per roving. Assuming that failure

test series. However, since the experimental setup was easily adjusted to produce thinner sections, 3 additional series of beams, *a6* - *a8*, were prepared with 1/8 in (3mm) thickness, containing 3 layers of fabric with 5 rovings each, with prestress levels of 0.1, 1, and 2 ksi (0 - 14 MPa), respectively.

5.2 Prestress Loss during Early Hydration

As described in the previous chapter, the tensile load carried by the aramid roving system was monitored not only prior to concrete placement, but also until load transfer at a concrete age of 20 hours. It was observed that a significant amount of force in the roving system was lost during the first few hours of hydration, in spite of the roving preconditioning and the fact that the reaction was still carried by the steel form. A typical force-time history is illustrated in Fig. 5.1, with two distinct phases, which are readily approximated by linear functions. The first phase, characterized by points P_1 and P_2, represents a period of relatively rapid tension loss, whereas during the phase between points P_2 and P_3, very small losses take place (Note that load is transferred at the time of P_3). The pertinent test data are listed in Table 5.1. Since roving systems of test series *a1* were not (or barely) prestressed, there were no losses to be recorded. In the case of series *a4*, problems with the data acquisition system allowed load monitoring only during the last few hours before load transfer, i.e. the tensile load was known only at a concrete age of 20 hours, besides the initial prestress.

Fig. 5.2 presents the glass concrete age at point P_2 and the rate of tension loss

---

of a single roving occurs at 120 lbs, a tensile load of 25 lbs per roving means, that the system is stressed to 21% of its load-carrying capacity.

Table 5.1: Force in Roving System during Early Hydration

Specimen #	Prestress (ksi)	P2 age (hours)	P2 load (%)	Slope P1_P2 (% per hour)	P3 age (hours)	P3 load (%)
a1_00	0.1		100.0			100.0
a1_01	0.1		100.0			100.0
a1_02	0.1		100.0			100.0
a1_03	0.1		100.0			100.0
a2_00	0.5	2.3	94.4	-2.4	19.2	93.7
a2_01	0.5	1.9	92.6	-3.9	19.3	91.8
a2_02	0.5	2.1	91.3	-4.1	19.4	90.6
a2_03	0.5	1.9	91.8	-4.3	19.5	91.4
a3_00	1.0	2.1	89.2	-5.1	18.6	88.4
a3_01	1.0	2.6	94.5	-2.1	18.8	93.7
a3_02	1.0	2.3	91.3	-3.8	18.9	90.5
a3_03	1.0	1.6	99.6	-0.2	19.0	98.8
a4_00	1.5					88.5
a4_01	1.5					88.5
a4_02	1.5					90.7
a4_03	1.5					86.7
a5_00	2.0	3.4	90.7	-2.7	18.8	90.3
a5_01	2.0	3.0	91.0	-3.0	18.6	90.6
a5_02	2.0	3.6	88.8	-3.1	18.5	87.6
a5_03	2.0	2.6	87.2	-4.9	18.4	86.8
Averages:						
a1	0.1		100.0			100.0
a2	0.5	2.1	92.5	-3.7	19.4	91.9
a3	1.0	2.3	91.7	-3.7	18.8	90.9
a4	1.5					88.6
a5	2.0	3.2	89.4	-3.4	18.6	88.8

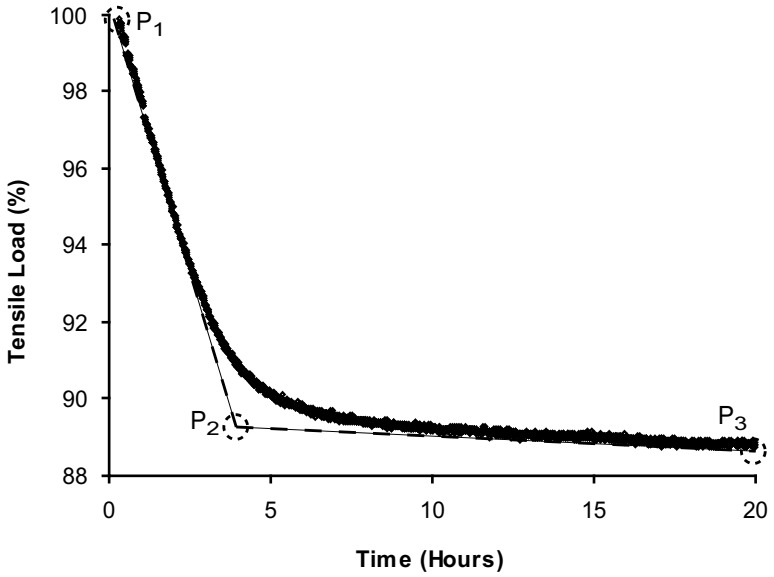

Figure 5.1: Force in Roving System during Early Hydration

between points P_1 and P_2, for the different levels of prestress. The rate of tension loss is given in percent of the initial force per hour. Whereas the duration of rapid tension loss appears to increase for higher prestress levels, the rate of decay is almost independent of it. As presented in Fig. 5.3, the total loss of tension during early hydration was of the order of $10\pm2\%$, slightly higher for higher prestress levels. Such a loss, at a rate of $\approx 3.5\%$ per hour, means that a system prestressed with 500 lbs (2 ksi) (2.2kN (14MPa)) looses twice as much total load in the same time period as a system, which is prestressed with the same number of rovings, but stressed to only 250 lbs (1.1kN) (to cause 1 ksi (7MPa) of uniform compression), namely 50 lbs (222N) and 25 lbs (111N), respectively, both in about 2.5 hours.

Fig. 5.4 shows the tensile forces recorded for specimens of series *a1* and *a2*, as functions of time, i.e. for specimens with very low levels of prestress. It is interesting to observe fluctuations, with even slight increases in tensile load during short periods.

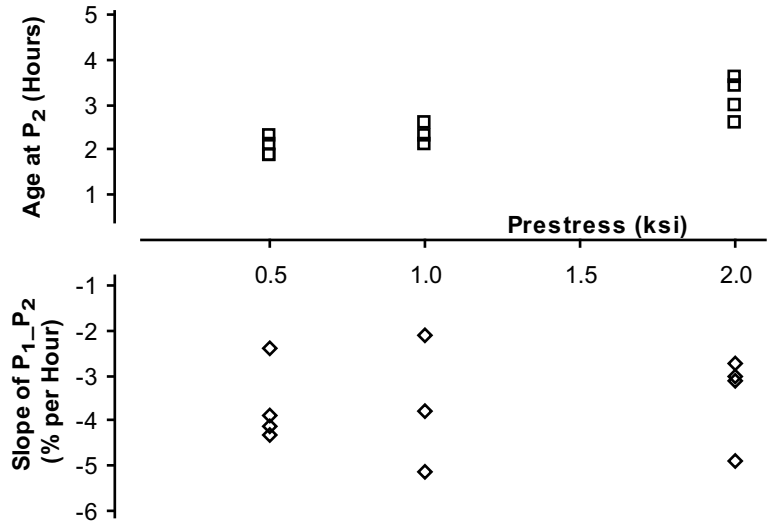

Figure 5.2: Duration and Rate of Prestress Loss During Early Hydration

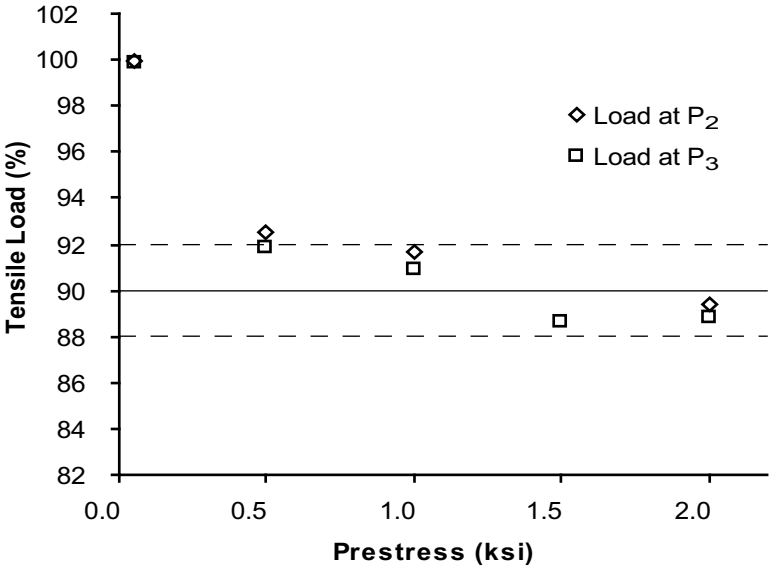

Figure 5.3: Amount of Prestress Loss During Early Hydration

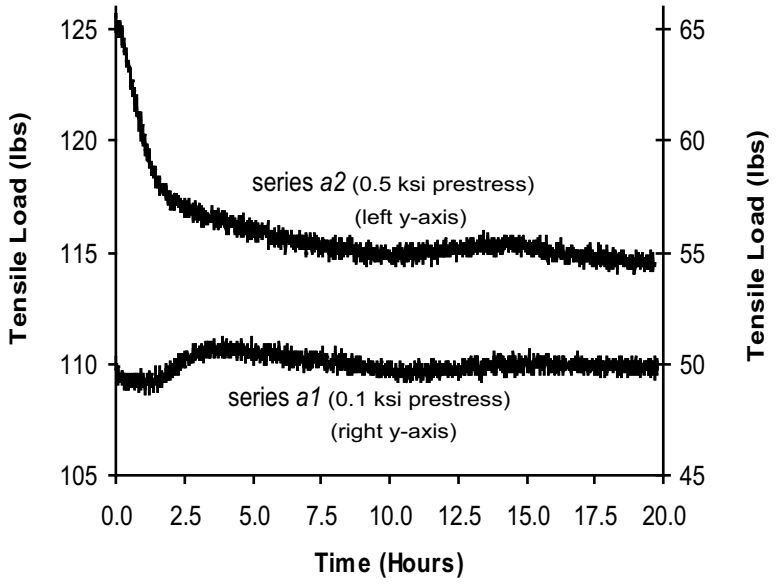

Figure 5.4: Load Histories of Specimens with Low Prestress Levels

These oscillations appear to correlate with the day and night cycle, which might point to small humidity changes within the daily 24 hour rhythm. No rational explanation of this phenomenon can be offered at this time.

The end of the period with rapid loss of pretension force (2 to 5% per hour), signified by point P_2, coincides with the time when the concrete sets and undergoes change from a plastic through a gel-like to a solid material. At this age the material develops its first capacity to resist shear and bond stresses. This finding is of significance for practical applications. 10% of prestress are lost in the first 2 - 3 hours, but afterwards the prestress level stabilizes. The factors, which cause this phenomenon are not completely understood and should be further investigated.

A different aspect of the same phenomenon is presented in Fig. 5.5. The complete loss of tensile force during early hydration is plotted in percent against the utilized capacity of the roving system, also in percent. As pointed out earlier, in

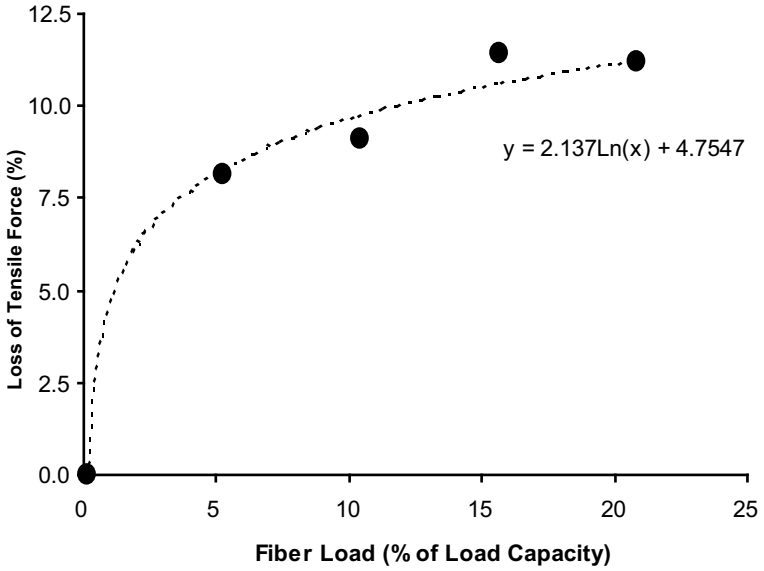

Figure 5.5: Prestress Loss per Used Roving Capacity During Early Hydration

the case of 2 ksi (14MPa) prestress, only 21% of the capacity of the roving system is utilized. At 1 ksi (7MPa), with the same number of rovings, the roving system is stressed to only 10% of its capacity. Yet, higher strain in the roving system implies only slightly higher loss over a longer time-span, Fig. 5.3 and Fig. 5.2. Whereas the stiffness of the roving system is a function of the number of parallel rovings, the loss of tension force during early hydration is a function of the strain, to which the rovings are stretched. If the 1 ksi (7MPa) system had not been produced with 20 rovings, utilizing only 10% of their strain capacity, but with 10 rovings at 20% of their capacity, the loss to be expected during hydration would have been about 11% instead of 9%. Also, it would have occurred over a longer time-span, i.e. point P_2 in Fig. 5.1 would have shifted towards the right.

Although a loss of pretension force of the order of 10% would be acceptable, as long as it is accounted for during design, the results presented in this section raise

a number of questions, which cannot be answered at this time:

- What exactly happens to a single aramid fiber under stress when it is exposed to the pore solution of fresh concrete? The fibrillar nature of the fibers suggests a change of material properties as a function of the distance to the fiber core, i.e. the whole fiber is not necessarily compromised, but only partially degraded, more on the outside, less towards the inside. It is expected that Twaron and Kevlar fibers exhibit different behavior than Technora fibers, since the production processes are different and Technora fibers are much more inert to moisture uptake and hydrolysis [85].

- Does the effect of the fresh concrete mix on aramid fibers diminish from the outside towards the inside of a roving with thousands of single fibers? Are hydration products able to penetrate into rovings and cause harm? How is this degradation mechanism influenced by different fresh concrete characteristics, such as flow, setting time, and hydroxide content, which in turn, is influenced by pozzolanic additives? Aramid fibers are known not to develop strong bond in composite matrixes [19]. Does this statement also apply to cement-based composites? The first hours of hydration should hold the answer to this question.

- What role does the coating of the fibers play? Is a roving, subjected to large strains, more vulnerable to alkali attack, because of larger, or more numerous cracks? Is a coated roving still a fiber bundle, or would one need to treat it as a composite [46]?

- Results were presented only for roving systems, which were stretched to 20% of their load bearing capacity. In view of the high cost of aramid fibers, the

roving systems should be better utilized, e.g. at about 50% of their capacity. The performance of fibers stretched to higher strains needs to be studied to verify the logarithmic trend suggested in Fig. 5.5. According to the trend line shown in Fig. 5.5, fibers stretched to 50% of their capacity would be expected to loose $2.137 \times \ln(50) + 4.7547 = 13.1\%$ of their prestress.

5.3 Load Transfer

By monitoring the distance between the two epoxy end-blocks during load transfer, using the clip-on LVDT (Fig. 4.8), one can calculate the average elastic shortening of the specimens. Fig. 5.6 summarizes the results for a number of specimens with different prestress levels. The 20-hour compressive strength of the glass concrete was found to be 5 ksi. Assuming that prestress up to 2 ksi does not exceed the linear range of the stress-strain curve of glass concrete at that age, a Young's modulus of $\approx 1.5 \times 10^6$ psi is derived from the data obtained at load transfer. After 7 days the compressive strength doubles from 5 to 10 ksi, and so does the Young's modulus, from 1.5 to 3.2×10^6 psi.

Elastic shortening of concrete during load transfer causes an instant loss of prestress force, since the aramid rovings shorten together with the concrete. For calculating the elastic shortening it is unimportant, how many rovings are used to generate the prestress. Only the prestress force, the axial stiffness of the concrete beam, and the modular ratio (which is about n=10 in this case) determine the elastic shortening. It is common knowledge in prestressed concrete theory, that the concept of prestressing of concrete works only if the prestressing wires are utilized at strains greater than the shortenings caused by load transfer, shrinkage and creep of the

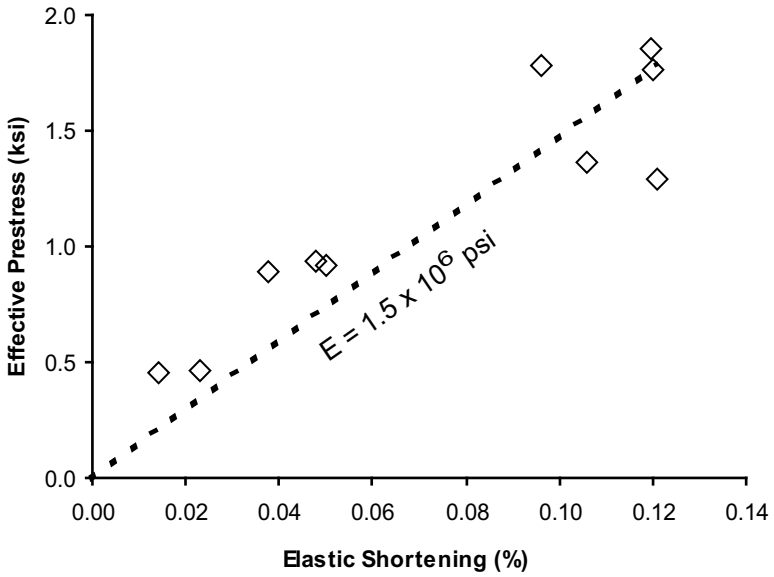

Figure 5.6: Elastic Shortening Observed during Load Transfer vs. Prestress

concrete matrix[4]. Smaller numbers of rovings, which are stretched to larger strains, will therefor cause smaller prestress losses. If the roving system shortens by a certain amount, for example 0.12%, caused by a prestress of 2 ksi (14MPa), Fig. 5.6, a system with 20 rovings, as used in this study, looses ≈90 lbs (400N), or ≈20% of its initial prestress. If the rovings were used more economically, for example, stressed to ≈50% of their capacity, the same prestress levels could be realized with 8 rovings and the loss of prestress during load transfer would be reduced by a factor of 2.5, namely from 20% to 8%.

Another way to reduce prestress losses during load transfer is to stiffen the matrix. The Young's modulus of concrete changes drastically during the first days

[4]Only the use of high-strength steels, which could be stretched to 0.7%, compared with 0.15% for normal-strength steels, combined with high-strength concrete, enabled Eugene Freyssinet in 1928 to successfully produce prestressed concrete for the first time [20].

of hydration, increasing from 1.5×10^6 psi (10.3GPa) after 20 hours to 3.2×10^6 psi (22.1GPa) after 7 days. If prestress could be transferred after 44 instead of 20 hours, the prestress losses could be reduced accordingly. From a commercial production viewpoint this measure might be uneconomical because it would tie up expensive formwork for an additional 24 hours.

5.4 Shrinkage and Early Creep

Knowledge of combined shrinkage and creep is essential in prestressed concrete design. The usage of linear-elastic fibers implies that any shortening of a prestressed concrete beam after load transfer immediately causes losses of prestress force.

The constituent materials used in this work were studied with regard to their long-term behavior under load. In Chapter 2 the relaxation characteristics of aramid fibers were explained with consideration of their micro-structure. It was observed that prestretching of fibers can greatly reduce their relaxation coefficient, but also, that embedding the fibers in an alkaline environment changes the relaxation properties. In Chapter 3 it was pointed out, based on published test data, that the creep properties of metakaolin-modified concrete are superior to those of other high-performance or regular concrete systems. Because of limitations of the available laboratory equipment, experimental data were obtained only for shrinkage, not for creep.

Determining the creep properties of concrete following standardized procedures involves large specimens with embedded strain sensors and an externally generated permanent load. A simple alternate experimental technique to observe combined shrinkage and creep for small-scale prestressed thin glass concrete beams was de-

scribed earlier. By leaving the clip-on LVDT of Fig. 4.8 in place after load transfer one can readily monitor the shortening of the beam specimen due to combined creep and shrinkage.

Because only one LVDT was available in the context of this study, it was impossible to equip all specimens with the necessary data acquisition system even for only one week after load transfer, when they were subjected to three-point bending. Only one specimen of a preliminary test series prestressed at 0.5 ksi (3.5MPa) was so monitored to demonstrate the experimental technique, with the test results shown in Fig. 4.9. 0.04% of the observed strain of 0.085% was caused by shrinkage, Fig. 3.7, and the remaining 0.045% were caused by creep. When concrete dries under load, the shortening strain is referred to as drying creep. In our case, it is caused by the prestress force after load transfer, i.e. 0.9 (hydration) $\times$ 0.8 (load transfer) $\times$ 125 lbs = 90 lbs (400N). The shrinkage and drying creep strains cause additional prestress losses of30 lbs (133N) and 33 lbs (147N), or 26% and 30%, respectively. As stated before, reducing the number of rovings will reduce the prestress loss caused by shrinkage and creep enormously.

5.5 3 Point Bending - Flexural Capacity and Ductility

At a concrete age of 7 days all beams were subjected to 3-point bending as illustrated in Fig. 4.10. The measured quantities were mid-point deflection, load and strain. The strain readings, obtained with a 1-inch clip gage attached to the bottom side of the test specimen, were utilized to control the bending experiments by means of closed-loop feedback control. Beams were loaded at a rate of 0.5%/min first to a strain of 0.5% and after unloading to 1.0%, and after another unloading to 1.5%. Representative load-strain curves for specimens with 0, 1, and 2 ksi (0 - 14 MPa)

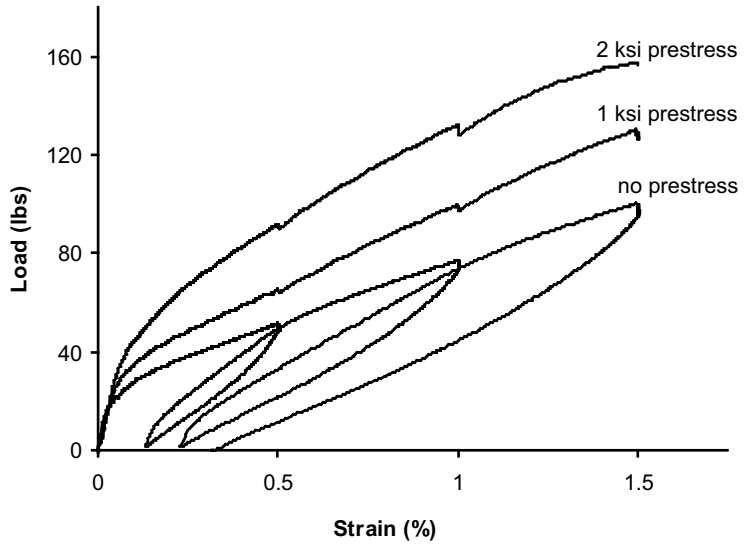

Figure 5.7: Load-Strain Curves for Various Prestress Levels

prestress are shown in Fig. 5.7. For clarity, the unloading branches of the two prestressed beams are not shown. The complete set of load-strain curves is compiled in Appendix A. Results of bending experiments are usually presented as functions of mid-point displacement, which is dependent on the span length. In this study it was decided to plot the curves as functions of strain, which correlates to curvature just as well as mid-point deflection. A useful measure would be the deflection-to-span ratio, which is commonly used in building codes and industry standards. The relation between strain s and mid-point deflection d, was experimentally found to be linear, Fig. 5.8, with d (in) $\times$ 11.5 = s (%), where 11.5 is a mean value, obtained from multiple strain vs. deflection curves. A strain of 1.5% in bending experiments thus corresponds to a mid-point deflection of $\approx$0.13 in (3.3mm), and a deflection-to-span ratio of 1/42.

The immediate observations from the load-strain curves in Fig. 5.7 correspond well with the established basic principles of prestressed concrete theory:

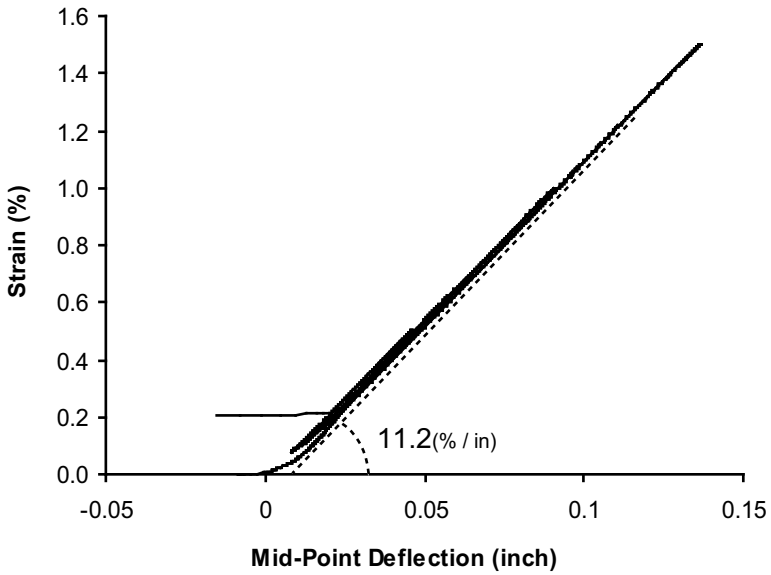

Figure 5.8: Typical Strain vs. Mid-Point Deflection Curve

- The formation of flexural cracks occurs gradually and is clearly delayed by the application of prestress.

- The load to produce a given strain (deflection) is greatly increased by prestress. The load difference between the specimens prestressed at 2 ksi (14MPa) and no prestress reaches its maximum at a strain of $\approx 0.75\%$.

- As expected, the stiffness of cracked sections increases with increasing prestress, because a larger concrete area is available to balance the prestress force.

- The load-strain curves indicate that ductility is inversely proportional to prestress level. Since the sections are over-reinforced, failure is typically initiated by concrete crushing, which will occur earlier in beams with higher prestress. An actual case of incipient concrete crushing is illustrated in Fig. A.4(b).

To quantify the effect of prestress level, Table 5.2 lists loads (relative to the

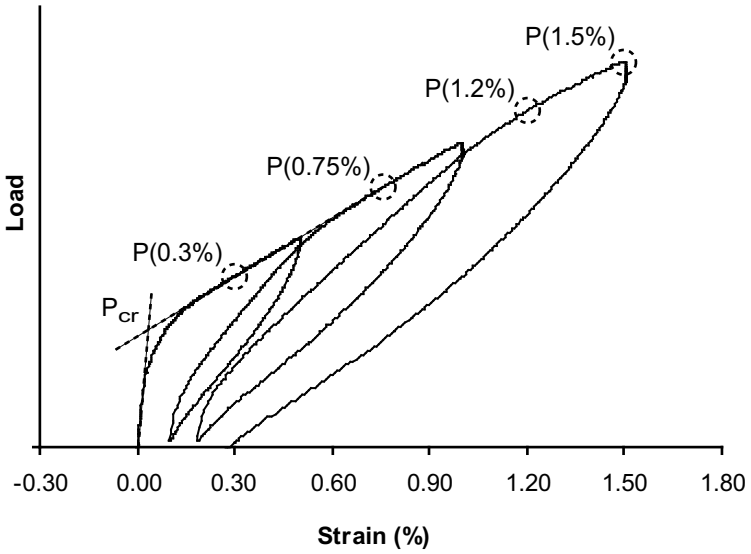

Figure 5.9: Representative Load-Strain Data Points

case of no prestress) required to produce various strains, Fig. 5.9. At strains up to 0.75%, load responses are increased by up to 72% by a prestress level of 2 ksi (14MPa). At the higher strain of 1.5%, the maximum gain in load capacity is only 45%. This observation is easily explained with incipient softening of the compression zone, which occurs at lower strains for beams with higher prestress levels. Beams prestressed at 2 ksi (14MPa) started to soften in compression at strains between 1% and 1.5%, as can be seen in Fig. 5.7. Beams with low prestress, in contrast, could be loaded to strains up to 2%, with considerably less softening of the compressive zone.

Also shown in Fig. 5.9 is a point P_{cr}, which signifies approximately the point of cracking. The corresponding load and strain coordinates for the various prestress levels are plotted in Fig. 5.10. Compared to the case of no prestress, a prestress level of 2 ksi (14MPa) increases the cracking strain from 0.035% to 0.06% and the applied load from 24 lbs (107N) to 39 lbs (173N). All test specimens exhibited linear-elastic

Table 5.2: Relative Load Levels as Function of Strain and Prestress (values are averages of 4 specimens per series)

	Strain (%)			
Prestress (ksi)	**0.30**	**0.75**	**1.20**	**1.50**
0	100	100	100	100
0.5	116	116	114	111
1.0	139	136	129	123
1.5	160	161	156	143
2.0	172	169	159	145

behavior until cracking. By determining the slope of the elastic loading branch, using the data of Fig. 5.10, it was possible to verify that the bending stiffness of the uncracked section is independent of the amount of prestress.

5.6 Prestress as a Function of Time

Beams were reloaded to strains of 1.5% after 14, 21 and 28 days. The loading was performed monotonically, not cyclically as in the case of the 7-day experiment. Fig. 5.11 shows the response of a specimen tested after 7 days and after 28 days, omitting the 14-day and 21-day experiments, for clarity. At a strain of 1.5% the specimen reached about the same peak load as in the three prior tests. The fact that the 28-day experiment was carried out on a specimen that had been cracked previously, is reflected in the lower applied load at lower strains and in a smaller amount of dissipated energy, i.e. the hysteresis area. Peak loads at 1.5% strain at the 4 different specimen ages for the different prestress levels are summarized in Table 5.3. It is interesting to observe that at small prestress levels, at which the compression zones are almost undamaged after the first cyclic bending experiments after 7 days, the peak loads at subsequent loading sessions were higher compared to the first loading. This observation is explained with the gain of compressive strength and Young's

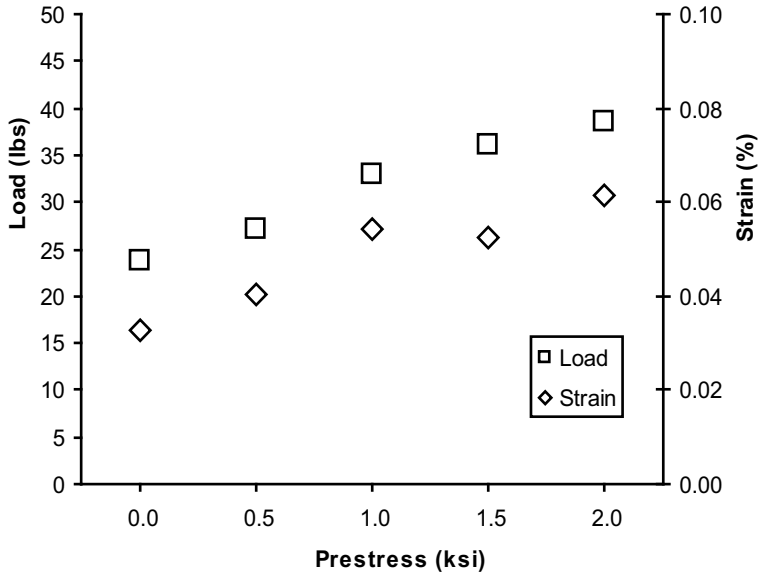

Figure 5.10: Load and Strain Values at Crack Initiation (Point P_{cr})

modulus of the concrete between 7 and 28 days. Only in cases of 1.5 (10.5MPa) and 2 ksi (14MPa) prestress the peak load decreased slightly when specimens were reloaded, due to the damage caused by the first test. Typical load-strain curves are shown in Fig. 5.12. A complete set of curves is compiled in Appendix B. A small number of specimens was tested yet again more than 3 months later, and no loss of flexural capacity was observed.

The results of repeated bending of specimens suggest that the prestress forces were maintained over time, even after subjection to severe flexure. Two observations support this statement. The specimens reached peak loads of similar magnitude at repeated loading sessions, which would not be possible if the prestress were reduced in the meantime. Also, the repeated load-strain curves of specimens without prestress were almost linear directly from the start, Fig. 5.12. Under prestress, however, the cracked sections returned to a state of uniform compression after the earlier bending

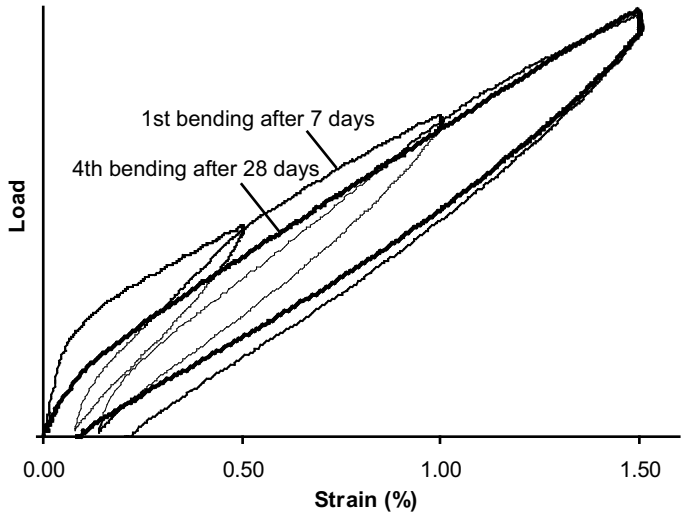

Figure 5.11: Typical Curves for Repeated Bending Experiments

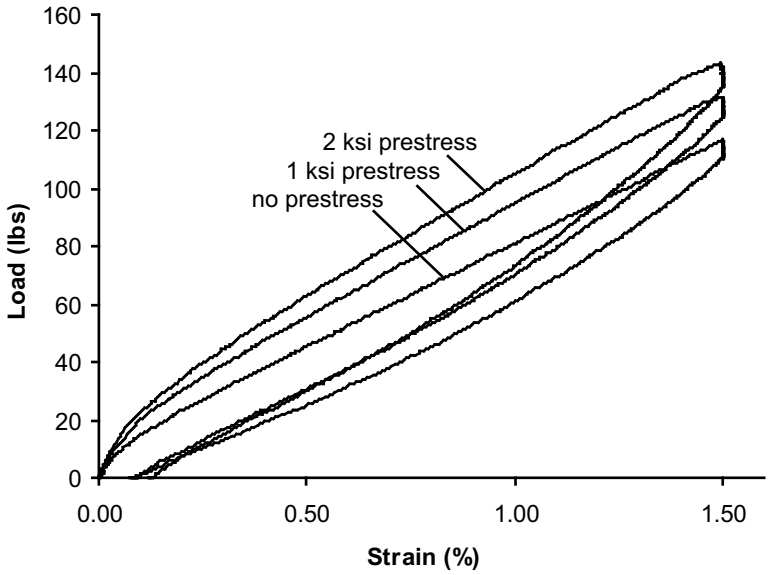

Figure 5.12: Typical Load-Strain Curves for Specimens Subjected to 3-Point Bending for the Fourth Time after 28 Days

Table 5.3: Flexural Capacity in lbs at 1.5% Strain as a Function of Specimen Age at Different Prestress Levels (values are averages of 4 specimens per series)

	Specimen Age (days)			
Prestress (ksi)	**7**	**14**	**21**	**28**
0	100	117	119	111
0.5	111	124	129	122
1.0	129	137	129	137
1.5	137	139	130	129
2.0	147	136	142	139

experiments. The compressive strain produced by the prestress had to be overcome in any subsequent 3-point bending experiment. This is reflected by the considerable reduction in slope of the load-strain curves at ≈0.1% strain, Fig. 5.12.

5.7 Permanent Strain and Durability Aspects

Permanent strain may be indicative of fiber slip, which also correlates to a residual deflection. A prestressed beam should theoretically return to a straight and uniaxially compressed state after bending. If fibers slip during a bending experiment, for instance because of inadequate development length, the permanent deflection measured after unloading might reveal details of the causative mechanism. In the early days of the life of the prestressed specimens the epoxy end-blocks ensured the transfer of prestress into the glass concrete matrix. After 7 days, however, two specimens of each series were subjected to three-point bending, after their epoxy end-blocks had been cut off. The length of those specimens was thus reduced from 7 in (180mm) (plus the two end-blocks), to about 5 in (127mm), Fig. 5.13. Bending experiments, however, were carried out on the same 4.5 in (114mm) span. The resulting load-strain curves (compiled in Appendix A) were no different than those obtained with specimens that were tested with their end-blocks in place. The residual strains of

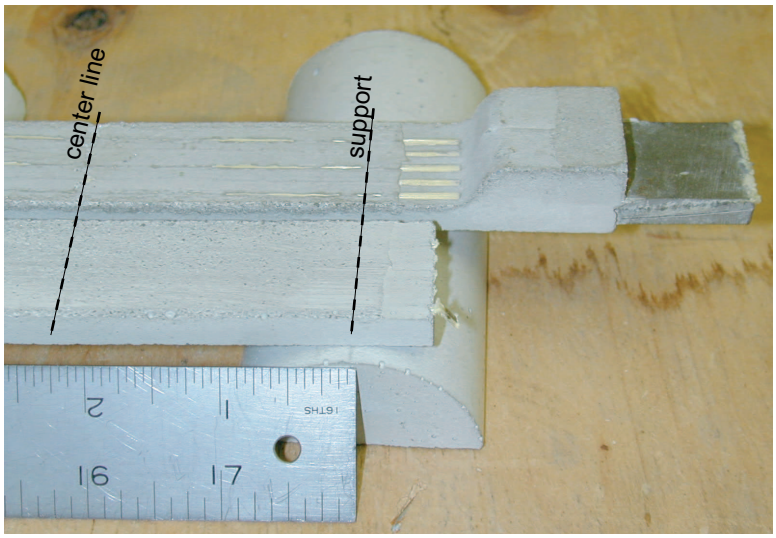

Figure 5.13: Prestressed Thin Beams with and without Epoxy End-Block

Table 5.4: Permanent Strain in % after Three-Point Bending (subscript "cut" indicates specimens with their end-blocks removed)

	Specimen			
Prestress (ksi)	**00**	**01**	**02**	**03**
0	0.50_{cut}	0.31	0.34	0.31_{cut}
0.5	0.35_{cut}	0.27	0.29	0.26_{cut}
1.0	0.24	0.22_{cut}	0.21_{cut}	0.21
1.5	0.18	0.29_{cut}	0.22_{cut}	0.23
2.0	n.a.	0.23_{cut}	0.22_{cut}	0.24

specimens (numbered 00, 01, 02, and 03) with and without end-blocks and at various prestress levels are summarized in Table 5.4. Apparently, enough bond was developed to transfer a prestress as high as 2 ksi (14MPa) into the concrete. Any fiber slippage would have reduced the stiffness of the cracked section and increased the permanent deflection after bending. Cracks were not noticeable with the naked eye after the 7-day bending experiment. Higher prestress seems to lead to more complete closure of cracks.

Table 5.5: Peak Loads in lbs of Reloaded Cracked Prestressed Thin Beams of Series *a2*(subscript "wet" indicates specimens, which were soaked in water prior to testing)

	Specimen			
Time (hours)	**00**	**01**	**02**	**03**
0	134	121	123	120
5	128	118	95_{wet}	94_{wet}
48	124	117	110	104

A separate issue is how the permanent deflection or strain increases after a large number of load applications. It was further observed, that the flexural performance of beams dropped considerably after they were submerged in water, and that their flexural capacity recovered when they were given time to dry. Specimens of series *a2*, prestressed with 0.5 ksi (3.5MPa), were investigated for the effect of moisture uptake on the flexural performance. Fig. 5.14 shows typical load-strain curves for a single specimen, which was bent in a dry state, then soaked in water for 5 hours, bent again, then dried for 2 days, and bent for a third time. Peak loads at 1.5% strain for all 4 specimens of test series *a2*, two of which were soaked prior the second loading, are summarized in Table 5.5. The load-strain curves are compiled in Appendix C. It is clear from the material properties of aramid fibers, that the stiffness of fibers is reduced upon moisture uptake, and that it recovers after drying. This explains Fig. 5.14, but the question, whether moisture uptake modifies the fiber-matrix or fiber-fiber friction remains.

To further investigate these two questions, specimens of series *a1*, *a3*, and *a5* were subjected to 100 load applications, cycling between 10 lbs (44N) and 70 lbs (311N) at a moderate loading rate of 10 lbs/s (44N/s) under load control. Half of the specimens were tested in dry condition, while the others were subjected to the cyclic loading after they had been fully saturated in water for 5 hours. Typical

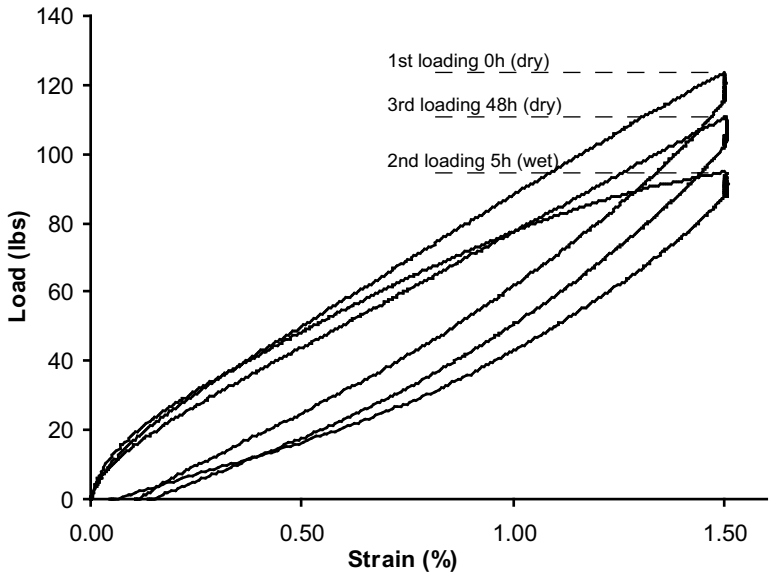

Figure 5.14: Repeated Loading (dry - wet - dry) of Specimen of Series *a2* (0.5 ksi prestress)

load-strain curves are shown in Fig. 5.15 and 5.16. The quantity of main interest is the accumulation of permanent strain, which in the illustrated cases were 0.21% and 0.44%, for the dry and the wet specimens, respectively. Complete results are summarized in Table 5.6.

There is a number of observations that can be made:

Table 5.6: Accumulated Permanent Strain in % of Prestressed Thin Beams due to Cyclic Loading (subscript "wet" indicates specimens, which were soaked in water prior to testing)

	Specimen			
Prestress (ksi)	**00**	**01**	**02**	**03**
0	0.42_{wet}	0.44_{wet}	0.21	0.11
1.0	n.a.	0.17	0.30_{wet}	0.36_{wet}
2.0	0.53_{wet}	0.14_{wet}	0.05	0.07

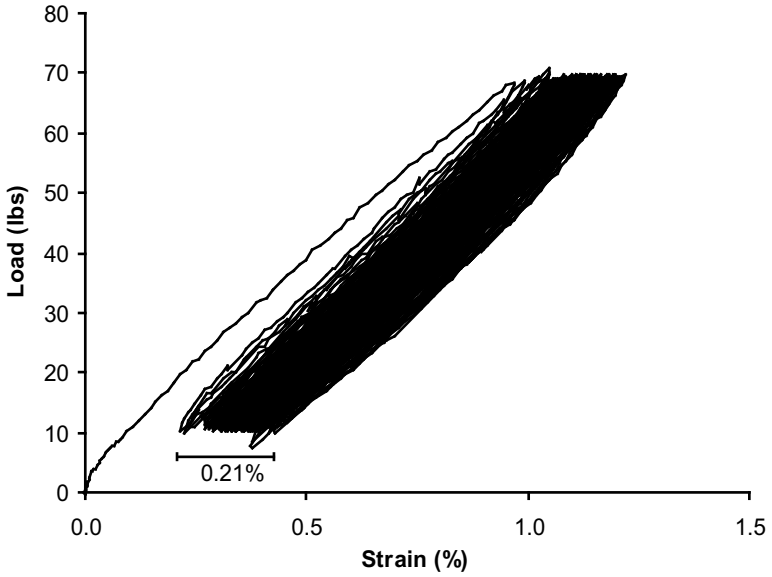

Figure 5.15: Cyclic Loading of a Dry Specimen (series *a1*)

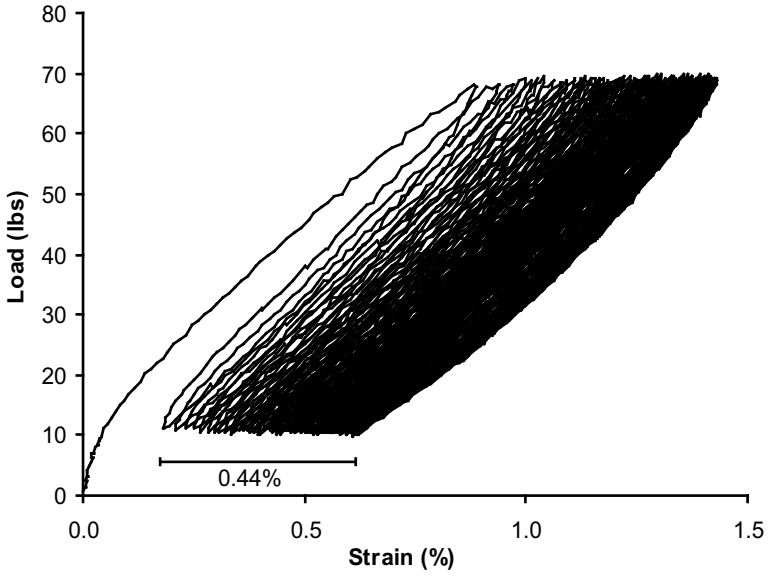

Figure 5.16: Cyclic Loading of a Wet Specimen (series *a1*)

- Residual strain accumulates upon repeated loading. It follows, that a certain, but small, slip of fibers may occur during each bending application. In environments with large repetitions of loadings, permanent deflections may be visible after some time.

- Applications in wet environments should be further investigated. The performance of prestressed elements will suffer, when they are wet. Fibers will be softer when wet, but they regain their original stiffness after drying. The flexural performance of concrete reinforced with aramid fibers varies accordingly.

- Wetting of specimens not only reduces the load response at a given strain, it also increases the permanent set when the specimen is subjected to a large number of loading cycles in a wet state. The moisture not only affects the fiber stiffness, but also the friction among them, i.e. the overall bond of the roving in the prestressed matrix.

5.8 Beams with 1/8 in Thickness

In addition to series *a1-a5*, three more series *a6-a8* were produced, but with 1/8 in (4mm) thickness. The beams were prestressed to 0, 1, and 2 ksi (0-14MPa), respectively. There are no observations, which have not already been pointed out in the previous sections. However, the slenderness of the specimens and their spectacular deformability, Fig. 5.17, are reasons for presenting them at this point. Note, that the specimen in the photograph fully recovers to its original shape upon removal of the loading and that cracks in the unloaded state are not noticeable with the naked eye. Fig. 5.18 shows load-strain curves of three representative specimens at the various prestress levels. The curves completely compiled in Appendix E showed a

Figure 5.17: 1/8 in Thin Prestressed Beam Specimen

much larger scatter of load responses for given strains than the corresponding results in the cases of 1/4 in (7mm) thick specimens. No attempt is made at this point to explain this observation.

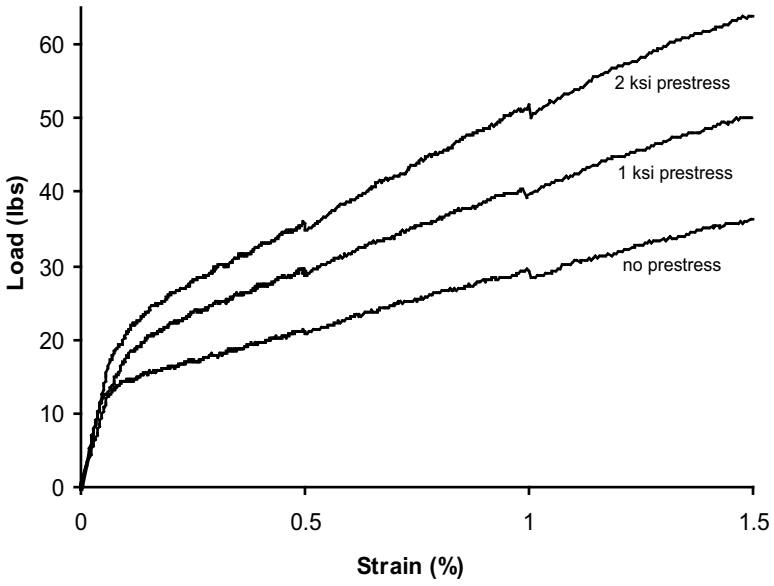

Figure 5.18: Load-Strain Curves for 1/8 in Thin Specimens for Various Prestress Levels

Chapter 6

Summary, Conclusions, and Future Research

6.1 Aramid Fibers

Within the context of this study, the presented body of knowledge and experimental evidence on aramid fibers can be summarized as follows:

1. Deformation mechanisms of highly orientated polymer fibers, such as aramid are well understood in the polymer research community. Numerical models successfully explain the time- and strain-dependent mechanical performance of aramid fibers in uniaxial tension as well as in compression.

2. The deformation mechanism of aramid fibers is twofold. The reversible linear elastic stretching of the molecular PpPTA chains is accompanied by the irreversible reorientation of crystallites towards the fiber axis. The second mechanism is strain-dependent and can almost be eliminated for consecutive loading by mechanically preconditioning, i.e. prestretching the fiber to a level just below ultimate strength.

3. High-modulus fibers deform upon tensile loading almost linear elastically up to fibrillar failure. When properly preconditioned and especially when several thousand single fibers are involved, perfectly linear elastic mechanical behavior can be assumed and a higher fiber stiffness be obtained.

4. The viscoelastic behavior is controlled by large primary and considerably lower secondary creep strains. Again, when properly preconditioned, primary creep or relaxation will be greatly reduced for consecutive loadings. The secondary creep or relaxation can be conveniently described by exponential or logarithmic decay functions of time with one single creep or relaxation coefficient.

5. The stiffness and the strength of fibers in compression is considerably lower than in tension. The dominant failure mode in compression is the formation of kink bands.

6. Aramid fibers are chemically highly inert. But under the impact of concentrated NaOH solution, stressed fibers will ultimately give up a considerable amount of prestress, not due to degradation, but because of weakened secondary bonds between fibrils within single fibers.

The single most important information obtained from investigating the fibers is the beneficial effect of mechanical preconditioning by means of prestretching the rovings to improve relaxation properties. Work should continue towards verifying the results, especially by applying the viscoelastic models supplied by the polymer research community.

More work is needed to understand the relaxation properties of aramid fibers in humid and alkaline environments, which is of great importance for actual prestressed concrete structures. When exposed to water or alkaline solutions in a strain-controlled loading setup, fibers rapidly loose some fraction of their loading, but then seem to stabilize. The mechanisms, which are responsible for this behavior are not yet fully understood.

6.2 Glass Concrete

Glass concrete has outstanding esthetic potential. Utilizing white cement with metakaolin generates a matrix with superior color stability over time. Colored matrixes can be combined with specific colors and particle sizes of glass particles to produce a variety of architectural concrete surfaces that can not be achieved with any other materials.

For prestressed thin sheets a glass concrete matrix was developed with a high-early strength of 5 ksi (14MPa) after 20 hours. The mix is of excellent workability, but due to the usage of metakaolin must be consolidated using brief external vibration. Mechanical properties and shrinkage deformations have been determined. For the practical aspects of prestressed glass concrete applications creep properties must also be determined, either according to ASTM standard C-512, or the non-standard setup discussed in Chapter 5.

Although glass concrete is already being produced commercially, it has not yet been shown what mechanisms exactly are responsible for successfully inhibiting ASR, when glass is used as the exclusive aggregate. It would be instructive to measure the amount of lime generated throughout the first hours of hydration, as well as concentration of hydroxide ions. Water and ion penetration through glass concrete should be studied, since ASR is closely tied to transport phenomena.

6.3 Generation of Prestress

An epoxy end-block system was developed to generate and hold prestress in several layers of fiber mesh. The system proved to be reliable to produce thin beams with cross-sections of $1/4 \times 1$ in^2 (7 mm $\times$ 25 mm) and $1/8 \times 1$ in^2 (3.5 mm $\times$ 25 mm) and

reinforced with roving systems containing 20 and 15 parallel rovings, respectively. Prestress levels up to 2 ksi (14MPa) were generated. To use the aramid rovings more economically, the number of rovings should be reduced, such that the fiber system can be used at about 50% of its capacity. This would reduce the number of rovings for the 2 ksi (14MPa) case by more than one half. The epoxy end-block system used in this study would not be able to hold the rovings at such a high load level.

The system developed for this study was adequate for investigating characteristics and properties of prestressed thin sheets on a small scale for research purposes only. For prestressed thin sheets closer to realistic applications, either the epoxy system needs to be modified to generate better bond, or an altogether different prestressing system would need to be developed. A first target application would be a thin sheet of at least 2×2 ft^2 (0.6×0.6 m^2) size.

6.4 Prestress Losses

1. Hydration

    - A tensile load of the order of 10% is lost during the first 3 hours of hydration. Since the rovings are held by steel formwork, the strain of the roving system remains constant. The stiffness of the roving system is also reduced by 10%.
    - The loss appears to be influenced by the early hydration characteristics of the concrete system, i.e. its alkalinity, flow and setting time.
    - The loss is independent of the target prestress, but a function of the strain, to which the rovings are stretched. The more strain, the more loss during hydration.

2. Load Transfer

   - The loss is caused by the elastic shortening of the concrete specimen during load transfer, which is a function of the stiffness of the concrete system and of the transferred prestress force.
   - The more rovings are used to generate the prestress, the more prestress is lost, due to the increased stiffness of the roving system.
   - The prestress loss observed for specimens prestressed with 20 rovings was 20%.

3. Combined Shrinkage and Drying Creep

   - This prestress loss is caused by the shortening of the concrete specimen as it dries under load, which is a function of the concrete system, the curing environment, and the amount of prestress.
   - The more rovings are used to generate the prestress, the more prestress is lost, due to the increased stiffness of the roving system.
   - The shrinkage observed for non-prestressed glass concrete specimens was 0.04%.
   - Combined shrinkage and drying creep observed on one specimen prestressed at 0.5 ksi (3.5MPa) over 7 days was 0.085%.

Prestress losses due to elastic shortening, shrinkage, and creep can be reduced by minimizing the number of rovings used to generate the required prestress, i.e. by stressing the rovings to higher levels. This should not affect losses due to relaxation, but could increase the loss of prestress force during early hydration. A sufficient

factor of safety must be maintained to exclude the possibility of brittle fiber failure when prestressed composites are subjected to flexural loading.

It is obvious that more testing is needed to better understand the creep behavior of glass concrete thin beams, also with higher amounts of prestress. It is further suggested to monitor creep over extended time spans, to compare the creep behavior of glass concrete with regular metakaolin modified concrete systems, Fig. 3.3.

The loss of prestress during early hydration is least understood, yet most fascinating. More tests are recommended to study how fresh concrete properties and different concrete systems in particular effect this phenomenon; whether a regular concrete system causes more tension losses; how much protection the rovings get from the proprietary coating; and how much more load the rovings loose if stressed to 50% of their load bearing capacity.

6.5 Flexural Performance

Principles of prestressed concrete theory apply well to thin glass concrete beams prestressed with unprotected aramid rovings. As expected, cracking was delayed, response at given load levels greatly improved, and ductility reduced by application of prestress. Cracks closed upon the removal of load, and beams could be loaded repeatedly to similar load levels, even months after the first bending experiment, during which the tensile zone of the concrete cracked. Permanent displacements after bending experiments were minimal, but accumulated under repeated load applications.

A certain bond between rovings and concrete matrix was developed. This observation is based on the distributed crack patterns in three-point bending as well

as the fact, that beams with their epoxy end-blocks removed performed just as well as beams with their end-blocks in place. Although three-point bending was found to be a simple and reliable way to test performance of prestressed thin beams, it would be instructive to perform uniaxial tension tests or single roving pull-out tests to study the bond in more detail. Also four-point bending should be performed on larger spans to study the cracking patterns (distances between cracks and crack widths). If the number of rovings is decreased to reduce prestress losses and to use the material more economically, bond stresses will increase eventually beyond the bond strength. The same is expected if the weight, that is the denier number of rovings is increased. Fibers located in the core of a roving will slip more easily in heavier rovings stressed to larger strains.

Considering the complexity of concrete thin sheets prestressed with aramid fabrics, it will be a challenge to model their flexural behavior numerically. Efforts to numerically simulate the bond and pull-out behavior of rovings (different fiber and matrix materials, coatings, prestress, number of filaments, etc.) are underway at different universities. Complex non-linear numerical models will have to rely not only on the material laws of the constituents of the prestressed composite, but especially on such bond and pull-out models. Since the matrix in this study was confined by prestressed rovings, aligned with very small spacings, size effects are also expected to play an important role.

6.6 Durability

Prestress levels appear to be stable over time, yet this has to be verified in practice. In the present study, specimens were subjected to bending after more than three months and the performance was not found to be affected by the age of the specimens. It has

been observed that beams prestressed with aramid fibers perform differently when tested in wet condition. The load response in a strain-controlled bending experiment decreased considerably, but then improved again after the specimen was dried. The increased accumulation of permanent set in cyclic loading tests suggests a different fiber-slip behavior in a wet environment. The effect might be expected to be more pronounced in larger rovings, because a higher percentage of the single fibers would be within the roving core, rather than in the outer ring of fibers, which could be penetrated by the concrete matrix. The performance of wet specimens is important, when wet-room and outdoor applications of prestressed thin sheets are considered. In addition, out-door applications call for more durability testing, such as resistance to freezing and thawing.

6.7 Summary of Findings

Although numerous questions and open problems were addressed in the last paragraphs, a number of findings and achievements was presented.

1. Aramid fibers are used in structural engineering mainly in the form of FRP. This is one of few studies, where unprotected aramid fibers were utilized to reinforce a Portland cement-based matrix. Despite the concern, that the alkalinity of concrete may cause severe damage, especially to prestressed aramid fibers, it was shown for the first time that such high-performance polymeric fibers can be used to produce thin sheets made of glass concrete with prestress levels up to 2 ksi (14MPa). It was found that during the first few hours of the hydration process, when the fibers are still anchored against the formwork, certain mechanisms cause a rapid loss of 10% of the prestress force, but that

the tension level of the rovings stabilizes as the concrete hardens after approximately 3.5 hours. Besides normal prestress losses due to elastic shortening during load transfer, shrinkage and creep, the prestress level was not found to decay within up to 3 months.

2. A glass concrete mix design was developed that combines excellent workability with high-early strength. Using glass concrete as the prestressed matrix will allow to further explore the great esthetic potential of this novel material in form of prestressed thin sheet applications. Compatibility of aramid fibers with ordinary concrete matrixes still has to be shown. It is assumed that some of the mechanisms, which inhibit ASR in glass concrete, also ensure the structural stability of the prestressed aramid fibers, for their primary degradation mechanism is hydrolysis caused by the same alkaline environment, which is responsible for the initiation of ASR.

3. Few studies in the field of structural engineering have investigated aramid fibers with regard to their microstructure. This work gives a detailed overview on what aramid fibers are, how they deform, and especially what makes them different from solid fibrous materials such as glass or carbon. Understanding their basic deformation mechanism allows for the utilization of mechanical preconditioning to greatly reduce tension losses caused by relaxation. This finding will also be of importance to conventional prestressing applications where aramid fibers are used as FRP.

4. Results from bending experiments carried out with prestressed beams with thicknesses of 1/4 in (7mm) and 1/8 in (3mm) are very promising. The relatively small rovings develop sufficient bond with the glass concrete matrix

to transfer prestress as high as 2 ksi (14MPa). The epoxy end-blocks developed especially for this study could be safely removed after 7 days, prior to the bending experiments, with no negative effect on the flexural performance. Basic principles of prestressed concrete theory apply also to prestressed thin sheets. Especially the large deformability of the 1/8 in (3mm) thin specimens may offer entirely new applications for concrete based materials.

5. Residual strains after bending experiments were found to be very small. Combined with a permanently compressed matrix, very large numbers of loading cycles need to be applied to produce permanent visible deflections. However, when the specimen is wet during load application, accumulation of residual strains can be greatly accelerated. This finding is critical for the development of prestressed thin sheets for outdoor or wet-room applications.

The use of aramid fibers for prestressing thin sheets made of glass concrete was at first inspired by their outstanding success as the basis material for the production of body armor. In this work, their ability to undergo large deformations by dissipating extensive amounts of energy was successfully extended to the similarly promising fields of textile-reinforced concrete and Portland cement-based thin sheet applications.

Appendix A

Load-Strain Curves of Three-Point Bending of Specimens with 1/4 in Thickness after 7 Days

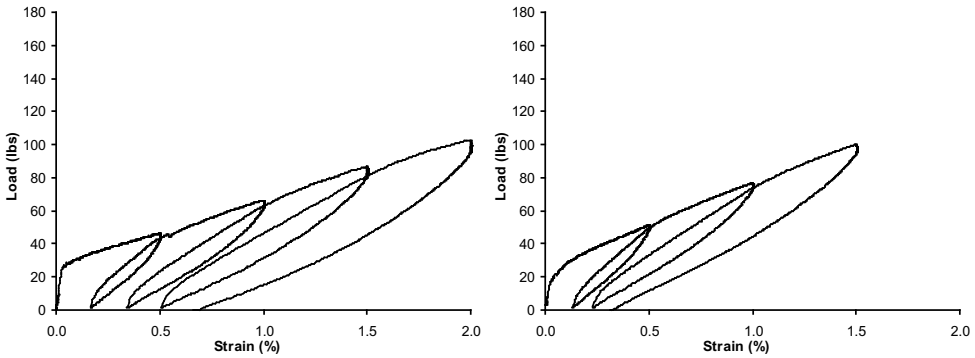

(a) Specimen 00 (no end-blocks)

(b) Specimen 01

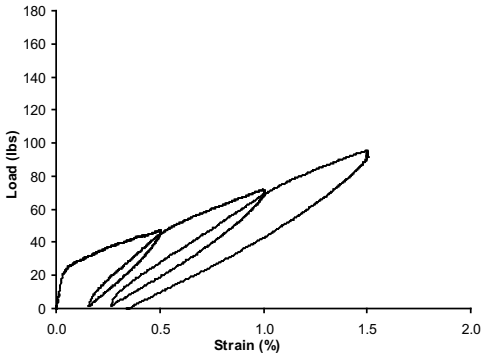

(c) Specimen 02

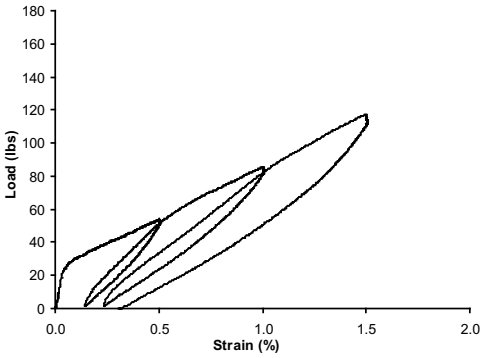

(d) Specimen 03 (no end-blocks)

Figure A.1: Cyclic Bending of Specimens of Series *a1* (no prestress)

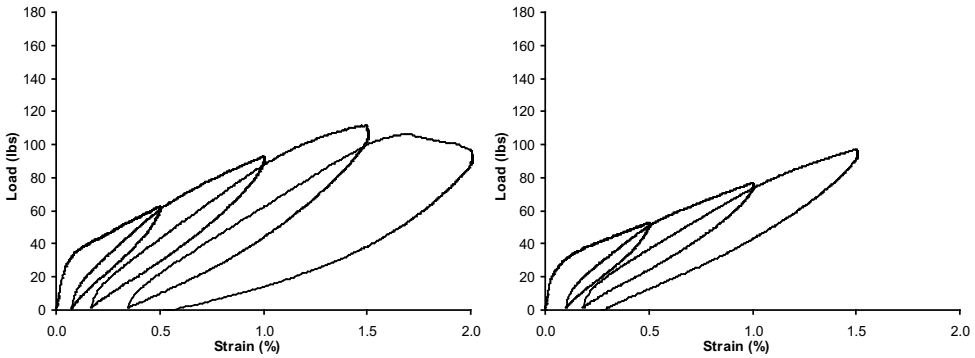

(a) Specimen 00 (no end-blocks)

(b) Specimen 01

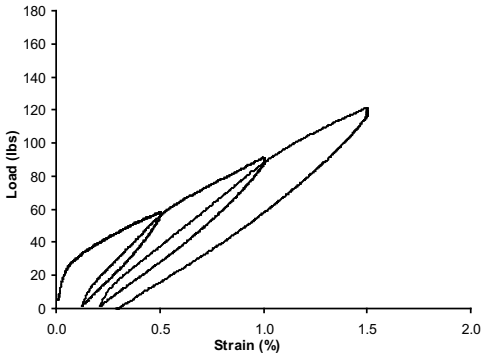

(c) Specimen 02

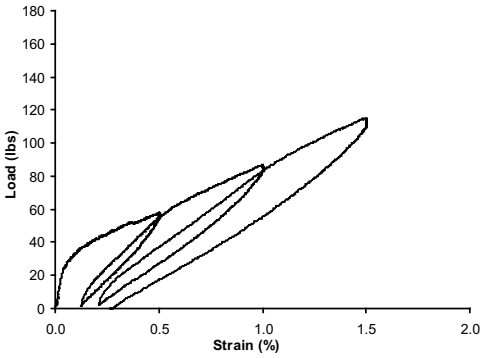

(d) Specimen 03 (no end-blocks)

Figure A.2: Cyclic Bending of Specimens of Series *a2* (0.5 ksi prestress)

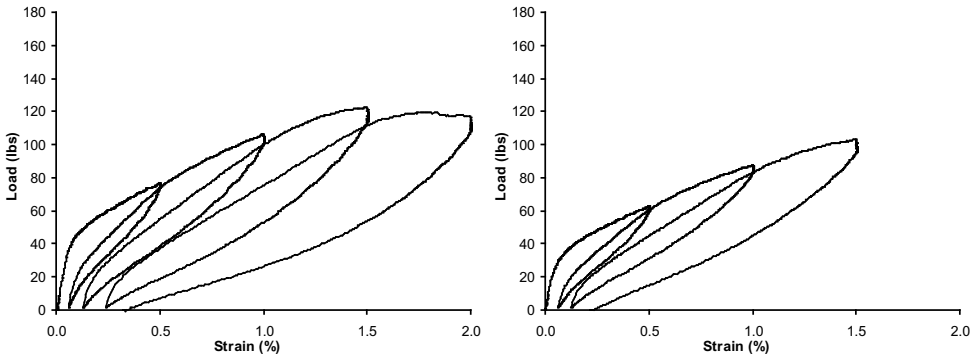

(a) Specimen 00

(b) Specimen 01 (no end-blocks)

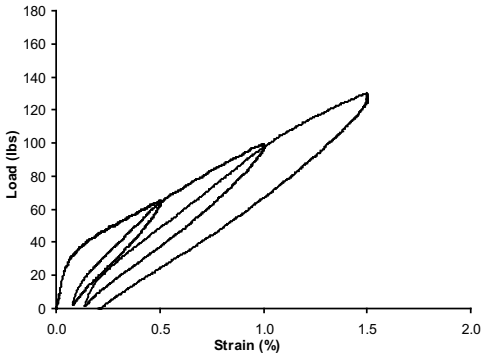

(c) Specimen 02 (no end-blocks)

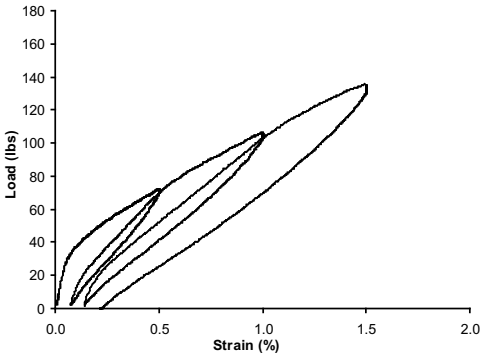

(d) Specimen 03

Figure A.3: Cyclic Bending of Specimens of Series *a3* (1 ksi prestress)

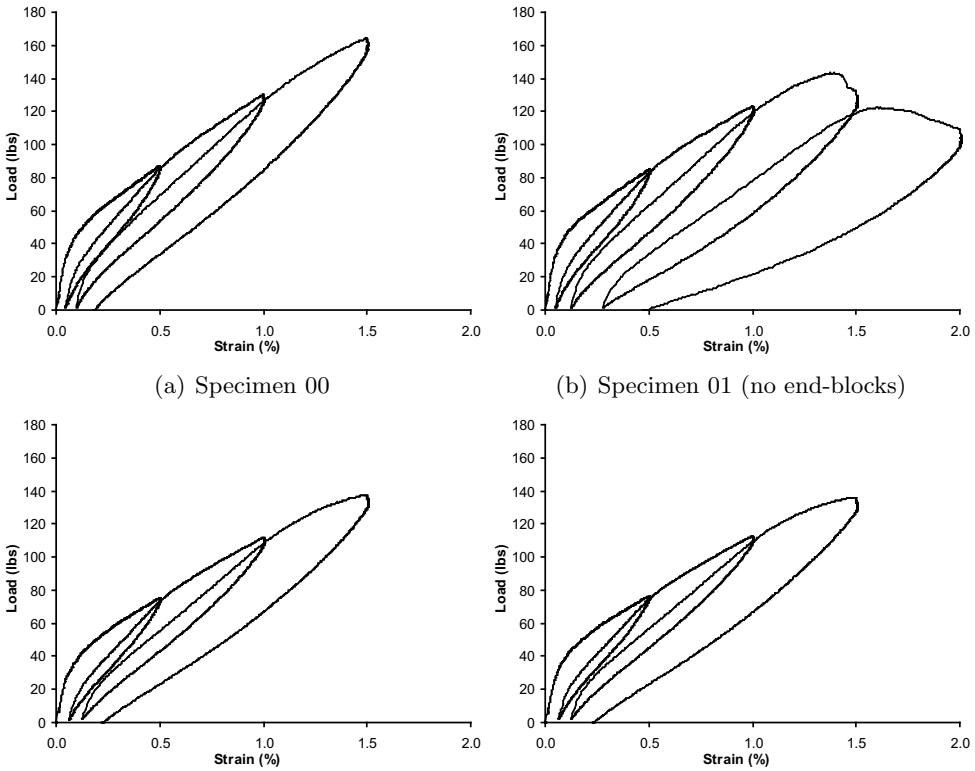

(a) Specimen 00

(b) Specimen 01 (no end-blocks)

(c) Specimen 02 (no end-blocks)

(d) Specimen 03

Figure A.4: Cyclic Bending of Specimens of Series *a4* (1.5 prestress)

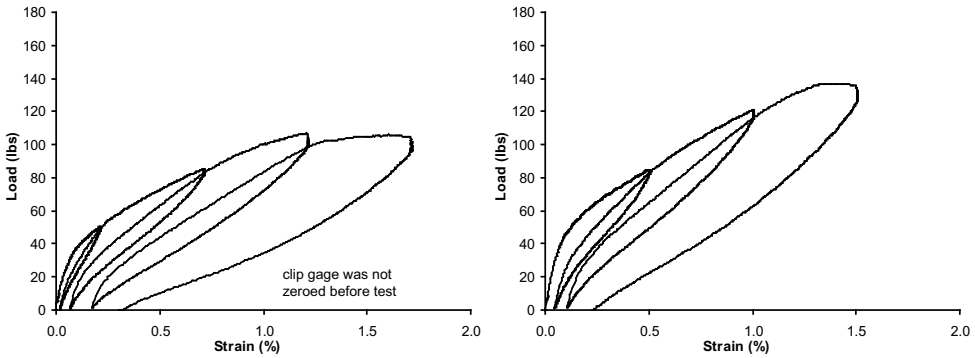

(a) Specimen 00

(b) Specimen 01 (no end-blocks)

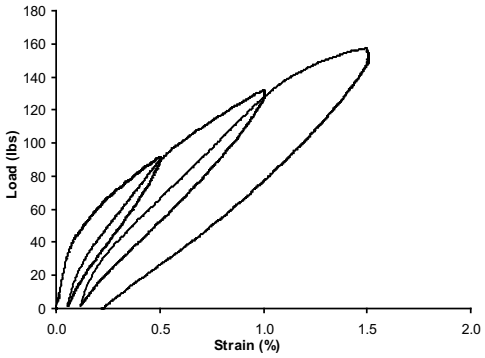

(c) Specimen 02 (no end-blocks)

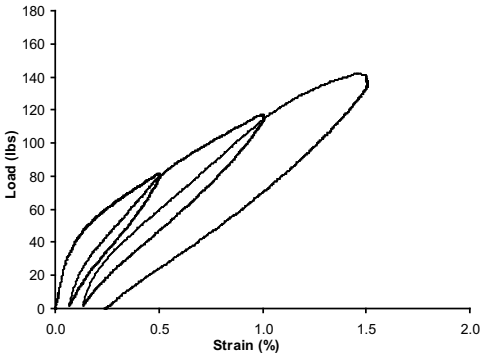

(d) Specimen 03

Figure A.5: Cyclic Bending of Specimens of Series *a5* (2 ksi prestress)

Appendix B

Load-Strain Curves of Repeated Three-Point Bending after 14, 21, and 28 Days

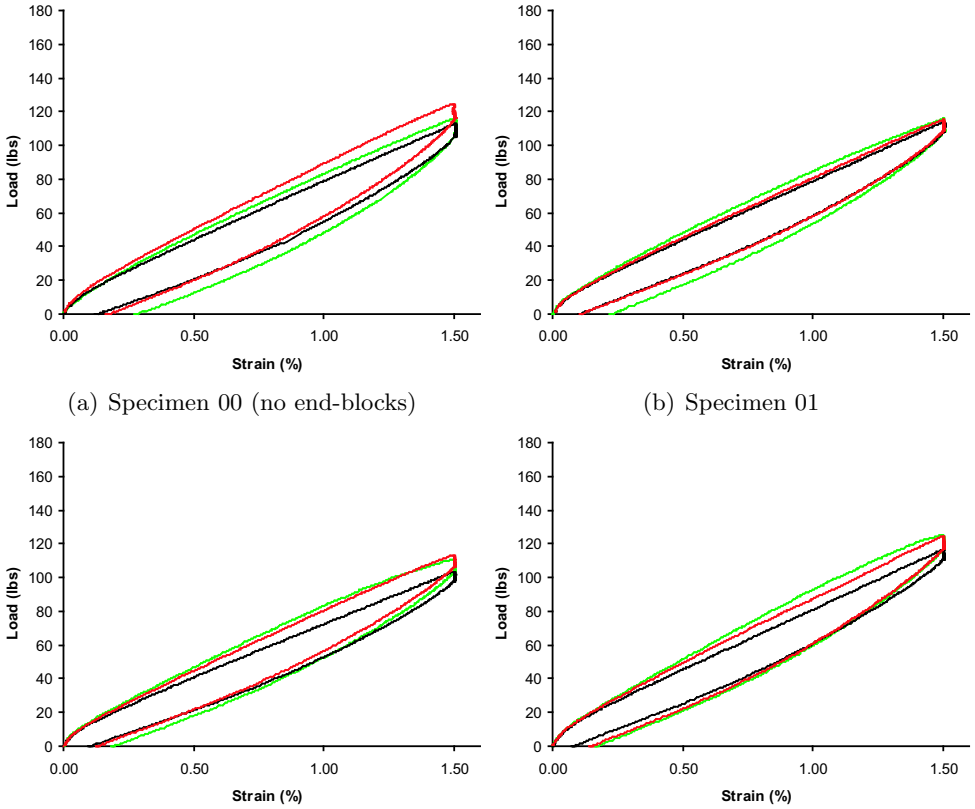

(a) Specimen 00 (no end-blocks)

(b) Specimen 01

(c) Specimen 02

(d) Specimen 03 (no end-blocks)

Figure B.1: Repeated Bending of Specimens of Series *a1* (no prestress) green - 14 days, red - 12 days, black - 28 days

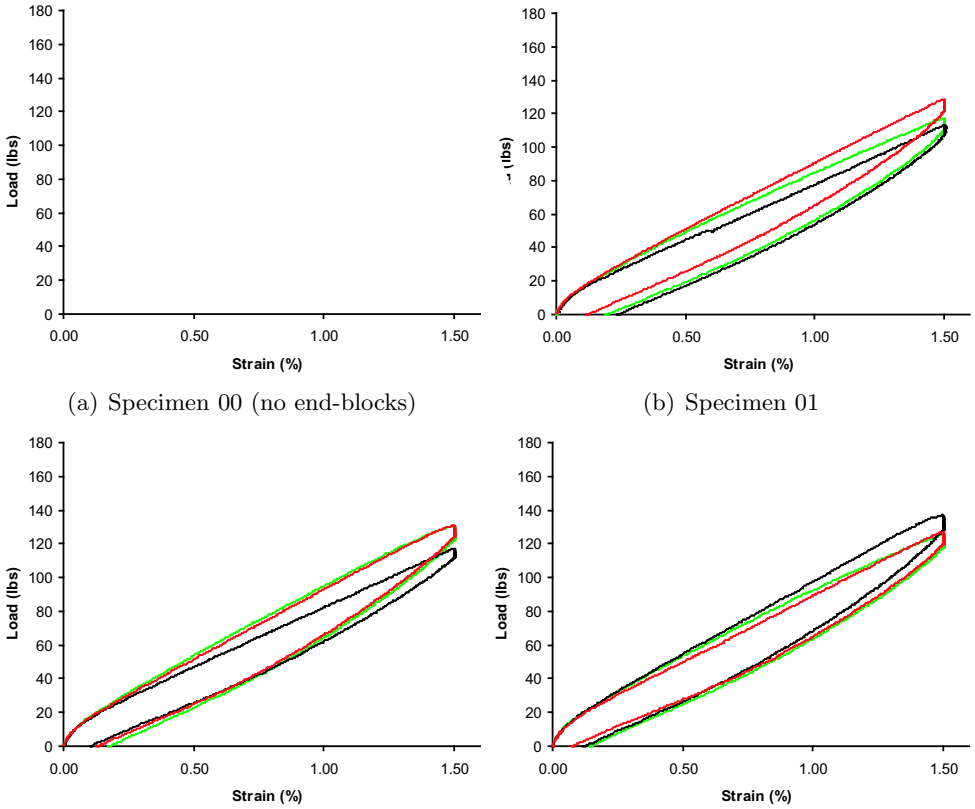

(a) Specimen 00 (no end-blocks)

(b) Specimen 01

(c) Specimen 02

(d) Specimen 03 (no end-blocks)

Figure B.2: Repeated Bending of Specimens of Series *a2* (0.5 ksi prestress) green - 14 days, red - 12 days, black - 28 days

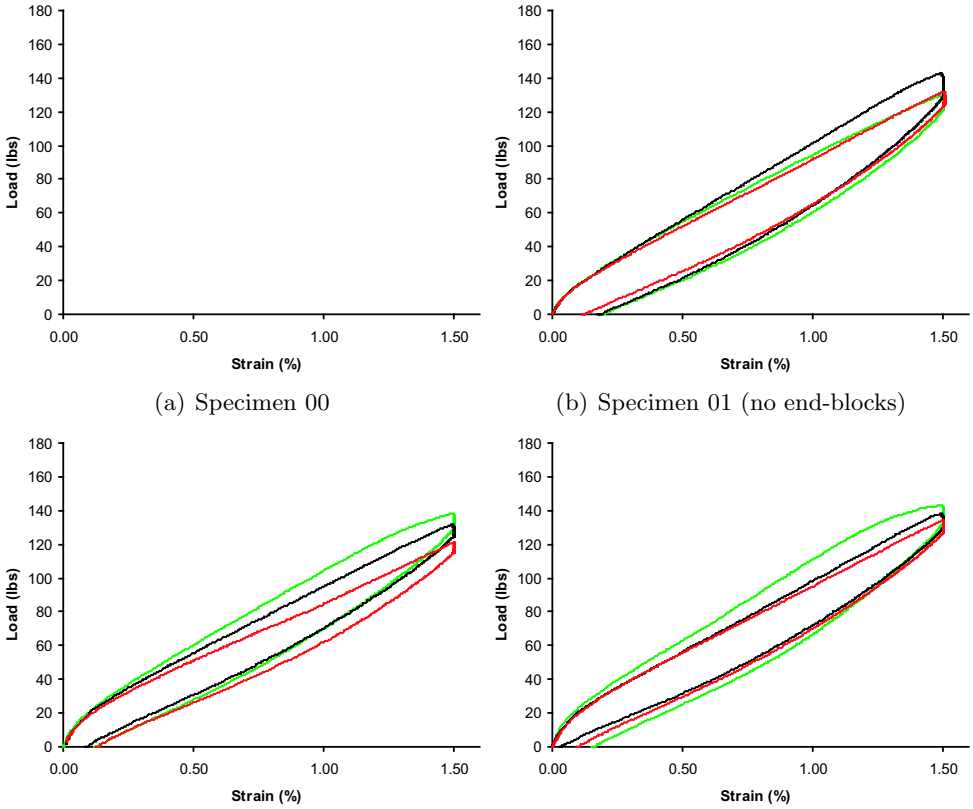

(a) Specimen 00

(b) Specimen 01 (no end-blocks)

(c) Specimen 02 (no end-blocks)

(d) Specimen 03

Figure B.3: Repeated Bending of Specimens of Series *a3* (1 ksi prestress) green - 14 days, red - 12 days, black - 28 days

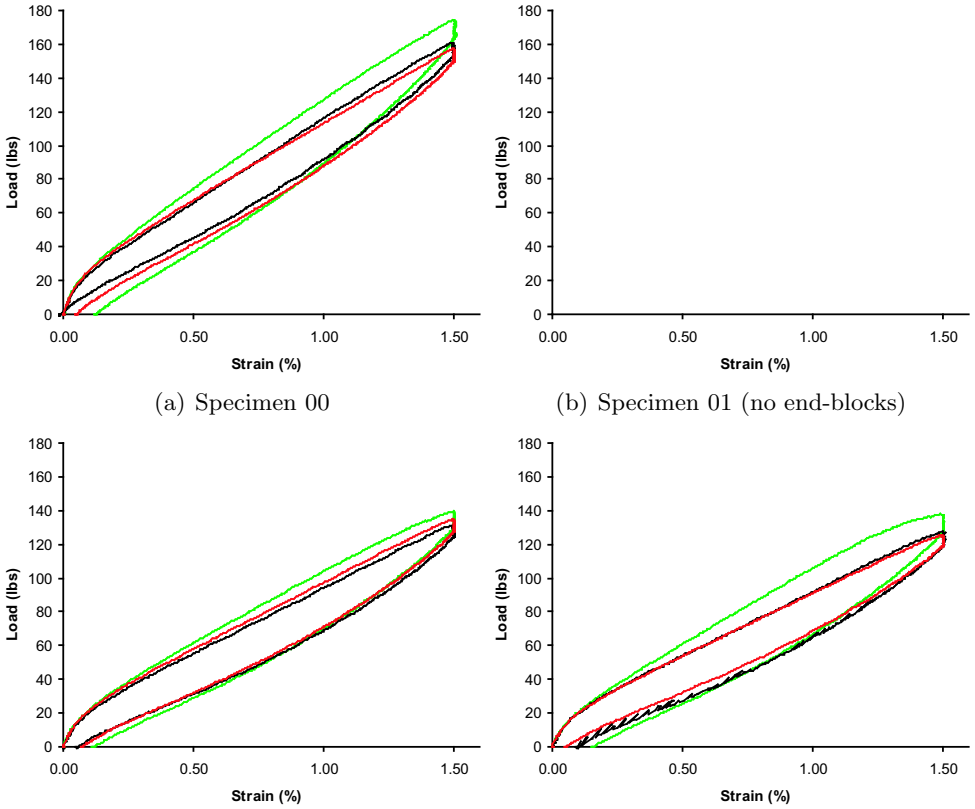

(a) Specimen 00

(b) Specimen 01 (no end-blocks)

(c) Specimen 02 (no end-blocks)

(d) Specimen 03

Figure B.4: Repeated Bending of Specimens of Series *a4* (1.5 prestress) green - 14 days, red - 12 days, black - 28 days

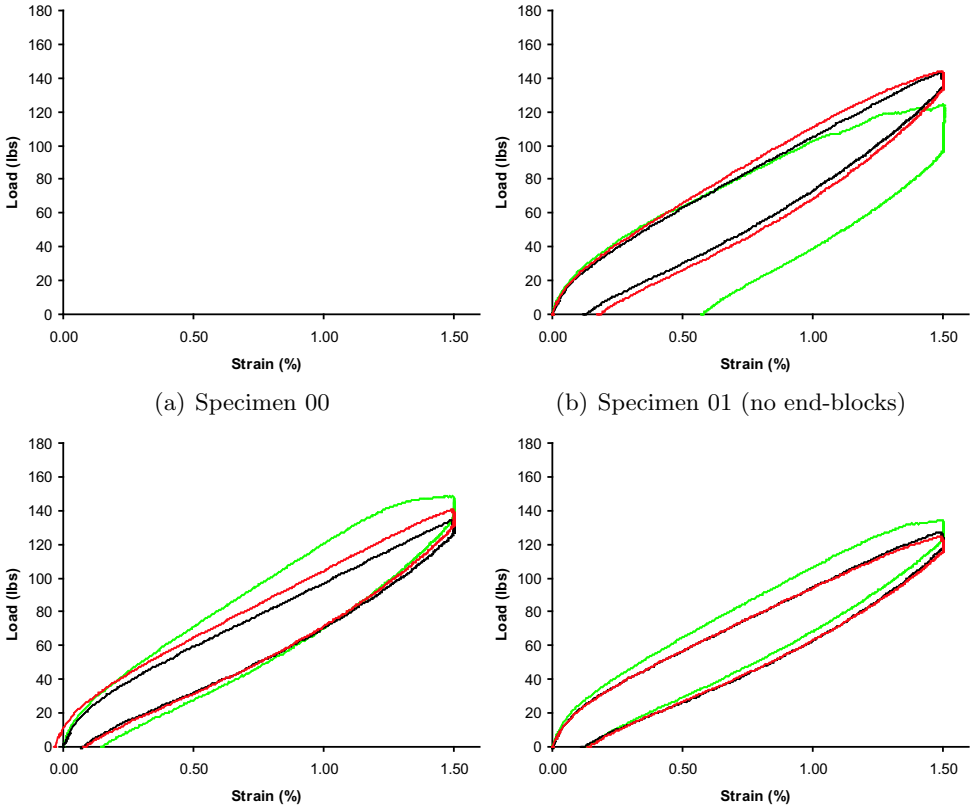

(a) Specimen 00

(b) Specimen 01 (no end-blocks)

(c) Specimen 02 (no end-blocks)

(d) Specimen 03

Figure B.5: Repeated Bending of Specimens of Series *a5* (2 ksi prestress) green - 14 days, red - 12 days, black - 28 days

Appendix C

Repeated Bending of Partially Wet Specimens of Series *a3* (1 ksi prestress)

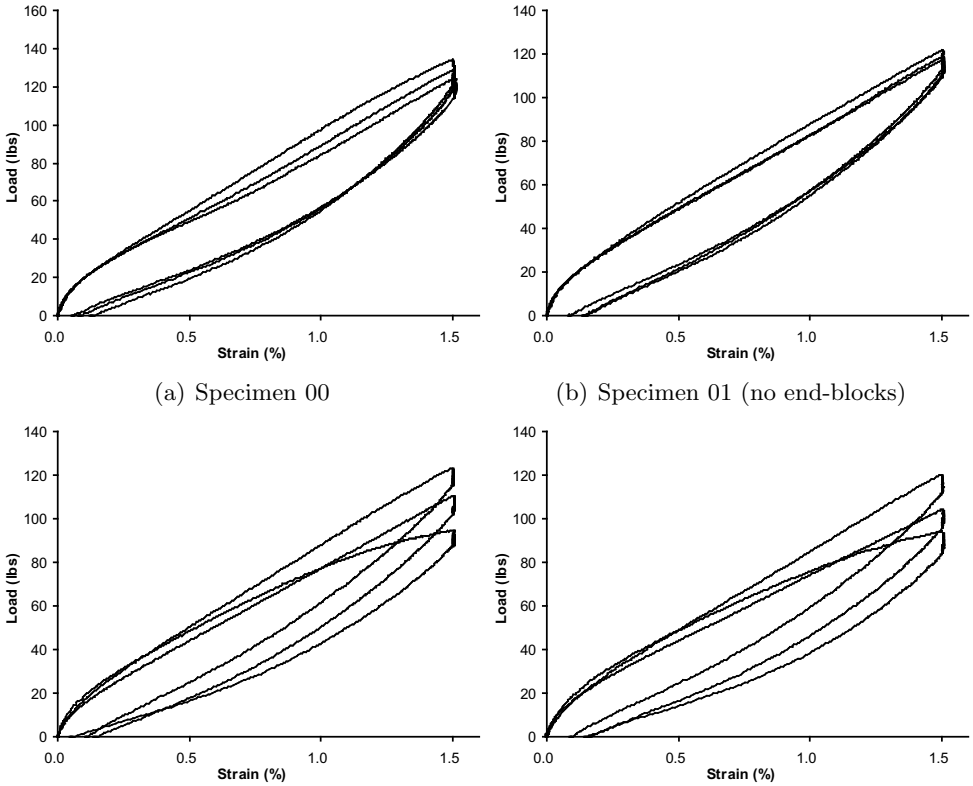

(a) Specimen 00

(b) Specimen 01 (no end-blocks)

(c) Specimen 02 (wet) (no end-blocks)

(d) Specimen 03 (wet)

Figure C.1: Repeated Bending of Partially Wet Specimens of Series *a3* (1 ksi pre-stress)

Appendix D

Cyclic Bending of Partially Wet Specimens of Series *a1, a3* and *a5* (0, 1, and 2 ksi prestress, respectively)

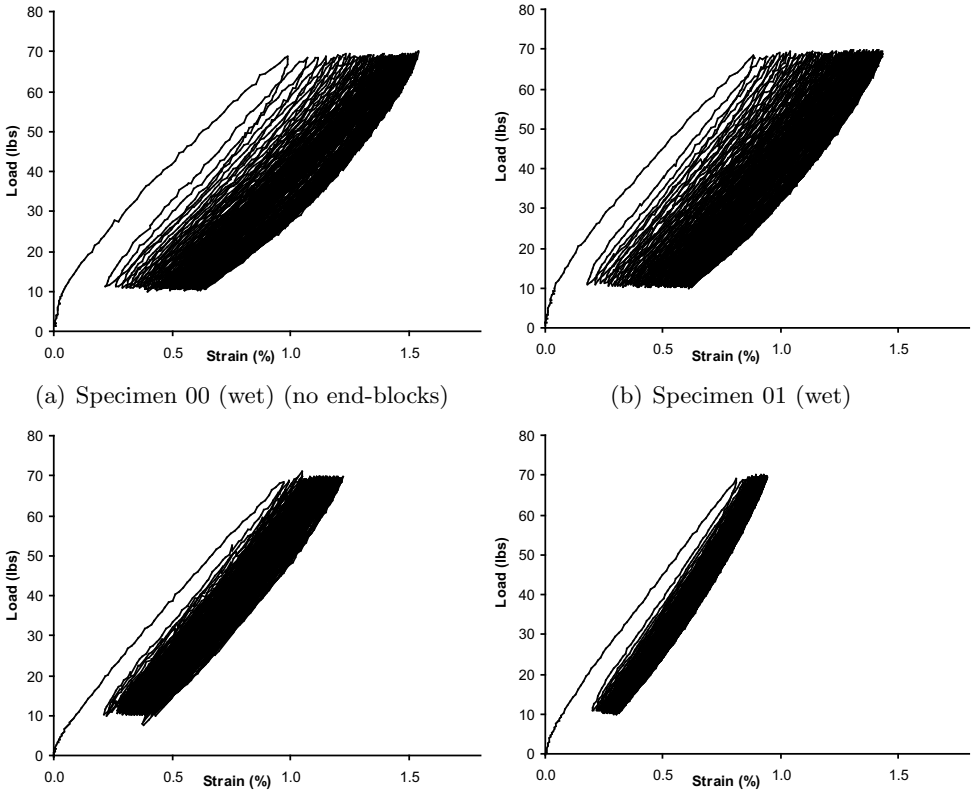

(a) Specimen 00 (wet) (no end-blocks)

(b) Specimen 01 (wet)

(c) Specimen 02

(d) Specimen 03 (no end-blocks)

Figure D.1: Cyclic Bending of Specimens of Series *a1* (no prestress)

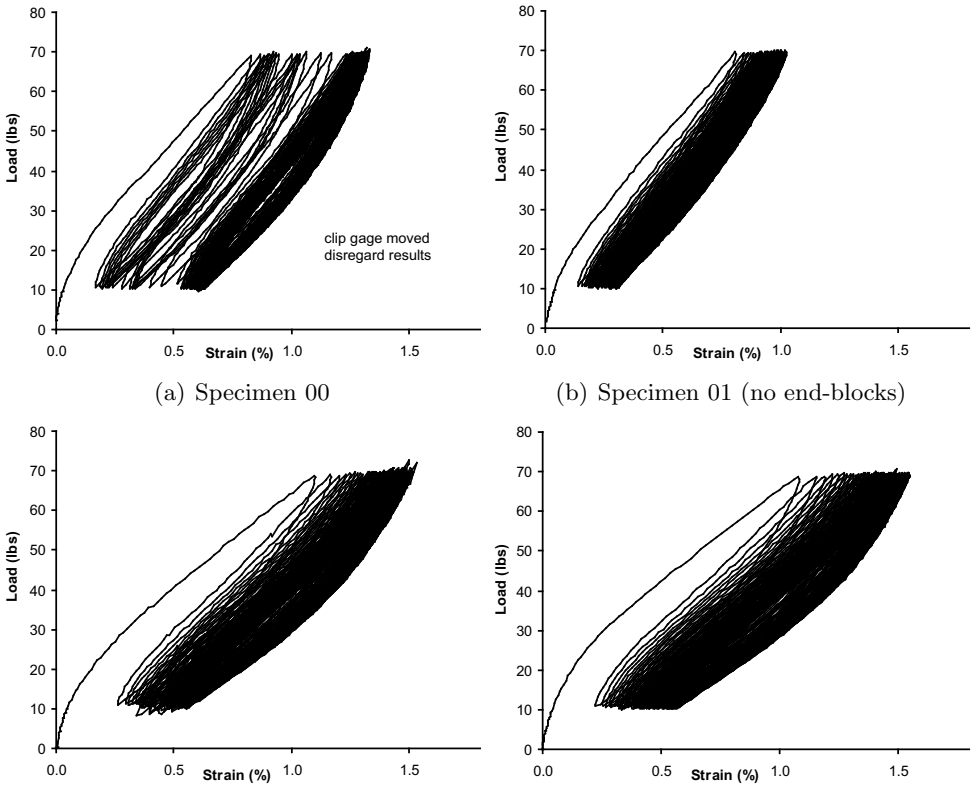

(a) Specimen 00

(b) Specimen 01 (no end-blocks)

(c) Specimen 02 (wet) (no end-blocks)

(d) Specimen 03 (wet)

Figure D.2: Cyclic Bending of Specimens of Series *a3* (1 ksi prestress)

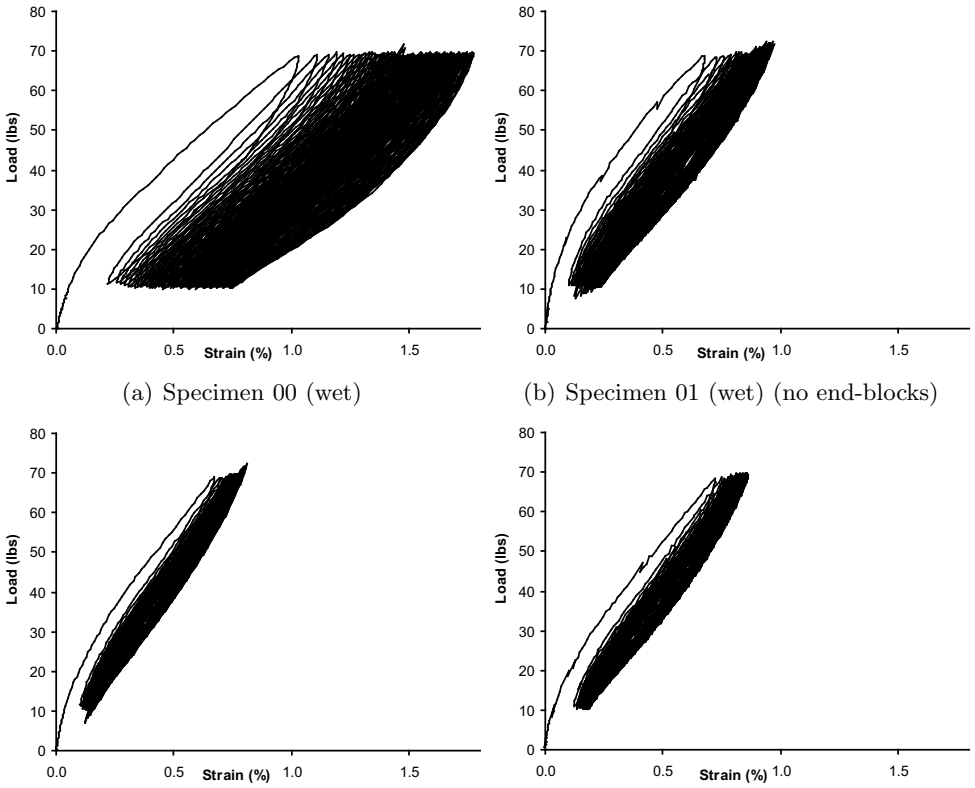

(a) Specimen 00 (wet)

(b) Specimen 01 (wet) (no end-blocks)

(c) Specimen 02 (no end-blocks)

(d) Specimen 03

Figure D.3: Cyclic Bending of Specimens of Series *a5* (2 ksi prestress)

Appendix E

Load-Strain Curves of Three-Point Bending of Specimens with 1/8 in Thickness after 7 Days

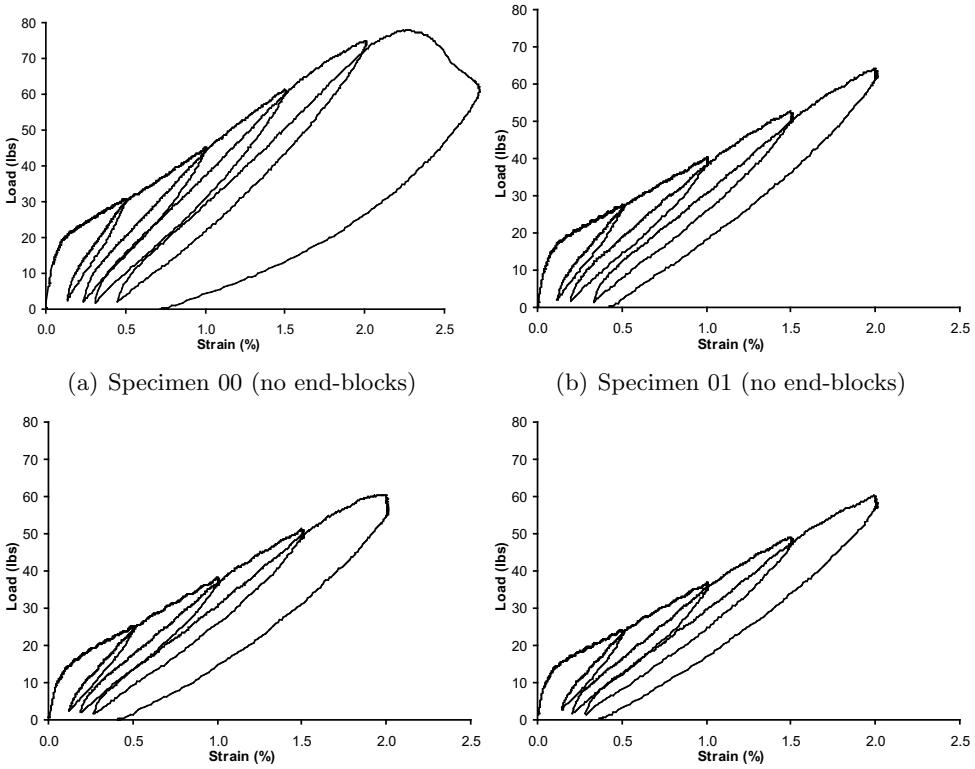

(a) Specimen 00 (no end-blocks)

(b) Specimen 01 (no end-blocks)

(c) Specimen 02

(d) Specimen 03

Figure E.1: Cyclic Bending of Specimens of Series *a6* (no prestress)

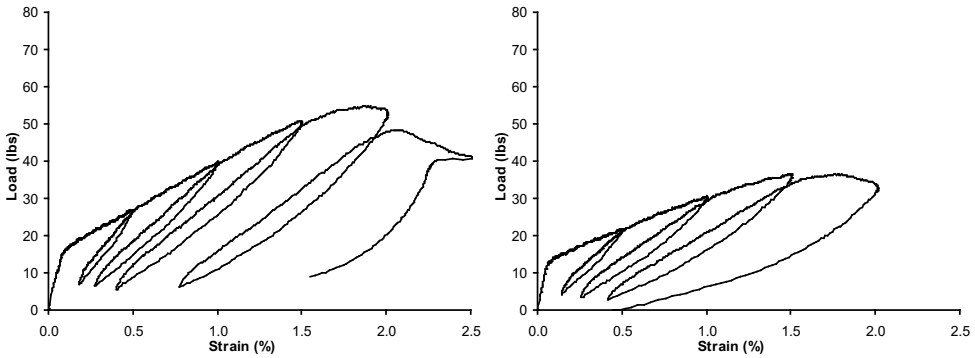

(a) Specimen 00

(b) Specimen 01 (no end-blocks)

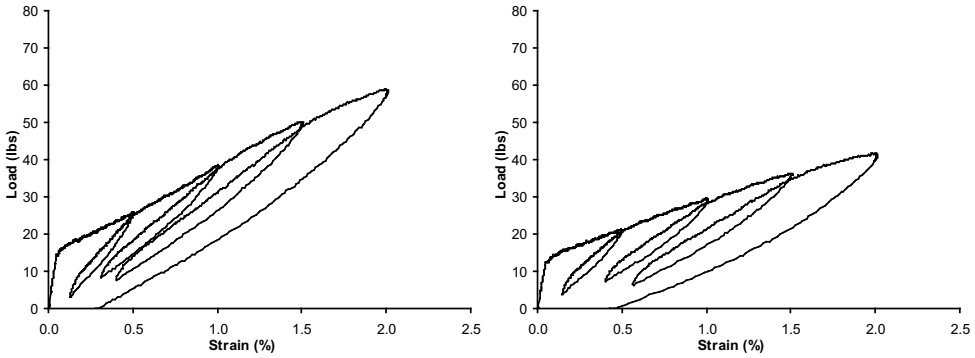

(c) Specimen 02

(d) Specimen 03 (no end-blocks)

Figure E.2: Cyclic Bending of Specimens of Series *a7* (1 ksi prestress)

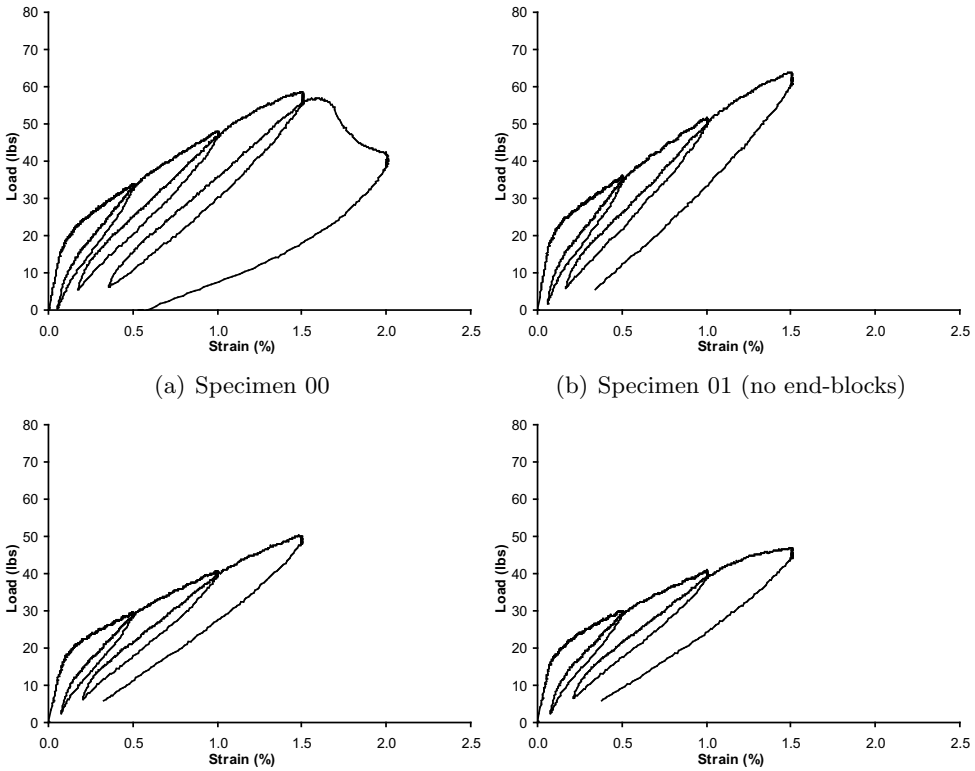

(a) Specimen 00

(b) Specimen 01 (no end-blocks)

(c) Specimen 02

(d) Specimen 03 (no end-blocks)

Figure E.3: Cyclic Bending of Specimens of Series *a8* (2 ksi prestress)

Bibliography

[1] American Concrete Institute Committee 318. *ACI Building Code and Commentary.* ACI, 2002.

[2] Allen and Roche. Deformation behaviour of kevlar. *Polymer*, 30:996–1003, 1989.

[3] Amaniampong. Variability and viscoelasticity of prallel-lay ropes. Ph.D. Dissertation at the University of Cambridge, UK, 1992.

[4] Amaniampong and Burgoyne. Statistical variability in the strength and failure strain of aramid and polyester yarns. *Journal of Materials Science*, 29:5141–5152, 1994.

[5] Amaniampong and Burgoyne. Analysis of the tensile strength of parallel-lay ropes and bundles of parallel elements by probability theory. *International Journal of Solids and Structures*, 32(24):3573–3588, 1995.

[6] Andrews, Lu, and Young. Compressive properties of aramid fibres. *Polymer*, 38(10):2379–2388, 1997.

[7] Norsk GlassGjevinning AS. Unlimited potential - glass concrete. http:// www.glassgjenvinning.no/ bruktnytt_eng/ muligheter.html, 1999.

[8] Asselanis and Mehta. Microstructure of concrete from a crack-free structure designed to last a thousand years. *Third CANMET/ACI International Sympo-*

sium on Sustainable Development of Cement and Concrete, ACI SP-202, pages 349–357, 2001.

[9] Balaguru, Naaman, and Weiss, editors. *Concrete: Material Science to Application, A Tribute to Surendra P. Shah, ACI SP-206*. ACI, 2002.

[10] Baltussen and Northolt. The elastic extension of polymer fibers in the glassy state: Experimental results. *Journal of Rheology*, 41(3):575–598, 1997.

[11] Baltussen and Northolt. The stress and sonic modulus versus strain curve of polymer fibres with yield. *Polymer*, 40:6113–6124, 1999.

[12] Baltussen and Northolt. The viscoelastic extension of polymer fibres: creep bahaviour. *Polymer*, 42:3835–3846, 2001.

[13] Baltussen, Northolt, and Hout. The continuous chain model for the elastic extension of polymer fibers in the glassy state. *Journal of Rheology*, 41(3):549–573, 1997.

[14] Baxter, Stokes, and Manissero. A lithium-based pozzolan for ASR control. *Proceedigns of the 11th International Conferece on Alkali-Aggregate Reaction, Quebec 2000*, pages 573–582, 2000.

[15] Brooks and Johari. Effect of metakaolin on creep and shrinkage of concrete. *Cement & Concrete Composites*, 23:495–502, 2001.

[16] Burgoyne. Rational use of advanced composites in concrete. *Structures & Buildings 146, Proceedings of the Institution of Civil Engineers*, (3):253–262, 2001.

[17] Chambers. Parallel-lay aramid ropes for use as tendons in prestressed concrete. Ph.D. Dissertation at the University of London, UK, 1986.

[18] Chambers and Burgoyne. An experimental investigation of the stress-rupture behaviour of a parallel-lay aramid rope. *Journal of Materials Science*, 25:3723–3730, 1990.

[19] Chawla. *Composite Materials, Science and Engineering*, pages 148–149. Springer, New York, 1998.

[20] Collins and Mitchell. *Prestressed Concrete Structures, 2nd Edition*. Prentice Hall, New Jersey, 1991.

[21] SEAS Columbia University. New concrete blends glass, engineering, art. *Engineering News*, (Spring):5, 2003.

[22] Daniel and Shah, editors. *Thin-Section Fiber Reinforced Concrete and Ferrocement, ACI SP-124*. ACI, 1990.

[23] University of Southern Mississippi Department of Polymer Science. Aramids. http://www.psrc.usm.edu/ macrog/ aramid.htm, 1995.

[24] Dobb and McIntyre. Properties and applications of liquid crystalline main chain polymers. *Advances in Polymer Science*, 60/61:61–98, 1984.

[25] Dolan, Rizkalla, and Nanni, editors. *Fiber Reinforced Polymer Reinforcement for Reinforced Concrete Structures, Fourth International Symposium, ACI SP-188*, 1999.

[26] Dyer and Dhir. Chemical reactions of glass cullet used as cement component. *Journal of Materials in Civil Engineering*, (11):412–417, 2001.

[27] Ericksen. Creep of aromatic polyamide fibres. *Polymer*, 26:733–746, 1985.

[28] Figg. Reaction between cement and artificial glass in concrete. *Proceedings of the Conference on Alkali-Aggregate Reaction in Concrete, Cape Town, South Africa*, 1981.

[29] Frias and Cabrera. Pore size distribution and degree of hydration of metakaolin-cement pastes. *Cement and Concrete Research*, 30:561–569, 2000.

[30] Gardner. Aramid fibers. http:// www.umaine.edu/ adhesion/ gardner/ 550lecture/ aramid%20fibers.ppt, 2000.

[31] Garland, Beyerlein, and Schadler. The development of compression damage zones in fibrous composites. *Composites Science and Technology*, 61:2461–2480, 2001.

[32] Grattan-Bellew, editor. *7th International Conference on Alkali-Aggregate Reaction in Concrete, Ottawa, Canada 1986*. Noyes Publications, Park Ridge, NJ, 1987.

[33] Grattan-Bellew. A critical review of ultra-accelerated tests for alkali-silica reactivity. *Cement and Concrete Composites*, 19:403–414, 1997.

[34] Gruber, Ramlochan, Boddy, Hooton, and Thomas. Increasing concrte durability with high-reactivity metakaolin. *Cement & Concrete Composites*, 23:479–484, 2001.

[35] Guimaraes and Burgoyne. Creep behaviour of a parallel - lay aramid rope. *Journal of Materials Science*, 27:2473–2489, 1992.

[36] US Gypsum. Durock brand cement board. http:// literature.usg.com/ pdf/ CB399.pdf, 2003.

[37] Hegger and Curbach, editors. *Textilbeton - 1. Fachkolloquium der Sonderforschungsbereiche 528 und 532*. E & FN Spon, London, 2001 (in German).

[38] Hudec and Ghamari. Ground waste glass as an alkali-silica reactivity inhibitor. *Proceedigns of the 11th International Conferece on Alkali-Aggregate Reaction, Quebec 2000*, pages 663–672, 2000.

[39] Echo Environmental Inc. Artistic impression of park bench assembly. Digital Graphics Composition, 2000.

[40] Jagasca. Modern day alchemy: Computational investigations into the molecular mechaniscms of kevlar & spectra fiber. http:// www.cmste.uncc.edu/ papers/ Final%20Draft.doc, 2001.

[41] Jin. Alkali-silica reaction in concrete with glass aggregate - a chemo-physico-mechanical approach. *Dissertation at the Department of Civil Engineering and Engineering Mechanics at Columbia University, New York*, 1998.

[42] Jin, Meyer, and Baxter. Glascrete - concrete with glass aggregate. *ACI Materials Journal*, 97(2):208–213, 2000.

[43] Johnston. Waste glass as coarse aggregate for concrete. *Journal of Testing and Evaluation*, 2(5):344–350, 1974.

[44] Kojima, Takagi, and Haruta. Expanding characteristics of mortar with glass powder produced from waste bottles. *Proceedigns of the 11th International Conferece on Alkali-Aggregate Reaction, Quebec 2000*, pages 673–682, 2000.

[45] Kozey, Jiang, Mehta, and Kumar. Compressive behavior of materials: Part ii. high performance fibers. *Journal of Materials Research*, 10(4):1044–1061, 1995.

[46] Krüger, Ožbolt, and Reinhardt. A new 3d discrete bond model to study the influence of bond on the structural performance of thin reinforced and prestressed concrete plates. *High Performance Fiber Reinforced Cement Composites - HPFRCC4, Proceedigns of the Fourth International RILEM Workshop, rilem PRO 30*, pages 49–63, 2003.

[47] Berkeley Lab. Kevlar - the wonder material. http:// www.lbl.gov/ MicroWorlds/ Kevlar/, 1996. Operated by the University of California for the U.S. Department of Energy.

[48] Lees. Flexure of concrete beams pre-tensioned with aramid frps. Ph.D. Dissertation at the University of Cambridge, UK, 1997.

[49] Liles. Lightweight structural concrte aggregate from municipal waste glass. *Proceedings of the 5th Mineral Waste Utilization Symposium of the IIT Research Institute, Chicago*, III:219–222, 1976.

[50] Litherland, Oakley, and Proctor. The use of accelerated ageing procedures to predict the long term strength of grc composites. *Cement and Concrete Research*, 11:455–466, 1981.

[51] Mehta and Monteiro. *Concrete: Structure, Properties, and Materials, 2nd Edition.* Prentice Hall, New Jersey, 1993.

[52] Meyer. Recycled glass - from waste material to valuable resource. *Proceedigns of the Int. Symposium on Recycling and Reuse of Glass Cullet at the University of Dundee, Scotland*, pages 1–10, 2001.

[53] Meyer, Egosi, and Andela. Concrete with waste aggregate. *Proceedigns of the Int. Symposium on Recycling and Reuse of Glass Cullet at the University of Dundee, Scotland*, pages 179–189, 2001.

[54] Meyer and Xi. Use of recycled glass and fly ash for precast concrete. *Journal of Materials in Civil Engineering*, (5):89–90, 1999.

[55] Millrath. Modifying concrete matrices with beneficiated dredged material or other clayed constituents. Ph.D. Dissertation at Columbia University New York, 2002.

[56] Mindess, Young, and Darwin. *Concrete, 2nd Edition*. Prentice Hall, New Jersey, 2003.

[57] Mobasher. Modeling of cement based composite laminates. *High Performance Fiber Reinforced Cement Composites - HPFRCC4, Proceedigns of the Fourth International RILEM Workshop, rilem PRO 30*, pages 81–94, 2003.

[58] n.a. Surprise for spiders. *Materials Today*, 5(10):9, October 1st 2002.

[59] Naaman and Reinhardt, editors. *High Performance Fiber Reinforced Cement Composites, HPFRCC2, RILEM Proceedings No. 31*. E & FN Spon, London, 1995.

[60] Naaman and Reinhardt, editors. *High Performance Fiber Reinforced Cement Composites, HPFRCC4, RILEM PRO30*. Rilem, 2003.

[61] Nanni and Dolan, editors. *Fiber-Reinforced-Plastic Reinforcement for Concrete Structures, International Symposium, ACI SP-138*, 1993.

[62] Neville. *Properties of Concrete*. John Wiley & Sons, Inc., 1997.

[63] Northolt. Tensile deformation of poly (p-phenylene terephthalamid) fibres, an experimental and theoretical analysis. *Polymer*, 21:1199, 1980.

[64] Northolt, Baltussen, and Schaffers-Korff. Yielding and hysteresis of polymer fibres. *Polymer*, 36(18):3485–3492, 1995.

[65] Northolt and Sikkema. Lyotropic main chain liquid crystal polymers. *Advances in Polymer Science*, 98:115–177, 1991.

[66] Parvizi-Majidi. *Fibers and Whiskers*, pages 25–88. Materials Science and Technology, Vol. 13, Structure and Properties of Composites. VCH, New York, 1993.

[67] Peled and Bentur. Cement impregnated fabrics for repair and retrofit of structural concrete. *High Performance Fiber Reinforced Cement Composites - HPFRCC4, Proceedigns of the Fourth International RILEM Workshop, rilem PRO 30*, pages 313–324, 2003.

[68] Peled, Shah, and Banthia, editors. *High-Performance Fiber-Reinforced Concrete Thin Sheet Products, ACI SP-190*. ACI, 2000.

[69] Phillips, Cahn, and Keller. Refuse glass aggregate in portland cement concrete. *Proceedings of the 3rd Mineral Waste Utilization Symposium of the IIT Research Institute, Chicago*, III:385–390, 1972.

[70] Pigliacampi. *Organic Fibers*, pages 54–57. ASM Handbook, Vol. 21, Composites. ASM International, 2001.

[71] Polley, Cramer, and Cruz. Potential for using waste glass in portland cement concrete. *Journal of Materials in Civil Engineering*, (11):210–219, 1998.

[72] Purnell, Short, Page, Majumdar, and Walton. Accelerated ageing characteristics of glass-fibre reinforced cement made with new cementitious matrices. *Composites: Part A*, 30:1073–1080, 1999.

[73] Ramlochan, Thomas, and Gruber. The effect of metakaolin on alkali-silica reaction in concrete. *Cement and Concrete Research*, 30:339–344, 2000.

[74] Reinhardt and Krüger. Vorgespannte dünne platten aus textilbeton. *Textilbeton - 1. Fachkolloquium der Sonderforschungsbereiche 528 und 532*, pages 165–174, 2001 (in German).

[75] Reinhardt and Naaman, editors. *High Performance Fiber Reinforced Cement Composites, HPFRCC3, RILEM PRO6*. Rilem, 1999.

[76] Rixom and Mailvaganam. *Chemical Admixtures for Concrete*. E & FN SPON, 1999.

[77] Rogers and Hooton. Reduction in mortar and concrete expansion with reactive aggregates due to alkali leaching. *Cement, Concrete, and Aggregates, CCAGDP*, 13(1):42–49, 1991.

[78] Sabir, Wild, and Bai. Metakaolin and calcined clays as pozzolans for concrete: a review. *Cement & Concrete Composites*, 23:441–454, 2001.

[79] Schmidt and Saia. Alkali-aggregate reaction tests on glass used for exposed aggregate wall panel work. *ACI Materials Journal*, 60:1235–1236, 1963.

[80] Shao, Lefort, Moras, and Rodriguez. Studies on concrete containing ground waste glass. *Cement and Concrete Research*, 30:91–100, 2000.

[81] Soukatchoff. Major improvements in long-term strength and toughness of glass-fiber reinfoced concrete. *High-Performance Fiber-Reinforced Concrete Thin Sheet Products, ACI SP-190*, pages 165–182, 2000.

[82] Tang, Xu, and Han. Alkali reactivity of glass aggregate. *Durability of Building Materials*, 4(4):377–385, 1987.

[83] Taylor. *Cement Chemistry, 2nd Edition*. Thomas Telford, 1997.

[84] Testa and Yu. Stress-strain relation for coated fabrics. *Journal of Engineering Mechanics*, 113(11):1631–1646, 1987.

[85] Twaron. Technora and twaron side by side in umbilicals. Twaron News 2002, No. 11, http:// www.twaron.com/ pdf/ news06/ Artikel4.pdf, 2002.

[86] Vaidya. Aramid fiber. http:// www.eng.uab.edu/ compositesLab/ b_fiber.htm, 2002.

[87] Varshneya. *Fundamentals of Inorganic Glasses*. Academic Press, Inc., 1994.

[88] Vlattas and Galiotis. Monitoring the behaviour of polymer fibres under axial compression. *Polymer*, 32:1788, 1991.

[89] Vlattas and Galiotis. Deformation behaviour of liquid crystal polymer fibres: 1. converting spectoscopic data into mechanical stress-strain curves in tension and compression. *Polymer*, 35:2335, 1994.

[90] Walton and Majumdar. Creep of kevlar 49 fibre and a kevlar 49 cement composite. *Journal of Materials Science*, 18:2939–2946, 1983.

[91] Wild and Khatib. Portlandite consumption in metakaolin cement pastes and mortars. *Cement and Concrete Research*, 27:137–146, 1997.

[92] Wild, Khatib, and Jones. Relative strength, pozzolanic activity adn cement hydration in superplasticised metakaolin concrete. *Cement and Concrete Research*, 26:1537–1544, 1996.

[93] Wortmann and Schulz. Non-linear viscoelastic performance of nomex, kevlar and polypropylene fibres in a single step stress relaxation test: 2. moduli, viscosities and isochronal stress-strain curves. *Polymer*, 36(12):2363–2369, 1995.

[94] Yang. *Aromatic high stregth fibers*. Wiley, 1989.

[95] Yeh and Young. Molecular deformation processes in aromatic high modulus polymer fibres. *Polymer*, 40(4):857–870, 1999.